12-2016

Quantifying terrestrial ecosystem carbon dynamics with mechanistically-based biogeochemistry models and in situ and remotely sensed data

Shaoqing Liu
Purdue University

Graduate School Form
30 Updated 12/26/2015

PURDUE UNIVERSITY
GRADUATE SCHOOL
Thesis/Dissertation Acceptance

This is to certify that the thesis/dissertation prepared

By Shaoqing Liu

Entitled

Quantifying terrestrial ecosystem carbon dynamics with mechanistically-based biogeochemistry models and in situ and remotely sensed data

For the degree of Doctor of Philosophy

Is approved by the final examining committee:

Yuch-Ning Shieh
Chair

Greg Michalski

Devdutta S Niyogi

Qianlai Zhuang

To the best of my knowledge and as understood by the student in the Thesis/Dissertation Agreement, Publication Delay, and Certification Disclaimer (Graduate School Form 32), this thesis/dissertation adheres to the provisions of Purdue University's "Policy of Integrity in Research" and the use of copyright material.

Approved by Major Professor(s): Qianlai Zhuang

Approved by: Indrajeet Chaubey 10/4/2016

Head of the Departmental Graduate Program Date

QUANTIFYING TERRESTRIAL ECOSYSTEM CARBON DYNAMICS WITH MECHANISTICALLY-BASED BIOGEOCHEMISTRY MODELS AND IN SITU AND REMOTELY SENSED DATA

A Dissertation

Submitted to the Faculty

of

Purdue University

by

Shaoqing Liu

In Partial Fulfillment of the

Requirements for the Degree

of

Doctor of Philosophy

December 2016

Purdue University

West Lafayette, Indiana

For my parents
my wife

ACKNOWLEDGEMENTS

First of all, I would like to thank my major advisor Prof. Qianlai Zhuang for his support on my research. I was so lucky that I had the opportunity to come to Purdue University and work with Prof. Zhuang in the Ecosystem Biogeochemistry and Dynamics Laboratory. His advices were always inspirational, encouraging and supportive. After Prof. Zhuang showed me a big picture of research about the biosphere and atmosphere interactions, his continuous support and advice help my growth to be a scientist. I shall never forget the research values and the dreams that he has passed to me.

I would like to thank my committee members: Profs. Yuch-Ning Shieh, Greg Michalski and Dev Niyogi. Their diverse research backgrounds help me a lot on such a complicated and interdisciplinary research project. Specifically, Prof. Shieh and Prof. Michalski are biogeochemistry scientists. Their theoretical instruction in isotope biogeochemistry provided me better understanding the two aspects of my PhD research. Prof. Niyogi is a biophysical and climate modeling expert. Technically speaking my thesis involved several biophysical concepts. His expertise helped me to solve my research questions successfully. I was deeply impressed by their great erudition and rigorous academic thinking. Their help are irreplaceable for me to successfully finish the dissertation.

I want to also thank my lab mates who enriched my life so much at Purdue. Finally, I would like to thank my wife. Without her support and encouragement, I may not be able to overcome so many difficulties to accomplish the dissertation research

TABLE OF CONTENTS

Page

Page

Page

LIST OF TABLES

LIST OF FIGURES

Figure Page

Figure Page

ABSTRACT

Shaoqing, Liu. Ph.D., Purdue University, December 2016. Quantifying Terrestrial Ecosystem Carbon Dynamics with Mechanistically-based Biogeochemistry Models and in Situ and Remotely Sensed Data. Major Professor: Qianlai Zhuang.

Terrestrial ecosystem plays a critical role in the global carbon cycle and climate system. Therefore, it is important to accurately quantify the carbon dynamics of terrestrial ecosystem under future climatic change condition. This dissertation evaluates the regional carbon dynamics by using upscaling approach, mechanistically-based biogeochemistry models and in situ and remotely sensed data.

The upscaling studies based on FLUXNET network has provided us the spatial and temporal pattern of the carbon fluxes but it fails to consider the atmospheric CO_2 effect given its important physiological role in carbon assimilation. In the second chapter, we consider the effect of atmospheric CO_2 using an artificial neural network (ANN) approach to upscale the AmeriFlux tower of net ecosystem exchange (NEE) and the derived gross primary productivity (GPP) to the conterminous United States. We found that atmospheric CO_2 effect on GPP/NEE exhibited a great spatial and seasonal variability. Further analysis suggested that air temperature played an important role in determining the atmospheric CO_2 effects on carbon fluxes. In addition, the simulation that did not consider atmospheric CO_2 failed to detect ecosystem responses to droughts in part of the US in 2006. The study suggested that the spatially and temporally varied atmospheric CO_2 concentrations should be factored into carbon quantification when scaling eddy flux data to a region.

The process-based ecosystem models are useful tools to predicting future change in the terrestrial ecosystem. However, they suffer the great uncertainty induced by model structure and parameters. The carbon isotope (13C) discrimination by terrestrial plants, involves the biophysical and biogeochemistry processes and exhibits seasonal and spatial variations, which may provide additional constraints on model parameters. In the third chapter, we found that using foliar 13C composition data, model parameters were constrained to a relatively narrow space and the site-level model simulations were slightly better than that without the foliar 13C constraint. The model extrapolations with three stomatal schemes all showed that the estimation uncertainties of regional carbon fluxes were reduced by about 40%.

In addition, tree ring data have great potentials in addressing the forest response to climatic changes compared with mechanistic model simulations, eddy flux measurement and manipulative experiments. In the fourth chapter, we collected the tree ring isotopic carbon data at 12 boreal forest sites to develop a linear regression model, and the model was extrapolated to the whole boreal region to obtain the water use efficiency (WUE) and GPP spatial and temporal variation from 1948 to 2010. Our results demonstrated that most of boreal regions except parts of Alaska showed a significant increasing WUE trend during the study period and the increasing magnitude was much higher than estimations from other land surface models. Our predicted GPP by the WUE definition algorithm was comparable with site observation, while for the revised light use efficiency algorithm, GPP estimation was higher than site observation as well as land surface model estimates. In addition, the increasing GPP trends estimated by two algorithms were similar with land surface model simulations.

CHAPTER 1 INTRODUCTION

1.1. Research background

Terrestrial ecosystem plays a critical role in the global carbon cycle and regulates the climate. On the one hand, the increasing greenhouse gas (GHG) emissions mainly due to the intensive anthropogenic activity have direct and indirect effects on the global terrestrial ecosystem carbon budget (Canadell et al., 2007). On the other hand, the capacity of absorbing CO_2 in terrestrial ecosystem would significantly impact the global climate through biophysical and biochemical feedbacks (Friedlingstein et al., 2006). Therefore, it is important to accurately quantify the carbon dynamics of terrestrial ecosystem under future climatic change condition, so as to facilitate the corresponding political decision making. At present, the global/regional carbon sink of terrestrial ecosystem can be estimated by using atmospheric inversion, satellite remote sensing approaches, data-driven methods and process-based ecosystem models. The magnitude of carbon sink/source using inversion models is based on the atmospheric observation, such as satellite retrievals and air flask samples. However, this approach is generally limited by the sparseness of observation network (Tans et al., 1990) and cannot differentiate the sink/source contribution from each vegetation type. Remote sensing can obtain the near real-time ecosystem productivity, but the accuracy is highly dependent on the model retrievals algorithm and quality images (Baldocchi et al., 2001).

Regional carbon dynamics estimation based on the data-driven methods relies on the ecosystem response to environmental condition derived from the site-level observation networks. Recently, the widespread eddy covariance towers have been intensively used to measure terrestrial land

surface exchanges of carbon, water and energy (Williams et al., 2009). The measurements of biometeorological variables (such as temperature, radiation, surface-atmosphere CO_2 exchange, latent heat flux) using the eddy covariance technique on a continuous basis started in the 1990s (Verma, 1990). At present, over 700 flux tower sites have been established to provide flux observation across a wide range of climate and biomes (except cropland), leading to the development of regional observation network (such as Ameriflux and FLUXNET: http://daac.ornl.gov/FLUXNET/fluxnet.shtml). Some sites also have the ecological measurement, such as the litter fall, leaf area index, soil organic carbon pool. The published datasets were generally composed of 4 levels data (level1 to level 4). Level 1 and level 2 include the raw observation and post-processed data (gap-filled) and the time step is generally 30 or 60 min. Level 3 is derived from the level 2 products, and the data is quality checked using standardized techniques, and level 4 is obtained from level 3 using ustar filter, gap-filled with different methods (e.g. marginal distribution sampling method and artificial neural network) and this product has the aggregated daily, weekly and monthly datasets. These continuous fluxes and meteorological variables measurements provide rich insights in the ecosystem response to environmental change at different time scales. To date, numerous studies have been conducted to explore the gross primary productivity (GPP)/net ecosystem exchange (NEE) temporal or spatial variation and its controlling factors in terrestrial ecosystems using those flux data (e.g. Valentini et al., 2000; Hirata et al., 2008; Lund et al., 2010; Bracho et al., 2012). Since the site-level observations cover a broad range of climate and biomes, the data-driven method is generally employed in the upscaling exercise by using eddy covariance flux sites at multiple representative sites. This approach generally employs the machine learning algorithm using meteorological data, vegetation properties, and remote sensing products and has great advantage in the simplicity without too many parameters compared with other mechanistically-based ecosystem models. For example, Xiao et al (2010) explored the regress tree to obtain the GPP and NEE in the continent

US by using Ameriflux level 4 data products and remote sensing variables. However, current upscaling studies have some limitations: First, simulations are vegetation type based: this means the model structure and parameters are invariant within an ecosystem (Alton, 2011); Second, the selected flux sites may contribute large uncertainties to the model development since regional ecoregions may not be well represented by these flux sites (Hargrove et al.2003); Finally, other controlling factors may not be considered in upscaling studies, such as land use change (Lambin et al., 2003), vegetation characteristics (e.g. tree age). Despite the drawbacks listed above, these data products derived from upscaling studies have been extremely useful for improving of our understanding of the processes and spatial and temporal patterns in terrestrial carbon dynamics (Luo et al., 2015).

The process-based ecosystem models, incorporating with key biophysical and biochemical processes including photosynthesis, respiration, and evapotranspiration, are now widely used in understanding and predicting carbon exchanges between terrestrial biosphere and the atmosphere. Most of process-based ecosystem models are conducted over relatively large spatial scales with short time scales, based on the meteorological forcings, vegetation characteristics and soil properties. Also some models incorporate the slow processes of vegetation dynamics (Sitch et al., 2008), such as the succession, competition and reproduction, with the fast exchanges of water, carbon. Although these models are useful tools to predict the likely future states of earth systems under anthropogenic forcings, the forecasts of global carbon dynamics show a great variability (Todd-Brown et al., 2013), indicating significant uncertainties exist in the representation of ecosystem processes (e.g. carbon/nitrogen interaction) and model structure (parameters). On the one hand, at a relatively short time scale, the response to light, temperature, precipitation are well-predicted by a series of physical and biochemical equations, however, the effects of disturbance (fire, land use change) and directional trends, including the increasing CO_2 and nitrogen deposition, are much less well understood (Luo et al., 2015). For example, the

performance capturing the long-term fertilization by ecosystem models is still very poor when compared with the in-situ free air enrichment (FACE) observations. Zaehle et al (2014) and Walker et al (2015) showed that most ecosystem models can reproduce the initial carbon sequestration under elevated CO_2 condition at the Duke and ORNL FACE sites. However, none of them were able to simulate the long term (10 years) response at both sites. The comparison suggested that the improved representation of nitrogen dynamics, carbon allocation and plant stoichiometry in ecosystem models is pivotal to reducing the uncertainty in the observed fertilization effects. On the other hand, most process-based models have detailed processes to allow the simulation of ecosystem's response to change in a realistic way (Prentice et al., 2015). And this generally results in the increasing model complexity and less traceability (Xia et al., 2013) due to the high non-linearity and groups of parameters. The inter-comparison studies of the 12 terrestrial ecosystem models showed that model structure and parameters were the main uncertainty sources (Schaefer et al., 2012). As for the model parameters, some measureable model parameters derived from experiment maybe valid under specific conditions (such as plant functional type and climate condition), while most other parameters are based on empirical or prior knowledge. In addition, the parameters equifinality often occurs (Tang and Zhuang, 2008) when different sets of parameters with a wide space are used to drive ecosystem models, which results in a large prediction variability.

In addition to carbon flux data, stable carbon isotope (^{13}C) observation may help constrain the carbon dynamics prediction. There are two naturally occurring stable isotopes of carbon, ^{12}C and ^{13}C. Most of the carbon is ^{12}C (98.9%), with 1.1% being ^{13}C. Due to the difference in atomic mass, the isotopologues exhibit different physical and chemical properties, resulting in different reaction kinetics and thermodynamic properties. The carbon isotope composition is usually expressed in δ notation (in ‰ units), relative to the international standard Vienna Pee Dee

Belemnite (VPDB). The carbon isotopic composition $\delta^{13}C$ of any sample is thus expressed as deviation from VPDB as shown:

$$\delta^{13}C = (\frac{R_{sample}}{R_{VPDB}} - 1) * 1000 \quad (1.1)$$

where R is the isotope (abundance) ratio ($^{13}C/^{12}C$) of a given sample (R_{sample}) and of VPDB (R_{VPDB} = 0.0111802), respectively. The carbon isotope discrimination ($\Delta^{13}C$) is defined as the depletion of ^{13}C during any process preferring the lighter isotopologue:

$$\Delta = (\frac{\delta^{13}C_s - \delta^{13}C_p}{1000 + \delta^{13}C_p}) * 1000 \quad (1.2)$$

where $\delta^{13}C_s$ is the carbon isotope signature of the source and $\delta^{13}C_p$ is the isotopic signature of the product of a process (Farquhar et al., 1989). On the VPDB scale, free atmosphere CO_2 currently has a value about -7.8‰, and typical C3 plant carbohydrate a deviation of δ_p of -27.6‰.

Generally, carbon isotope fractionation during photosynthesis in C3 plants is described according to the following equation (Farquhar et al., 1982):

$$\Delta = a_b \frac{P_a - P_s}{P_a} + a \frac{P_s - P_i}{P_a} + (e_s + a_l) \frac{P_i - P_c}{P_a} + b \frac{P_c}{P_a} - (\frac{eR_d / k}{P_a} + \frac{f\Gamma^*}{P_a}) \quad (1.3)$$

Where P_a , P_s , P_i and P_c are the CO_2 partial pressures in ambient air, at the leaf surface, in the leaf intercellular airspace and in the chloroplasts, respectively. a_b and a describe the carbon isotope fractionation during diffusion through the boundary layer (2.9 ‰) and into the leaves through the stomata (4.4 ‰), respectively. e_s is the fractionation occurring as CO_2 enters an aqueous solution (1.1 ‰ at 25 ◦C) and a_l the fractionation during diffusion through the liquid phase (0.7 ‰ at 25 ◦C), k is the carboxylation efficiency and b the net fractionation during

carboxylation. R_d is the respiration rate in the light, Γ_* is the CO_2 compensation point in the absence of day respiration, and e and f are the fractionation factors during day respiration and photorespiration.

According to Farquhar photosynthesis formula (Farquhar et al., 1980), the carbon assimilation rate is a function of the intercellular CO_2 concentration. Therefore, the in-situ observation of carbon fluxes combined with the measurements of isotopic signal of plant tissues, which integrate all the biophysical and biogeochemical processes, may be expected to have good constraints on the parameters related to biophysical and biochemical processes at the canopy scale. For example, plant ecosystem respired CO_2 has been shown to negatively relate with vapor pressure deficit, which is consistent with stomatal regulation of gas exchange and photosynthetic carbon discrimination (Bowling et al., 2002). In addition, the highly frequent respired CO_2 isotopic signals have provided a new tool to partitioning GPP and respiration. However, since plant ^{13}C tissue observation is closely associated with the plant physical and biochemical processes, few studies have incorporated the observation into the process-based ecosystem models to constrain relative parameters or physical/biochemical processes, and therefore the regional/global carbon dynamics. Ballantyne et al (2011) compared the simulated isotope composition of CO_2 using the Simple integrated Biosphere2 (SiB2) with in-situ atmosphere $^{13}CO_2$ measurement to evaluate Ball-Berry and Lenuing model schemes. Bodin et al (2013) incorporated the three stomatal models into a LSM to simulate the carbon isotope ratio of tree leaves ($\delta^{13}C_{leaf}$) and tree rings ($\delta^{13}C_{stem}$) over a period of 53 years, and comparing the results with carbon isotope ratios obtained from measured at six sites in northern Europe. As for the water use efficiency study based on tree rings, previous studies were mainly focused on site-level.

In addition, the isotopic records in tree ring are particularly useful for understanding tree response to long term environmental change. The annual tree rings are formed through cambial

cell division, enlargement and lignification, which are influenced by multiple environmental condition and occasional disturbance events (insect, fire) (Babst et al., 2014). Despite the complex processes (e.g. carbon allocation) resulting in the final tree ring characteristics, it still provides us an opportunity to investigate the effects of mutilple environmental conditions on tree ring properties (Billings et al., 2016). The ratio of intercellular CO_2 to ambient CO_2 (C_i/C_a), which links the photosynthetic activity and stomatal closure and drives the signal of carbon discrimination at the leaf scale, can be used to infer the physiological processes. Previous studies have used the tree ring isotopic carbon data to reconstruct past-climate variables (radiation, precipitation) (Loader et al., 1996; Holzkämper et al., 2009) since C_i/C_a is strongly modulated by environmental change. In addition, the intrinsic water use efficiency variation, which is often explored as an indicator of long term regulation of plant carbon uptake and water loss in plants (Keenan et al., 2009), can be also derived from tree ring isotopic record. For example, Saurer et al (2004) investigated the response of 126 trees (Larix, Pinus and Picea) in northern Eurasia to climatic change and increasing CO_2 over the last century by using tree ring data, and their findings suggested an 19.2% increase in WUE_i in these species. Dekker et al (2016) derived the global ecosystem water use efficiency based on tree ring data and FLUXNET by exploring a new stomatal algorithm, which is based on the optimal stomatal behavior. These site-levels studies help us understand how certain plant species respond to climatic change, especially the CO_2 fertilization effect. However, few have conducted the regional WUE estimation based on the tree ring carbon data.

1.2. Research Objective

Terrestrial ecosystems absorb around one-third CO_2 emissions from anthropogenic activities (Le Quere et al., 2009) and its feedback would have a large impact on the global climate system

(Friedlingstein et al., 2006). Therefore, it is important to accurately quantify the regional/global carbon dynamics in terrestrial ecosystems given the predicted continuous increasing GHG emissions in future. In the Introduction section above, I briefly reviewed two methods to quantify regional/global carbon dynamics: upscaling studies based on Fluxnet and process-based ecosystem models. Although the upscaling studies based on FLUXNET network has provided us the spatial and temporal pattern of the carbon fluxes and can serve as the benchmark products for the ecosystem modeling community, it fails to consider the atmospheric CO_2 effect given its important physiological role in carbon assimilation (e.g. Ainsworth and Long, 2005). The process-based ecosystem models are useful tools to predicting future change in the terrestrial ecosystem. However, they suffer the great uncertainty induced by model structure and parameters.

Therefore, my first two chapters will focus on the upscaling approach and using process-based ecosystem models to quantify carbon dynamics. In addition, compared with the complex land surface models, tree ring isotopic record has great advantage to address plant response to long term environmental variations. My specific research objectives are:

(1) Evaluate the atmospheric CO_2 effects on the regional GPP/NEE estimation using FLUXNET and machine learning algorithms.
(2) Constrain the carbon dynamics by using process-based ecosystem models where isotopic fractionation process is incorporated into a process-based model to reduce the estimation uncertainty.
(3) Derive the regional long term WUE variation and estimate the inter-annual GPP based on the derived WUE using tree ring carbon isotopic record.

CHAPTER 2 EVALUATING ATMOSPHERIC CO_2 EFFECTS ON GROSS PRIMARY PRODUCTIVITY AND NET ECOSYSTEM EXCHANGES OF TERRESTRIAL ECOSYSTEMS IN THE CONTERMINOUS UNITED STATES USING THE AMERIFLUX DATA AND AN ARTIFICIAL NEURAL NETWORK APPROACH

Abstract: Quantitative understanding of regional gross primary productivity (GPP) and net ecosystem exchanges (NEE) and their responses to environmental changes are critical to quantifying the feedbacks of ecosystems to the global climate system. Numerous studies have used the eddy flux data to upscale the eddy covariance derived carbon fluxes from stand scales to regional and global scales. However, few studies incorporated atmospheric carbon dioxide (CO_2) concentrations into those extrapolations. Here, we consider the effect of atmospheric CO_2 using an artificial neural network (ANN) approach to upscale the AmeriFlux tower of NEE and the derived GPP to the conterminous United States. Two ANN models incorporating remote sensing variables at an 8-day time step were developed. One included CO_2 as an explanatory variable and the other did not. The models were first trained, validated using eddy flux data, and then extrapolated to the region at a $0.05^o \times 0.05^o$ (latitude x longitude) resolution from 2001 to 2006. We found that both models performed well in simulating site-level carbon fluxes. The spatially-averaged annual GPP with and without considering the atmospheric CO_2 were 789 and 788 g C m^{-2} yr^{-1}, respectively (for NEE, the values were -112 and -109 g C m^{-2} yr^{-1}, respectively). Model predictions were comparable with previous published results and MODIS GPP products. However, the difference in GPP between the two models exhibited a great spatial and seasonal

variability, with an annual difference of 200 g C m^{-2} yr^{-1}. Further analysis suggested that air temperature played an important role in determining the atmospheric CO_2 effects on carbon fluxes. In addition, the simulation that did not consider atmospheric CO_2 failed to detect ecosystem responses to droughts in part of the US in 2006. The study suggests that the spatially and temporally varied atmospheric CO_2 concentrations should be factored into carbon quantification when scaling eddy flux data to a region.

2.1 Introduction

Net ecosystem carbon exchange (NEE) and gross primary productivity (GPP) are two major fluxes involved in the ecosystem biogeochemical carbon process. Quantification of GPP and NEE and their responses to environmental changes would improve our understanding of the ecosystem carbon cycling and its feedbacks to the global climate system. At present, GPP and NEE at regional scales are often quantified using atmosphere inverse models (e.g. Prince and Goward, 1995), process-based biogeochemical models (e.g. White et al., 2000), and satellite remote sensing approaches (e.g. Running et al., 2000). The estimation of NEE based on the inverse models is limited by the sparseness of the carbon dioxide (CO_2) observation network (Tans et al., 1990); and this approach cannot differentiate the carbon source/sink contributions of each ecosystem (Janssens et al., 2003). Process-based models generally first derive the GPP and ecosystem respiration, which are modeled as a function of physical and biological variables and thus can be applied at regional and global scales. However, large uncertainty still exists in current quantification due to complex model structure, uncertain parameters, and model input (Chen et al., 2011). Satellite remote sensing approaches have advantages in GPP quantification that is based on a near real-time dataset, instead of broadly parameterized ecosystem models. However, they

are highly dependent on the accuracy of the model algorithms and the quality of satellite imageries (Baldocchi et al., 2001).

The eddy covariance technique provides direct measurement of net carbon and water fluxes between vegetation and the atmosphere (Baldocchi et al., 1988; Foken and Wichura, 1996; Aubinet et al. 1999). At present, over 500 flux tower sites have been operated to measure the exchanges of carbon fluxes continuously over a broad range of climate and biome types (FLUXNET http://daac.ornl.gov/FLUXNET/fluxnet.shtml). These towers also provide calibrated, validated NEE data and the derived GPP product. To date, numerous studies have been conducted using those flux data to explore the GPP and NEE temporal or spatial variation and their controlling factors in terrestrial ecosystems (Valentini et al. 2000; Law et al. 2002; Baldocchi, 2008; Hirata et al. 2008; Kato and Tang 2008; Lund et al., 2010; Bracho et al., 2012). Eddy flux data have also been widely used for model calibration (Hanan et al., 2002; Reichstein et al., 2002; Hanson et al., 2004) and to upscale from stands to regional levels. The upscaling exercises generally employ the machine learning algorithm that uses meteorological data, vegetation properties, and remote sensing products, which have been conducted for Asia (Zhu et al., 2014; Fu et al., 2014), Europe (Jung et al., 2008; Vetter et al., 2008), the US (Yang et al., 2007; Xiao et al., 2008; Xiao et al., 2010) and even at global scales (Beer et al., 2010; Yuan et al., 2010).

However, few studies have incorporated the atmospheric CO_2 concentrations into regional GPP and NEE extrapolations when using eddy flux tower data. Increasing CO_2, which is mainly due to the burning of fossil fuels and, to a much lesser extent, land-cover change (Keeling et al., 1995; Hartmann et al., 2013), will have substantial direct and indirect effects on the carbon budget (Canadell et al., 2007). Numerous studies have been conducted to understand how plants and ecosystems will respond to elevated CO_2 (Ainsworth and Long, 2005). The large-scale free-air CO_2 enrichment experiment (FACE) showed that increasing CO_2 would reduce the stomatal

conductance (Curtis and Wang, 1998; Medlyn et al., 2001; Ainsworth and Rogers, 2007) over a short time period, resulting in decreased transpiration, enhanced water-use efficiency (Conley et al., 2001; Wall et al., 2001) and increased soil moisture (Bunce, 2004). In addition, stimulated photosynthesis (e.g. Li et al., 2014) would increase the above and below-ground biomass production (Piao et al., 2006, Los, 2013; Wan et al., 2007; Deng et al., 2010) and hence accelerate the CO_2 loss from heterotrophic respiration (Luo et al., 1996). Generally, long-lived plant biomass (trees) is more responsive to increasing CO_2 than herbaceous species (Ainsworth and Long, 2005). However, increased plant production with high carbon (C) to nitrogen (N) ratio under elevated CO_2 results in low quality litter input and slows the soil N mineralization, thus triggering the negative feedback to plant biomass over time (Oren et al., 2001; Gill et al., 2002; Luo et al., 2004) if there is no extra nitrogen input. This conceptual framework about progressive N limitation is more obvious in long-lived plants (trees) (Luo et al., 2004) and has been supported by few experiments (Oren et al., 2001; Norby et al., 2010). In addition, the climate drivers and their interaction with soil resources (Reich et al., 2014) would also constrain the ecosystem response to CO_2 fertilization. For example, increasing N mineralization due to warming temperature would further promote plant growth (Peltola et al., 2002; Dijkstra et al., 2010) whereas the drought stress may diminish this positive effect under elevated CO_2 condition (Dermody et al., 2007; Larsen et al., 2011). Moreover, altered water, energy balance (Drake et al., 1997, Keenan et al., 2013), and vegetation physiology due to increasing CO_2 would in turn affect the carbon cycling. Therefore, incorporating atmospheric CO_2 concentrations into the regional GPP and NEE estimation should be a research priority. In addition, previous upscaling flux studies that exclude the atmospheric CO_2 concentration assume that CO_2 variations were spatially and temporally uniform in a region. Although atmospheric CO_2 is generally well-mixed globally since it is chemically inert (Eby et al., 2009), it actually exhibits a large seasonal and spatial variability at the regional scale (Miles et al., 2012). The seasonal and spatial characteristics have

previously been reported at site and regional levels (Davis et al., 2003; Haszpra et al., 2008; Miles et al., 2012). For example, the summer measurement of the atmospheric boundary layer CO_2 mole fraction from a nine-tower regional network deployed during the North American Carbon Program's Mid-Continent Intensive (MCI) during 2007 to 2009 shows that the seasonal CO_2 amplitude is five times larger than the tropospheric background and the spatial gradient across the region is four times the inter-hemispheric gradient (Miles et al., 2012).

In this study, we used an artificial neural network (ANN) approach to upscale the AmeriFlux tower derived GPP and NEE to the conterminous US from 2001 to 2006 by considering the atmospheric CO_2 concentrations as an independent factor. We developed two sets of ANN models linking GPP and NEE and remote sensing variables for each vegetation type: the first considered the atmospheric CO_2 concentration effects (CO_2 incorporated simulation, S0) and the other did not (non-CO_2 incorporated simulation, S1). After the training and validation procedure, we then used the two models to extrapolate GPP and NEE to the conterminous US. We hypothesized that: (1) both models would capture the GPP and NEE variation at the calibration stage; (2) the two simulations would exhibit spatiotemporal differences which associate with climate drivers; and (3) ecosystems with high productivity (e.g., forest, cropland) would show greater differences between the two simulations.

2. 2 Method

2.2.1 Overview

From the AmeriFlux network, we selected the key ecosystem types in the conterminous US including: evergreen forest, deciduous forest, grassland, mixed forest, savannas, shrubland, and cropland. Day land surface temperature (D_LST) and night land surface temperature (N_LST),

leaf area index (LAI), fraction of absorbed photosynthetically active radiation (fPAR), normalized difference vegetation index (NDVI), enhanced vegetation index (EVI), CO_2 measurement and derived GPP and NEE from the eddy flux towers were organized into an 8-day time step. To explore the atmospheric CO_2 concentrations' effect on the GPP and NEE, we constructed two sets of ANN models for each vegetation type: one incorporated CO_2(S0) in addition to D_LST, N_LST, LAI, fPAR, NDVI and EVI; and the second did not incorporate with CO_2 (S1) with the same explanatory variables in S0. After the training and validation of the two sets of ANN models, the regional estimation of GPP and NEE was driven by the explanatory variables at a spatial resolution of $0.05^\circ \times 0.05^\circ$ on an 8-day time step. The difference between S0 and S1 was then analyzed, considering the controls of environmental variables.

2.2.2 Explanatory variables

NEE is the difference between photosynthesis and ecosystem respiration, which is influenced by a variety of physical, physiological, hydrological, and atmospheric variables. As for the plant photosynthesis, current ecosystem models have incorporated various mechanisms related to these factors to simulate GPP, such as the bio-chemical model (e.g. Farquhar et al., 1980), light use efficiency equation (e.g. Running et al., 2000), and the semi-empirical relationship (e.g. Raich et al., 1991). Ecosystem respiration (Re) includes autotrophic (Ra) and heterotrophic respiration (Rh). Ra is generally modeled as a function of temperature and plant biomass, while Rh is empirically modeled as a function of soil temperature, moisture, and soil organic carbon stocks. Many of these factors influencing GPP and NEE can be assessed by satellite remote sensing products. NDVI is closely correlated to the photosynthetic activity, vegetation biomass, and fractional vegetation cover, which have been widely used in production efficiency models. We also incorporated the EVI to improve the ANNs performance due to the several limitations of

normalized difference vegetation index (NDVI), including the saturation in a multilayer closed canopy and sensitivity to atmosphere aerosols and soil background. The LST derived from the Moderate Resolution Imaging Spectroradiometer (MODIS) corresponds the surface soil temperature, which is known to strongly control the Re as both Ra and Rh. Previous studies demonstrated that satellite-derived LST was strongly correlated with Re, especially in dense-vegetated ecosystems (Rahman et al., 2005). The estimation of LAI and fPAR, characterizing the vegetation canopy function and energy absorption capacity, are key parameters in most biogeochemical models due to the high correlation with GPP. Taken together, we selected LST, NDVI, EVI, fPAR, and LAI as explanatory variables to account for the GPP and NEE variation.

2.2.3 Data Organization

We organized AmeriFlux site-level data of carbon flux and meteorology, MODIS land-cover, spatially and seasonally explicit CO_2, and the remote sensing products derived from MODIS. The AmeriFlux network coordinates regional analyses of observations from eddy covariance flux towers across the US. The Level-3 and Level-4 data for 36 AmeriFlux sites over the period 2000–2006 that contained CO_2 measurements were ultimately organized (Table 2-1 & Fig 2.1). In the Level-3 product, the half-hourly $CO_2$was aggregated into 8-day time step values. The Level-4 product consists of two types of GPP and NEE data: standardized (GPP_st and NEE_st) and original (GPP_or and NEE_or). Here, we used the same method in Xiao et al. (2010) to select the type of GPP and NEE product. Explanatory variables, GPP and NEE values derived from the selected sites were organized to develop the ANN models for each ecosystem type.

We used the following four MODIS data products (Collection 4), including daytime and nighttime LST (MOD11A2; Wan et al., 2002), EVI (MOD13A1; Huete et al., 2002), and LAI/fPAR (MOD15A2; Myneni et al., 2002).EVI is at a spatial resolution of 500 m x 500m,

while LAI, fPAR, and LAI are at spatial resolutions of 1 km x 1km. These MODIS data were resampled to the same resolution of $0.05^{\circ} \times 0.05^{\circ}$ (longitude x latitude). The explicitly spatial and seasonal CO_2 data was obtained from the National Oceanic and Atmospheric Administration (NOAA) gridded CO_2 product (ftp://aftp.cmdl.noaa.gov/products/carbontracker/CO_2/). The product is based on global CO_2 observation network data, employing a novel ensemble assimilation method to accurately model atmospheric CO_2 mole fractions (Peters et al., 2007). Land cover was obtained from the MODIS product Land Cover Types Yearly L3 Global 0.05 Deg CMG (MOD12C1) (Year 2005) from the NASA Goddard Space Flight Center website (http://modis-land.gsfc.nasa.gov). The classification of the International Geosphere and Biosphere (IGBP) land-cover classification system was used to reclassify the land-cover map of the conterminous United States into seven major vegetation types in the ANN model. To be more specific, the evergreen needleaf forest and evergreen broadleaf forest were combined into evergreen forest (same for deciduous forest); and closed shrubland and open shrubland were merged into shrubland. Therefore, the model calibration and simulation were based on the seven vegetation types: evergreen forest, deciduous forest, grassland, mixed forest, savannas, shrubland, and cropland.

2.2.4 Neural Network Development

We used a General Regression Neural Network (GRNN) algorithm (Specht, 1991) to represent the input-output relationship between the independent variables and dependent variables. The GRNN scheme can model the nonlinear system without specifying the algebraic relationship or internal mechanism. With the advantage of a fast-learning speed and good convergence with a large number of training datasets, GRNN can be a useful tool to estimate GPP and NEE based on the explanatory environmental variables. The training data set, including input and output values

of measurements, is fed into the multilayer neural network. The network is trained to obtain a set of optimized interconnected network weights, which are used to produce the most probable value for the outputs. More details about the GRNN algorithm and optimization procedure are provided in the supplementary information (GRNN algorithm and Fig. 2.2). To develop the GRNN model for each ecosystem type, we first randomly divided each dataset into two sets: a training set (75% of whole data for each vegetation type) used to construct the GRNN model and a testing set (25% of whole data for each vegetation type) used to evaluate the performance of constructed GRNN. MATLAB codes were used for developing the model (The MathWorks Inc., Natick, MA, USA).

The uncertainty of GRNN model prediction is mainly from three sources: input variables, ANN model structure, and model parameters. Here we focused on the uncertainties associated with the model structure because we do not have sufficient knowledge about the uncertainty of input variables. We used the “delete-one” method (Zhuang et al., 2012) through developing a number of alternative ANN models to quantify the uncertainty of GPP and NEE due to uncertain model structures. To be more specific, we randomly selected 75% of the observed data for each ecosystem type to develop a new ANN model. The new model was then scaled up to obtain the new GPP and NEE estimation at the regional scale. The process was repeated for 100 times in S0 and S1 for each ecosystem type, respectively. The averaged GPP and NEE of all estimations were used to analyze the differences among simulations. The 95% confidence intervals were considered to be the range of model uncertainty to define the upper and lower bounds of the GPP and NEE estimation.

2.3 Results

2.3.1 Annual GPP and NEE and spatial difference

The simulated GPP, NEE with the two sets of ANN models were both close to the observed GPP and NEE for each ecosystem type (Fig. 2.3). We applied the two sets of models to calculate the annual averaged GPP and NEE of terrestrial ecosystems for the conterminous US at an 8-day time step from 2001 to 2006 (Fig. 2.4(a), 2.4(c)). Both models showed a high spatial variability with a clear gradient from west to east. The Gulf Coast and parts of the Southeastern US were the most productive regions, with GPP greater than 2000 g C m^{-2} yr^{-1}. Most parts of the Southeast and coastal Pacific Northwest also possessed high GPP (1250-1500 g C m^{-2} yr^{-1}). The Northeast had intermediate GPP (500–1000 g C m^{-2} yr^{-1}), where was mainly dominated by deciduous forest. The Midwest, Southwest and Rocky Mountain areas generally had relatively low GPP (<500 g C m^{-2} yr^{-1}). As for spatial patterns of NEE, the greatest net carbon uptake took place in the Gulf Coast and Mideast, with the annual averaged value of -800 g C m^{-2} yr^{-1}. By contrast, the Rocky Mountain area had the highest contribution to carbon release across the conterminous US. The uncertainty analysis based on the 100 ANN models (Fig. 2.5) demonstrated that our ANNs models predicted GPP and NEE with a small uncertainty across the whole ecosystem type. Overall, both simulations indicated that the East and Pacific Northwest showed high ecosystem productivity, acting as a carbon sink, while the Rocky Mountain region had the lowest GPP value and acted as a carbon source to the atmosphere.

The two simulations however, diverged in regions including the Pacific Northwest coast, Gulf coast and most parts of Southeast dominated by evergreen forests, savannas and mixed forest (Fig. 2.4(b), 2.4(d)). S0 exhibited lower GPP (-200 ~ -100 g C m^{-2} yr^{-1}) and more positive NEE (100 ~ 250 g C m^{-2} yr^{-1}) value in most Southeastern US than that of S1 (Fig. 2.4b). In contrast, west North Central region had higher GPP (100 ~ 200 g C m^{-2} yr^{-1}) and more negative NEE (-150 ~ -

50 g C m^{-2} yr^{-1}) in S0. From the vegetation perspective, the relative difference of GPP and NEE in the mixed forest and cropland showed a spatial variability. Specifically, the lower estimation of GPP in mixed forests and cropland was mainly found in the Southeast and east of South Central, while a higher GPP was observed in the North Central in S0. These patterns were similar to the NEE estimation (Fig. 2.4(d)).

2.3.2 Seasonal GPP and NEE difference

Our 8-day GPP and NEE estimation based on the two ANN models both captured the seasonal flux variability in the conterminous US (Fig.2.6 and Fig.2.7). Take the GPP seasonal pattern, for example; in spring (March to May), the Gulf Coast and the Pacific Northwest region began to assimilate carbon at 100–200 g C m^{-2} yr^{-1}, followed by the Southeast and the South Central. In contrast, most of the Northeast and Rocky Mountain area possessed a low GPP due to the relatively cold weather or late leaf-out. Plants reached the greatest productivity in summer (June–August) with the highest GPP of 300–400 g C m^{-2} yr^{-1} in the Northeast regions. From fall (September–November) to winter (December–February), GPP decreased drastically to either a low level (50–100 g C m^{-2} yr^{-1}) in the Gulf Coast, Pacific Northwest and South Central or nearly zero in most parts of Rocky Mountains throughout the US.

The obvious difference between seasonal GPP and NEE generally occurred in mixed forests and croplands (Fig.2.8 and Fig.2.9). In the early spring (March–April), the mixed forest in the Southeast began to exhibit lower GPP and more positive NEE in S0, and this difference was much stronger from late spring (May) to early fall (September). However, for the mixed forest in North Central and the Northeast, the difference only took place in June, July, and August. And this was similar for cropland in North Central, which only showed higher GPP and more negative

NEE in these three months. No obvious difference was observed between the two simulations in winter.

2.3.3 GPP and NEE response to CO_2concentrationsunder drought condition

Annual GPP and NEE both exhibited positive and negative anomalies each year. The anomalies could have been due to climate variability, disturbances, management practices, or model errors. The severe drought affected over 50% of the country, including the Southwest, the Great Plains, the Gulf Coast, the coastal Southeast, and particularly Texas and Oklahoma. Therefore, we evaluated the GPP and NEE response to the drought condition in 2006. Both models showed negative anomalies in most regions, like the Great Plains (Fig.2.10). However, as for the Southeast and parts of North Central, the S0 exhibited the negative GPP and positive NEE anomalies when compared with S1. According to the US Drought Monitor (http://www.drought.unl.edu) and the PRISM database, these regions showed around 250 mm less precipitation in 2006. Without considering the CO_2 effect in upscaling GPP and NEE, the S1 failed to show the ecosystem response to severe drought condition.

2.4 Discussion

2. 4.1 Comparison of S0 and S1 with other studies

Our estimation of GPP and NEE and their spatial variations agreed well with previous published results. For example, Xiao et al. (2010) estimated that the spatially averaged GPP across the conterminous US scaled at 907 g C m^{-2} yr^{-1}. Our simulation showed that the Gulf Coast and parts of the Southeast were the most productive regions, with GPP greater than 2000 g C m^{-2} yr^{-1}, and was consistent with previous studies (Yang et al., 2007; Xiao et al., 2010; Chen et al., 2011). The total gross carbon uptake estimated in both models was 4.00 and 3.95 Pg yr^{-1}, respectively, and was lower than the results of Xiao et al. (2010) because we did not reclassify the cropland/natural vegetation mosaic in MODIS land cover product as cropland ecosystems. In addition, the estimation of GPP (1250–1500 g C m^{-2} yr^{-1}) in the Southeast was much lower than Xiao's (Xiao et al., 2010) prediction (>2250 g C m^{-2} yr^{-1}), but was comparable with Chen's (Chen et al., 2011) study and the MODIS GPP product (Running et al., 2004). The spatially averaged GPP in two simulations generally agreed well with MODIS GPP (Fig.2.11) (R^2>0.8). However, MODIS GPP (<800 g C m^{-2} yr^{-1}) was markedly underestimated in cropland compared with our models (>1000 g C m^{-2} yr^{-1}). This large difference may be attributable to that MODIS GPP, which was based on the light use efficiency algorithm while ANN was based on the site-level flux tower data. The key parameter, the maximum light use efficiency in the MODIS GPP algorithm, was always underestimated and thus led to lower estimation in high productivity areas (Turner et al., 2006; Xiao et al, 2010).Recently, Madani et al. (2014) used eddy flux carbon data to show that the optimum light use efficiency in cropland was twice as much as that in the MODIS GPP algorithm.

2. 4.2 Climate controls on the CO_2 effects on GPP and NEE

Previous studies have evaluated the interactions between elevated CO_2 and other environmental variables, such as increasing temperature (Peltola et al., 2002; Tingey et al., 2003; Hovenden et al., 2008; Dijkstra et al., 2010) and hydrological conditions (Morgan et al., 2004; Nowak et al., 2004). Increasing CO_2 with enhanced N mineralization at higher temperatures may further promote plant growth (Kirschbaum et al. 1994), whereas the positive effect may be ameliorated in a reduced precipitation environment due to the slow turnover rate of N belowground (Emmett et al., 2004; Sowerby et al., 2008). The seasonal GPP and NEE difference in our simulations also indicated there were interactions between CO_2 effect and climate drivers. Obvious GPP and NEE difference can only been observed from late spring to summer in the Northern forest ecosystem (Fig.2.8 and 2.9), suggesting that the temperature controlling the plant phenology may play a key role in CO_2 effects on the carbon fluxes. In addition, evergreen forest in Pacific Northwest exhibited lower GPP in May and October (Fig.2.8), indicating that drought or the soil water deficit (Law et al., 2000; Schwarz et al., 2004) may impact the CO_2 effects. The seasonal variation of NEE difference was slightly different from GPP (Figs.2.8 and 2.9). NEE differences were shown earlier than GPP in spring, especially in the Northern forest. The enhanced heterotrophic respiration due to soil warming (Raich and Schlesinger, 1992; Lloyd and Taylor, 1994) may result in the asynchronicity of GPP and NEE's response to the atmospheric CO_2 effect.

We analyzed the causes for the spatial variability of GPP difference using annual averaged air temperature (Ta) and vapor pressure deficit (VPD) (Fig. 2.12). We obtained the Ta and VPD from North American Regional Reanalysis dataset (Mesinger et al., 2006). The atmospheric CO_2 concentration showed negative effect on the evergreen forest and the effect was more obvious under high temperature condition (>285 K). Both deciduous forest and shrubland did not show an obvious difference across the Ta and VPD ranges. However, for the mixed forests, the difference

could be divided by the Ta value around 285 K. The GPP estimation in S0 was generally lower when Ta >285 K but higher when Ta <285 K, when compared with S1. This was similar for the cropland; a lower GPP estimation occurred in S0 when Ta >285 K and it had a higher estimation when Ta <285 K. In addition, the negative effect was much stronger in lower VPD ranges (VPD < 600 Pa), indicating that the CO_2 had stronger effect in the humid area. As for the savannas, no obvious Ta threshold was observed and the negative effect generally located in the high Ta range. CO_2 concentration showed complex effect on grassland, but overall, had a small influence on GPP estimation. Figure 5 also gave the statistical values (mean and standard deviation) of the GPP difference between the two simulations in each ecosystem type. Although the spatially averaged GPP difference was generally small (< 50 g C m^{-2} yr^{-1}), the coefficient of variation (the ratio of standard variation to mean value) was great in mixed forest and evergreen forest, followed by cropland and savannas.

2.4.3 GPP and NEE response to atmospheric CO_2 under drought condition

Remote sensing has been widely used to monitor the spatial patterns of drought and its related changes in global ecosystems. Previous studies implemented the vegetation indices (NDVI, NDWI) from Advanced Very High Resolution Radiometer (AVHRR) (Tucker, 1979) and MODIS to detect drought conditions over the Great Plains in the US (Gu et al., 2007), East Asia (Song et al., 2004), and Amazonian forest (Anderson et al., 2010). Due to the lagged response of vegetation to the drought events, these vegetation indices were combined with land surface thermal infrared information to improve drought detection (Singh et al., 2003; Park et al., 2004; Wan et al., 2004; Son et al., 2012). In this study, the negative anomalies of GPP in the Southeast only occur in S0, although both simulations captured the vegetation response to drought events in 2006, especially in the low biomass ecosystem (grassland, shrubland), by exploring the

vegetation indices and thermal information. The spatial pattern of GPP anomalies in S1 was similar with Xiao et al. (2010), which also incorporated MODIS products using the regression tree model. Park et al. (2004) demonstrated that soil water-holding capacity affected the drought detection when using MODIS vegetation indices and thermal information. Gu et al. (2008) also pointed out that the various correlations between MODIS, NDVI, NDWI and drought events were highly dependent on the vegetation structure and soil types. Drought stress with reduced soil moisture can constrain plant nutrient uptake by reducing nutrient supply through mineralization(Emmett et al., 2004; Sowerby et al., 2008, Larsen et al., 2011), also by reducing nutrient diffusion and mass flow in soils (Lamber et al., 2008). Therefore, the induced drought condition may potentially decouple the soil microbial carbon and soil CO_2 fluxes with canopy photosynthesis (Ruehr et al., 2009), increasing the residence of recent assimilated carbonate in vegetation (Deng et al., 1990; Li et al., 2003) and thus affecting the whole ecosystem carbon and nitrogen cycling. Some studies also pointed out the great contribution of drought to the surface CO_2 variability (Knorr et al., 2005; Keppel-Aleks et al., 2014). The climate of the Southeast is predicted to be warmer and drier in future (Dai, 2013). Therefore, incorporating the atmospheric CO_2 concentration into an upscaling practice using the flux site data should improve the qualification of GPP and NEE and strengthen our understanding of vegetation's response to environmental condition.

2.4.4 CO_2 induced uncertainty

CO_2 data used here may result in our estimation uncertainty. First, the gridded CO_2 product was developed using a global inversion model, whose accuracy is highly dependent on the prior CO_2 fluxes (Masarie et al., 2011). In addition, inaccurate weather data in complex terrain also introduces errors by using the transport model (TM5) at coarse spatial resolutions (Geels et al.,

2007). The uncertain CO_2 product may bias our GPP and NEE estimations. To assess the uncertainty of the NOAA CO_2 products, we did a comparison analysis between the 8-daily averaged NOAA gridded CO_2 values and the in-situ CO_2 observation in summer season at seven sites (Fig. 2.13). Generally, the extracted CO_2 seasonal variations from NOAA products were comparable with the CO_2 measurement at forests (Fig. 2.13a, 2.13b and 2.13c) and crop sites (Fig. 2.13g), with the differences ranging from 5 to 15 ppmv. The site-level sensitivity analysis (Fig.2.14) showed that these CO_2 input data differences would change annual GPP by 8 -50 g C (2%-6% relative change) using ANN models. In particular, the GPP changes in the mixed forest and croplands were almost two times larger than in other ecosystems. Despite the uncertainty of the gridded CO_2 product, we used it to gain insight into the effects of CO_2 on regional GPP and NEE prediction when upscaling site-level data. High frequency, stable CO_2 measurements (Andrews et al., 2014) and high-density observation networks (Lauvaux et al., 2012) are needed to accurately quantify the atmospheric CO_2 effects on GPP.

In addition, the simplistic aggregation of CO_2 hour by hour into 8-day averages may bias our quantification without considering the influence of the planetary boundary layer (PBL) development. The PBL depth and turbulence intensity have a strong impact on the vertical and horizontal distribution of CO_2 in the atmosphere (Yi et al., 2001). The covariance between surface fluxes of CO_2 and the atmospheric mixing process has a strong seasonal character (Helliker et al., 2004). Since the rectifier effect influences the horizontal and vertical distributions of CO_2 in the atmosphere, it can bias carbon flux quantification (Denning et al., 1995). We further noted that we have not explicitly differentiated CO_2 fertilization effects and its indirect effects on CO_2 uptake through affecting stomata openness in these ANN simulations. Process-based ecosystem models shall incorporate both fertilization and indirect effects into regional GPP and NEE quantification.

2.5 Conclusion

Two sets of artificial neural networks incorporating remote sensing variables to upscale the AmeriFlux site-level data to the region for seven ecosystem types: one that incorporated CO_2 and a second that did not. Our results showed that both sets of models showed good performance and were able to capture the GPP and NEE variation when compared with previous published results and MODIS products. However, the GPP and NEE difference between two models exhibited a great spatial and seasonal variability, which was closely related with climate drivers (air temperature and vapor pressure deficit). In addition, the simulation without considering CO_2 effects fails to detect the ecosystem response to droughts in the southeastern US in 2006, indicating that drought-induced surface CO_2variation could have more constraint on the regional GPP and NEE qualification. This study is among the first to explore the CO_2 influence on the regional GPP and NEE estimation in upscaling eddy flux data to regional scales.

Table 2-1 Ameriflux Sites used in ANN models

Site Name	Site ID	Vegetation Type	Data range	Site Name	Site ID	Vegetation Type	Data range
ARM SGP Control	US-Arc	GR	2005-2006	Mead Irrigated Rotation	US-Ne2	CP	2001-2005
ARM SGP Main	US-Arm	CP	2003-2006	Metolius Intermediate Pine	Us-Me2	EF	2003,2005
Bartlett Experimental Forest	US-Bar	EF	2004-2005	Metolius Second Young Pine	Us-Me3	EF	2004-2005
Blodgett Forest	US-Blo	EF	2000-2006	Morgan Monroe State Forest	US-MMS	EF	2000-2005
Duke Forest Hardwoods	US-Dk2	MF	2001-2005	Lost Creek	US-Los	SR	2001-2005
Duke Forest Loblolly Pine	US-Dk3	EF	2001-2005	Missouri Ozark	US-MOz	EF	2004-2006
Fermi Agricultural	US-IB1	CP	2005-2006	North Carolina Loblolly Pine	US-NC2	EF	2005-2006
Fermi Prairie	US-IB2	GR	2004-2006	Ohio Oak Openings	US_Oho	EF	2004-2005
Fort Dix	US-Dix	MF	2005-2006	Santa Rita Mesquite Savanna	US-SRM	SA	2004-2006
FreemanRanch Mesquite Juniper	US-FR2	SA	2004-2006	Sky Oak Old	US-SO2	SR	2005-2006
Harvard Forest	US-Ha1	EF	2000-2006	Sky Oak Young	US-SO3	SR	2005-2006
Harvard Forest Hemlock	US-	EF	2004	Sylvania Wilderness	US-Syv	MF	2002-

	Ha2						2006
Howland Forest Main	US-Ho1	EF	2000-2004	Tonzi Ranch	US-Ton	SA	2001-2006
Kendall Grassland	US-Wkg	GR	2004-2006	Univ of Mich Biological Station	USMS	MF	2000-2003
Kennedy Space Center Scrub Oak	US-KS2	SR	2000-2006	Vaira Ranch	US-Var	GR	2001-2006
Mead Rainfed	US-Ne3	CP	2001-2005	Willow Creek	US-Wcr	EF	2000-2006
Mead Irrigated	US-Ne1	CP	2001-2005	Wind River Field Station	US-Wrc	EF	2000-2004
Wisconsin Mature Red Pine	US-Wi4	EF	2002-2005	Wisconsin Intermediate	US-Wi1	EF	2003

*Evergreen needleleaf forest = EF; Deciduous broadleaf forest = DF; Mixed forest = MF; Croplands = CP; Woody Savannas = SA; Grasslands = GR; Shrublands = SR.

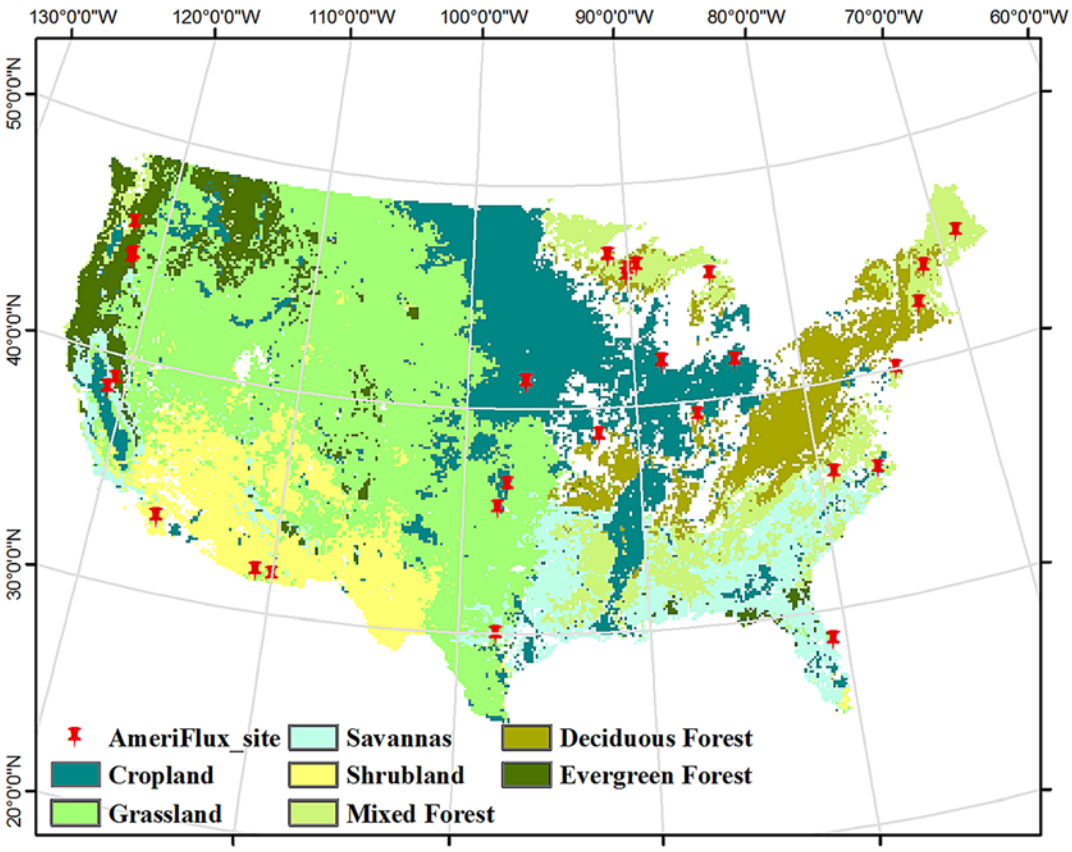

Figure 2.1. Selected AmeriFlux tower sites in this study

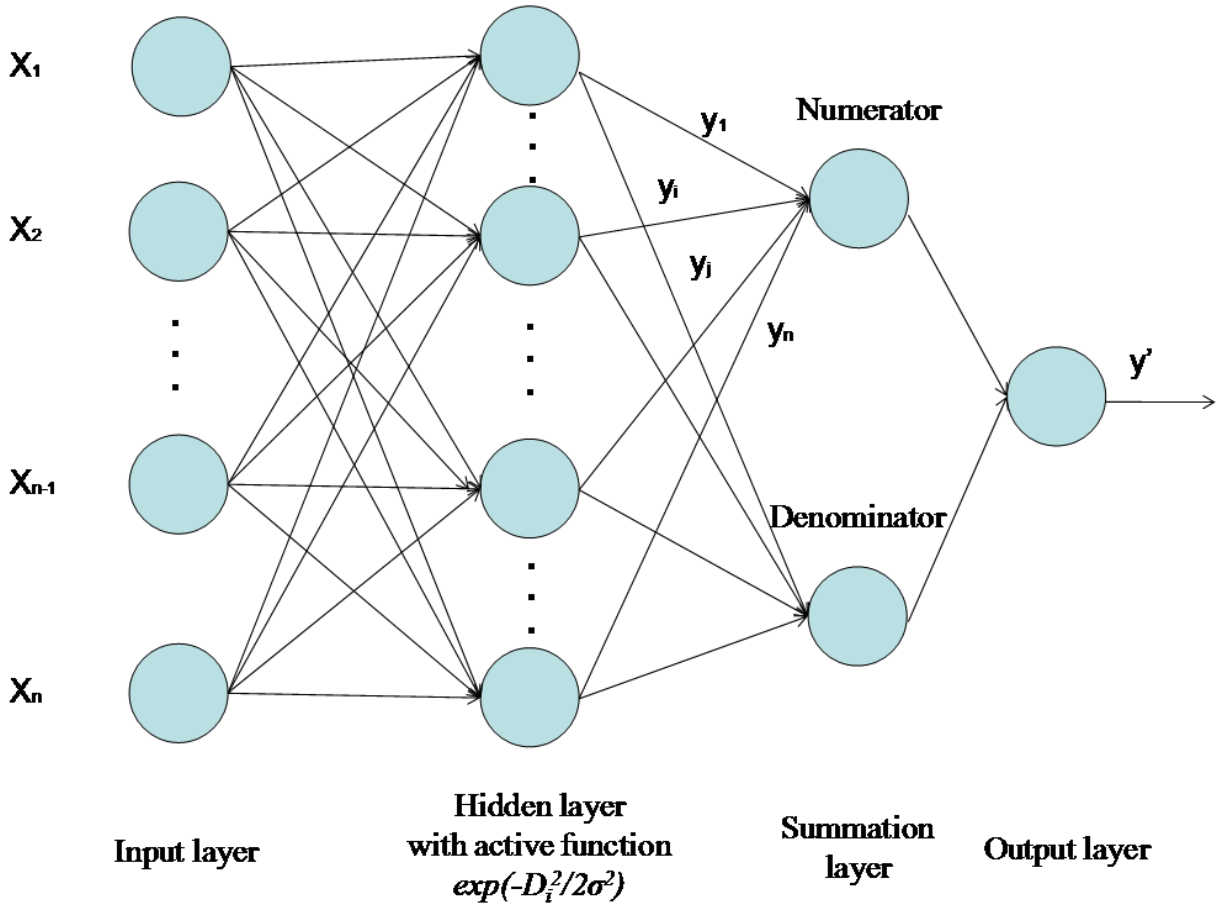

Figure 2.2 Schematic diagram of the generalized regression neural network architecture based on Cigizoglu and Alp (2006)

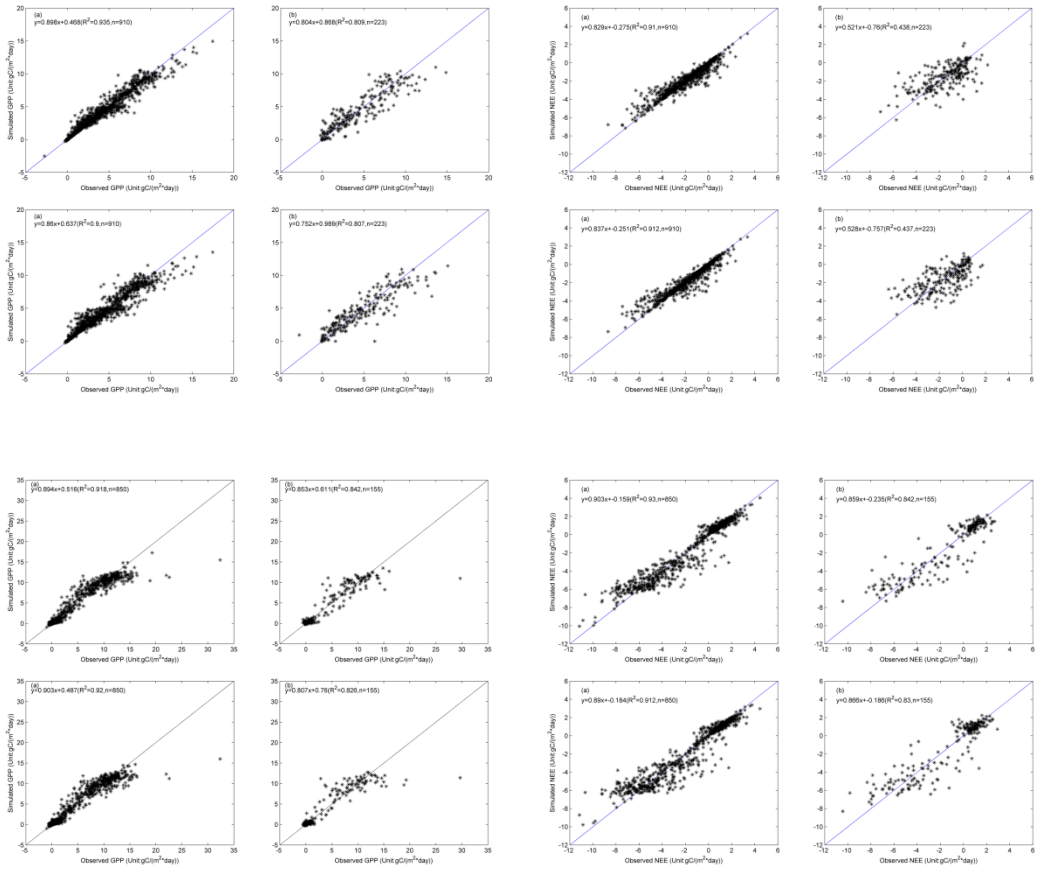

Figure 2.3 Comparisons between the measured and modeled 8-day averaged GPP (left two columns) and NEE (right two columns) at the selected Ameriflux sites for each vegetation type: (a) Evergreen forest (b) Deciduous forest (c) Grassland (d) Mixed forest (e) Savannas (f) Shrubland (g) Croplands. The ANN models (CO_2 incorporated model is at each section's first row, No-CO_2 incorporated model is at the second row)for each vegetation type were constructed based on the training data set (the first and third column), and (b) the validation data set was used to test the performance of the model (the second and fourth column). The blue line is the 1:1 line, and the solid line is the fitted line.

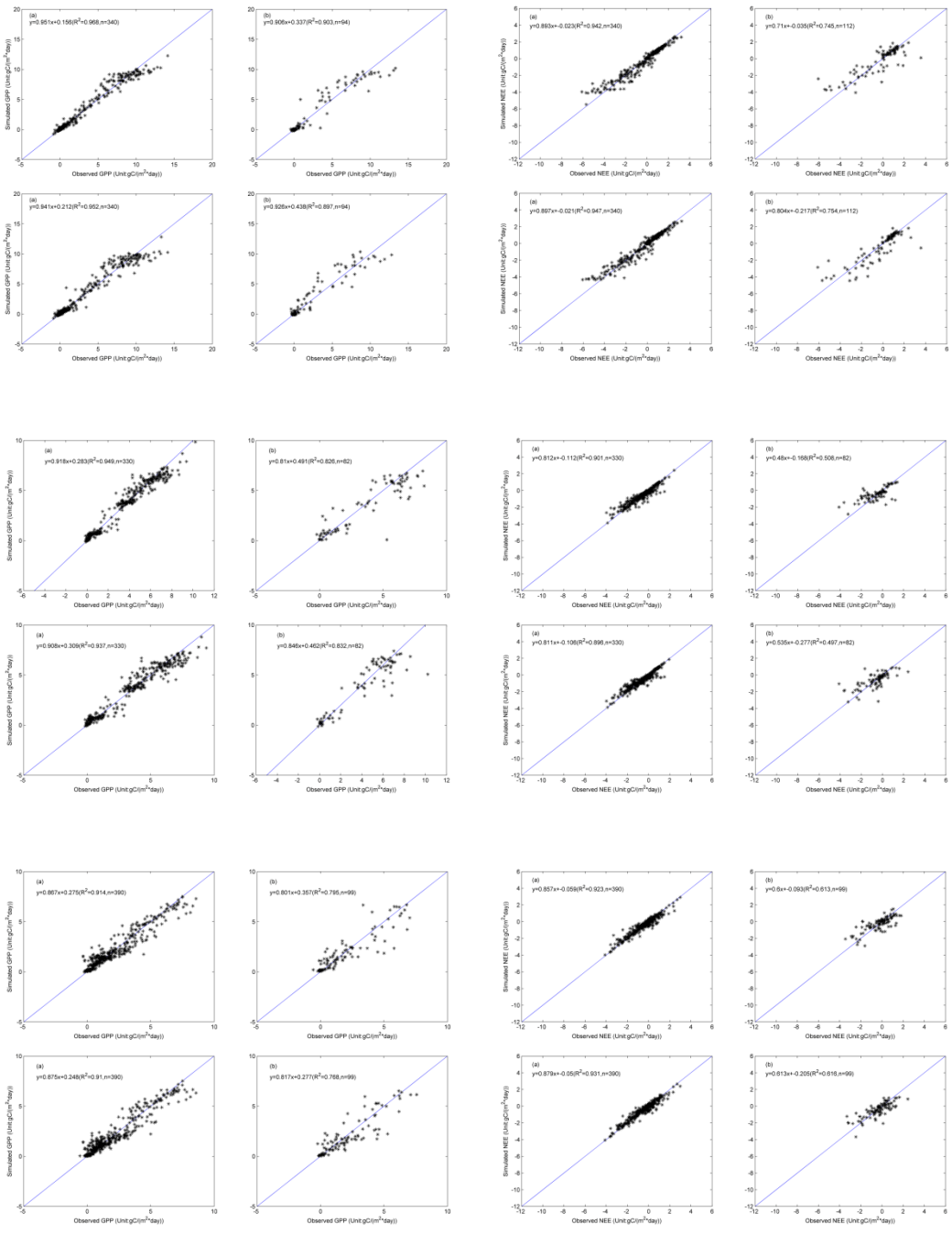

Figure 2.3 continued

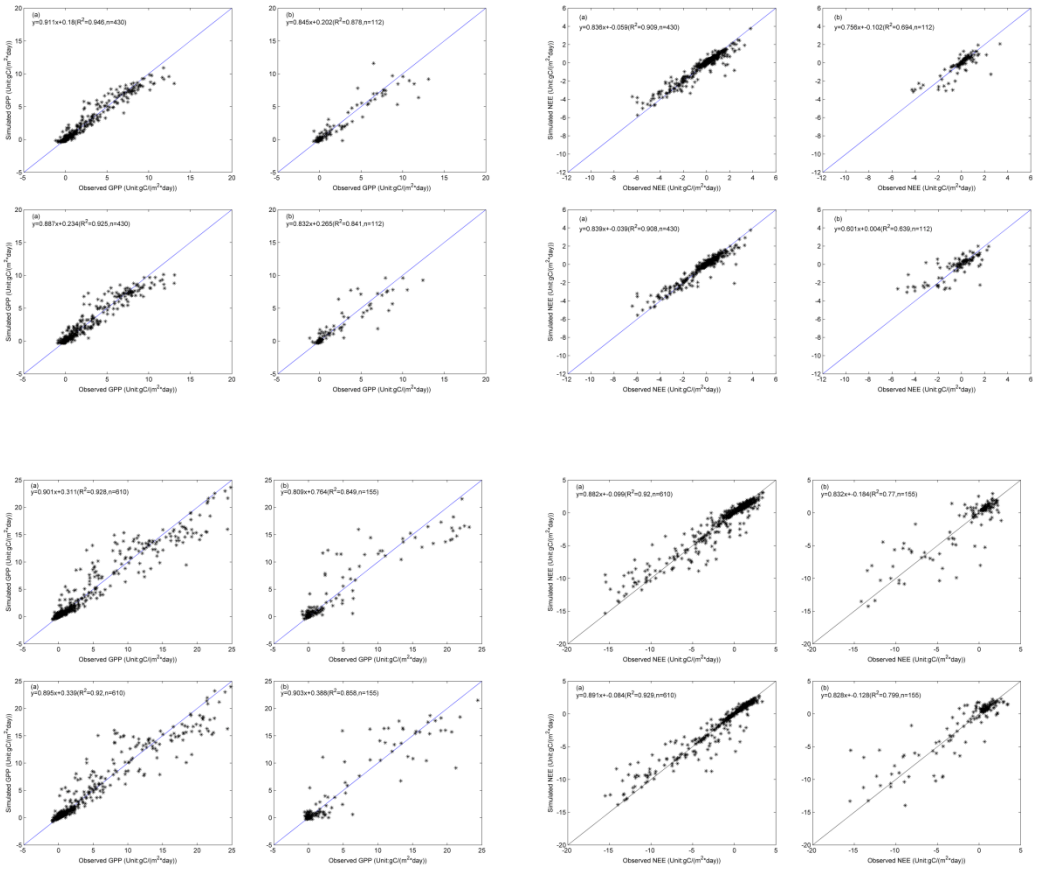

Figure 2.3 continued

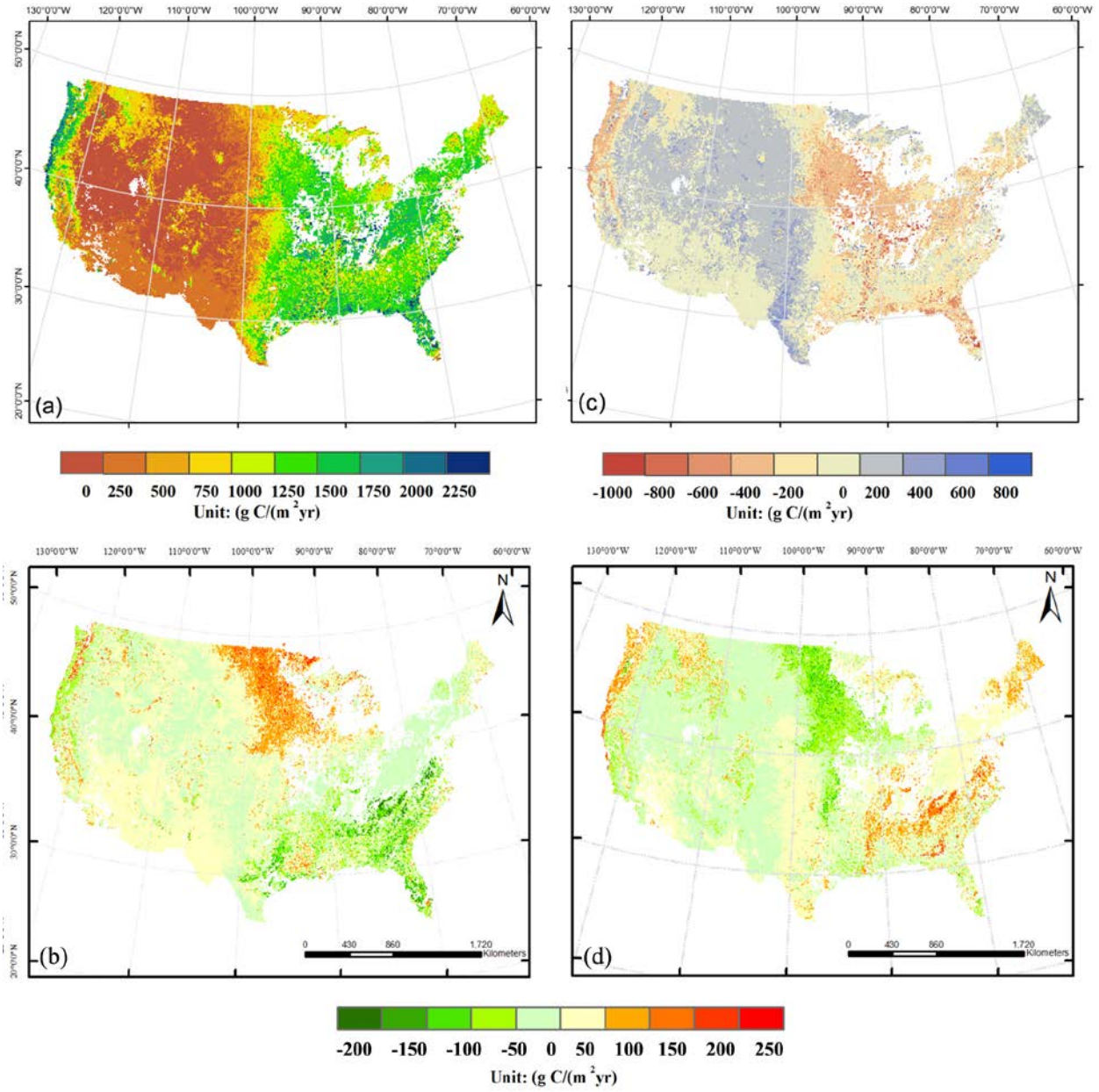

Figure 2.4 Annual averaged GPP (a) and NEE (c) in S0 and their differences (GPP (b), NEE (d)) between S0 and S1across the conterminous US scale from 2001 to 2006 (Unit: g C m^{-2} yr^{-1}). The difference is calculated as S0 minus S1. S0 and S1 are the simulations with and without considering the atmospheric CO_2 concentration, respectively

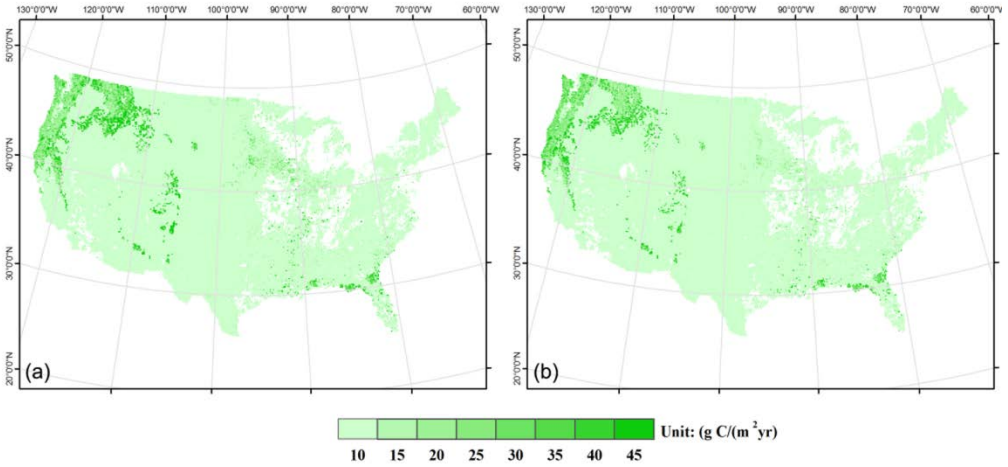

Figure 2.5 Uncertainties of GPP (a) and NEE (b) in S0 across the continental US scale from 2001 to 2006 (Unit: g C m^{-2} yr^{-1}) (The uncertainties in S1 is similar with S0).

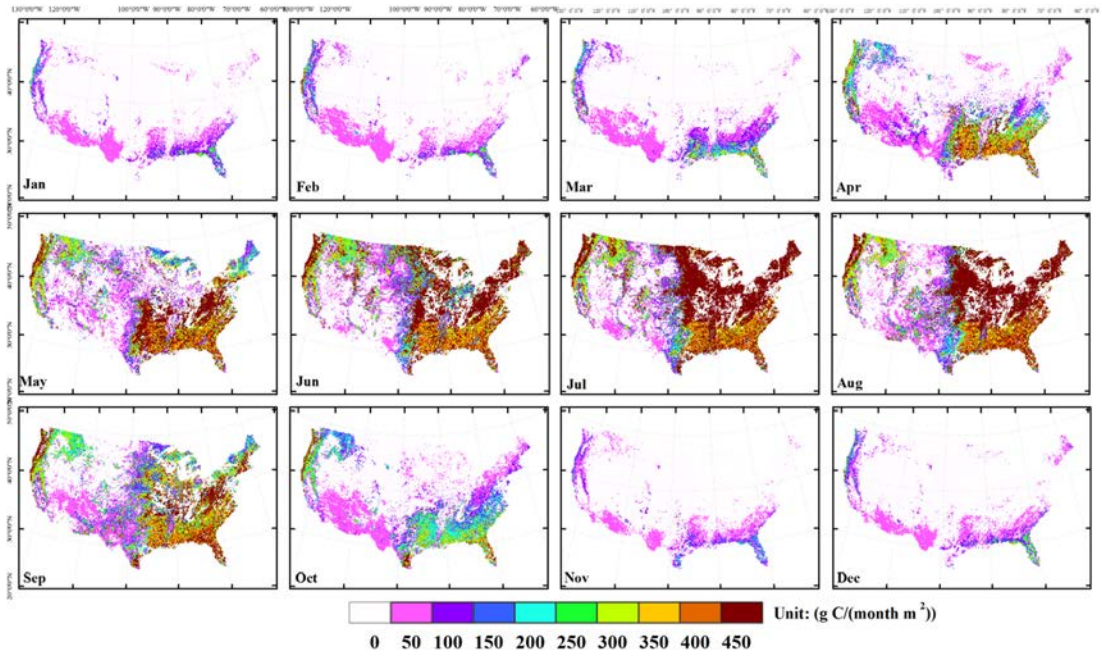

Figure 2.6 Averaged monthly GPP (g C m^{-2} $month^{-1}$) for the conterminous U.S. from January through December from 2001 to 2006 in S0. S0 is the simulation with considering the atmospheric CO_2 concentration.

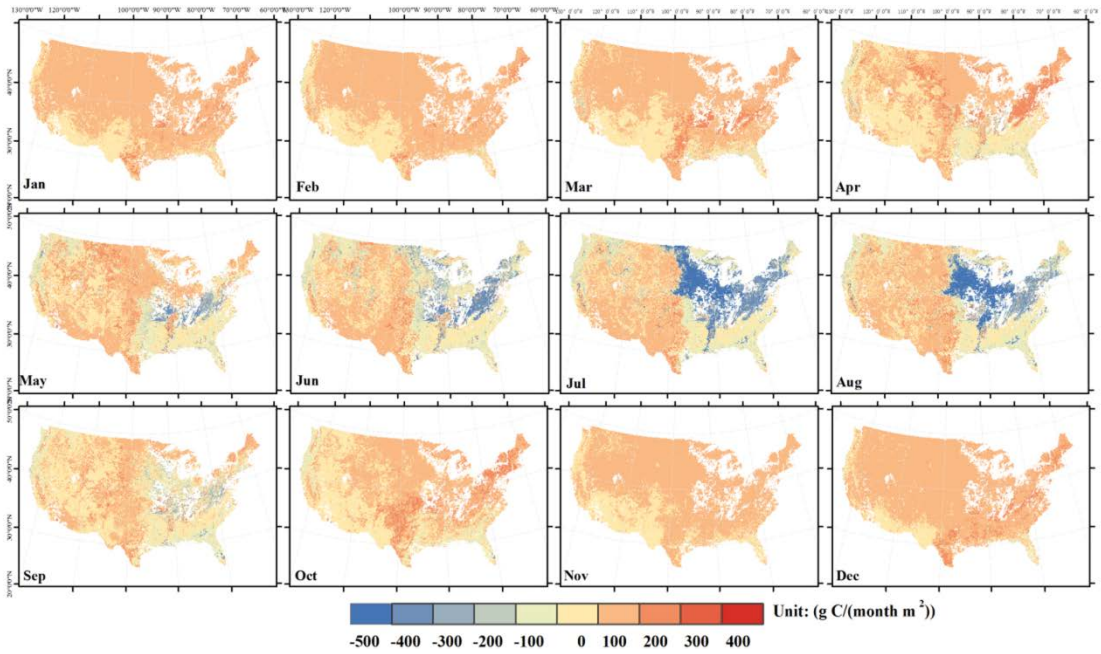

Figure 2.7 Averaged monthly NEE (g C m^{-2} $month^{-1}$) for the conterminous U.S. from January through December from 2001 to 2006.

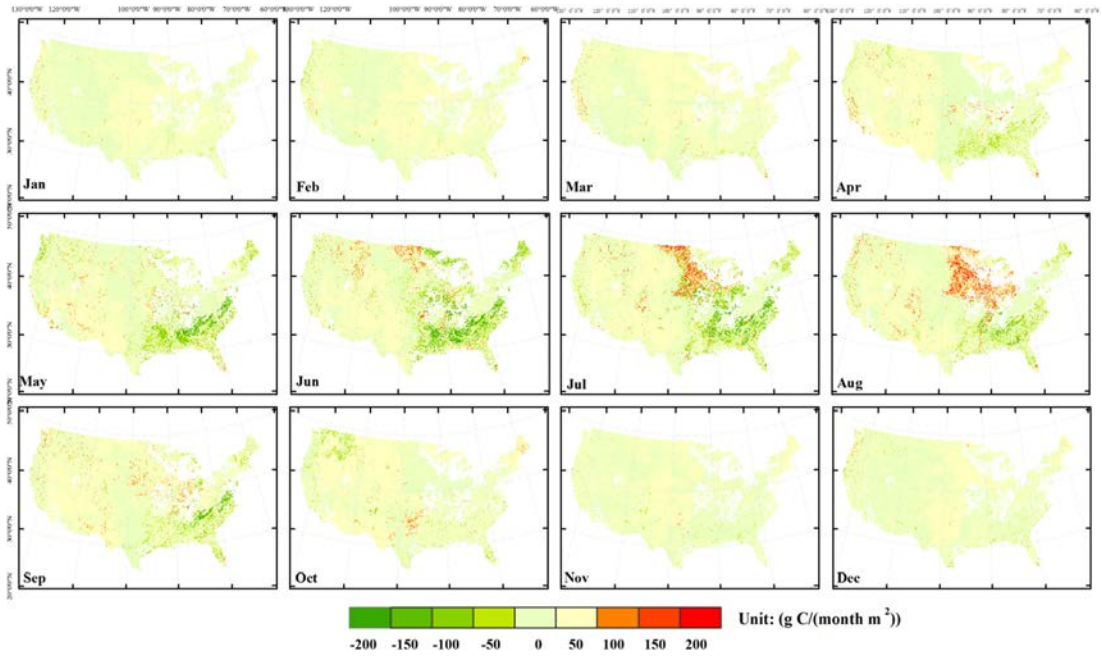

Figure 2.8 Averaged monthly GPP difference (g C m^{-2} $month^{-1}$) between S0 and S1 for the conterminous U.S. from January through December from 2001 to 2006. The difference is calculated as S0 minus S1.S0 and S1 are the simulations with and without considering the atmospheric CO_2 concentration, respectively

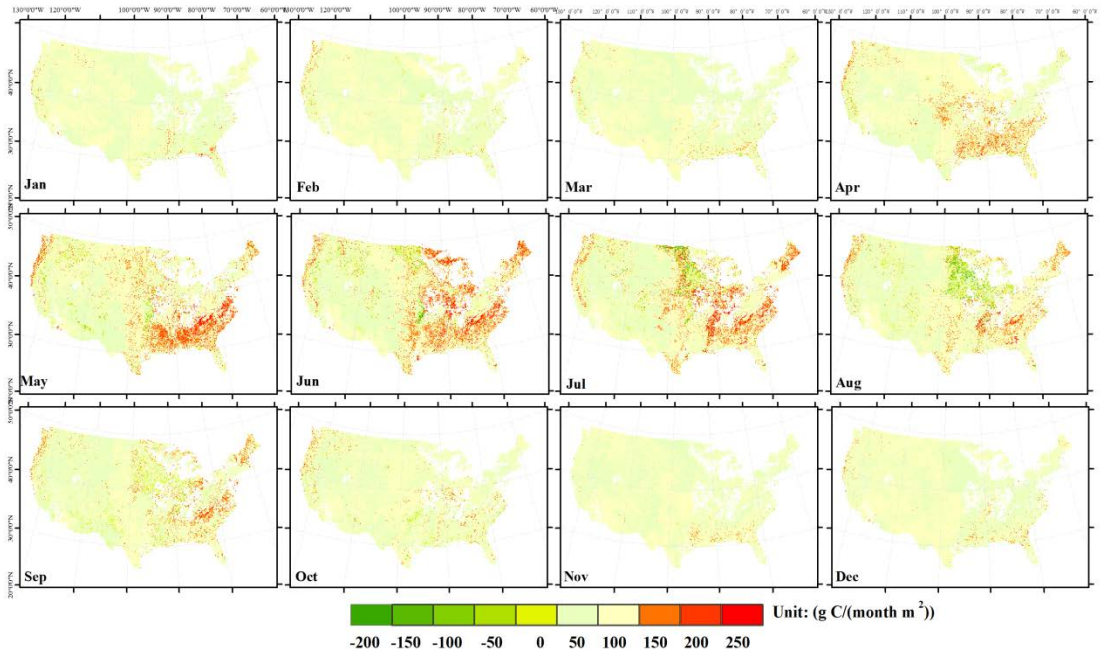

Figure 2.9 Averaged monthly NEE difference (g C m^{-2} $month^{-1}$) between S0 and S1 for the conterminous U.S. from January through December from 2001 to 2006. The difference is calculated as S0 minus S1

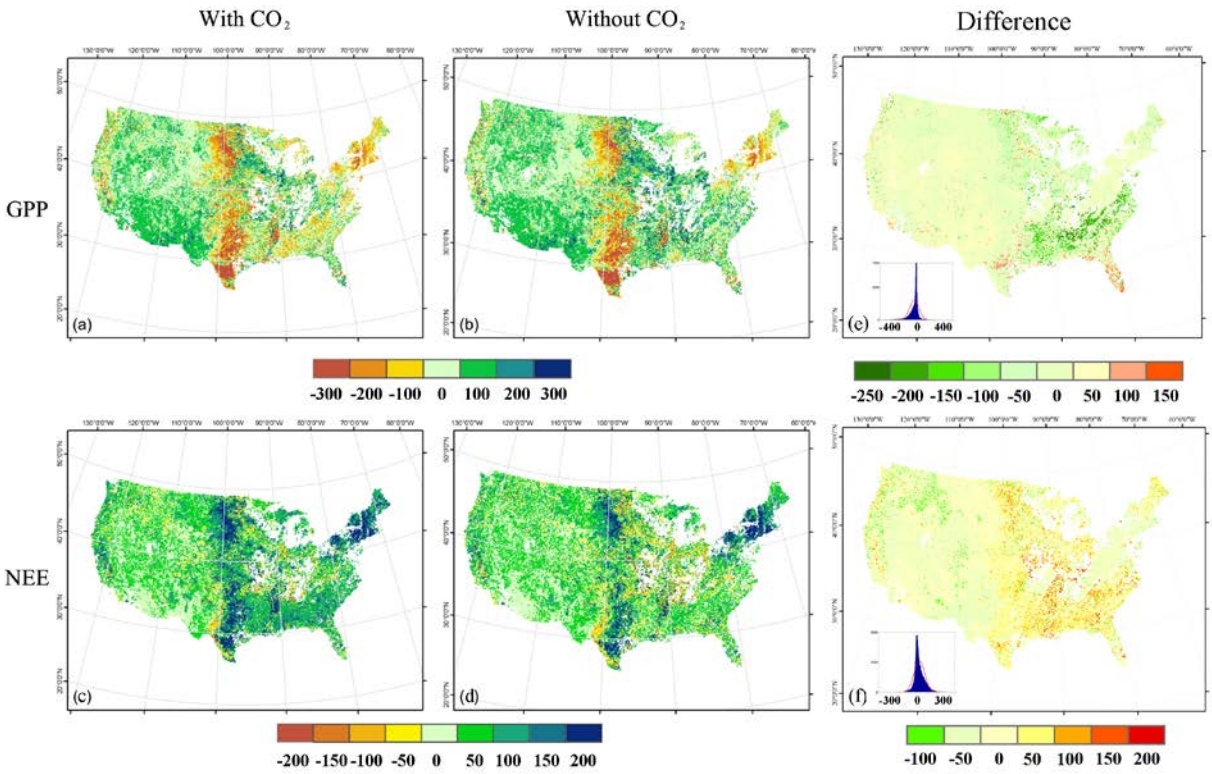

Figure 2.10 Annual GPP (a, b), NEE (c, d), and anomalies in S0 and S1 for the conterminous U.S. at 2006. The anomalies of annual GPP and NEE at 2006 were relative to the 6-year average value. The anomalies difference (e and f) is calculated as S0 minus S1.S0 and S1 are the simulations with and without considering the atmospheric CO_2 concentration, respectively.

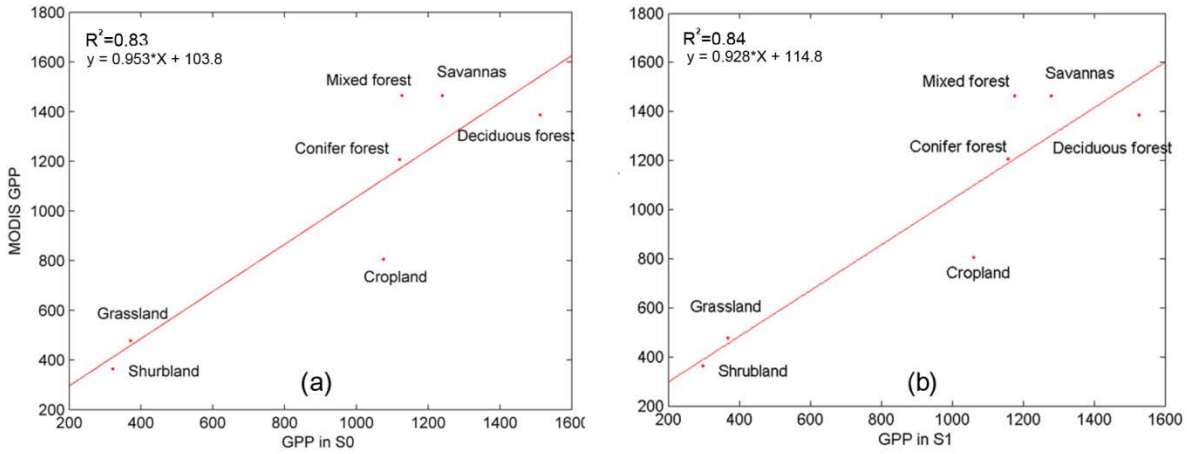

Figure 2.11 Comparison between the annual averaged GPP in S0 (a), S1(b) with MODIS GPP in each vegetation type.

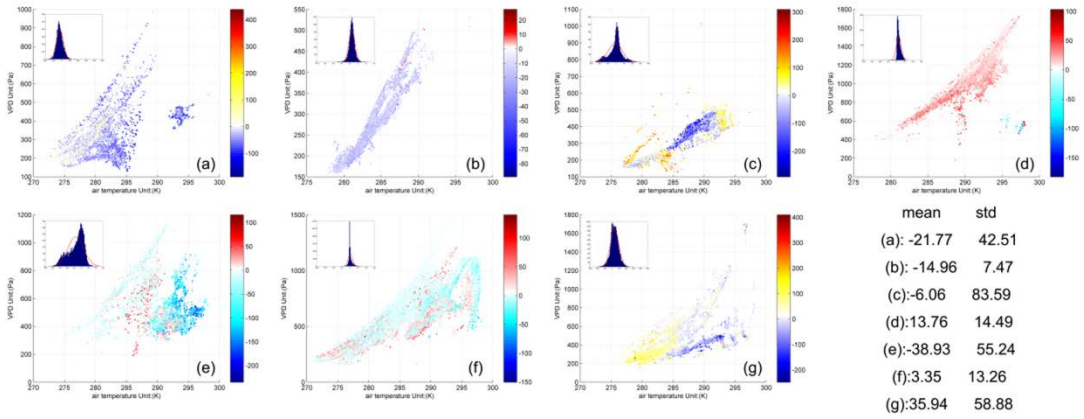

Figure 2.12 Air temperature and VPD controls on the annual GPP difference (the difference is calculated as S0 minus S1) spatial variability for each vegetation type:(a) Evergreen forest; (b) Deciduous forest;(c) Mixed forest; (d) Shrubland; (e) Savannas; (f) Grassland; and (g) Cropland. The mean values and standard deviations of GPP difference in each vegetation types are presented. S0, and S1 are the simulations with and without considering the atmospheric CO_2 concentration, respectively.

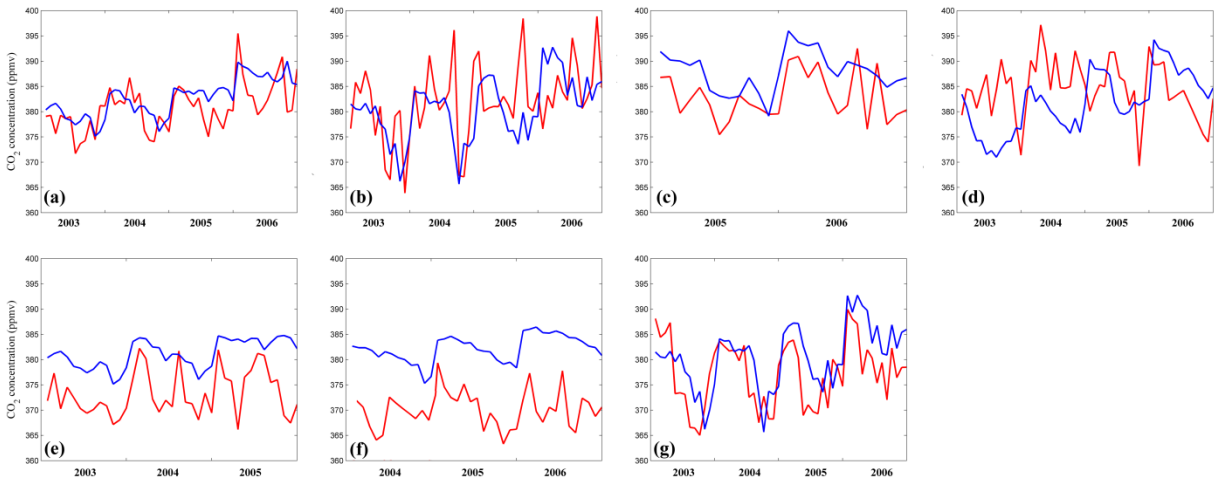

Figure 2.13 Comparison between the 8-day averaged NOAA CO_2 value and the site-level CO_2 observation in summer season at seven sites: (a) Blodgett Forest (evergreen forest), (b) Morgan Monroe State Forest (deciduous forest), (c) Fort Dix (mixed forest), (d) Kenndy Scrub Oak (shrubland), (e) Tonzi Ranch (savannas), (f) Kendall Grassland (grassland), and (g) Mead Irrigated (cropland).

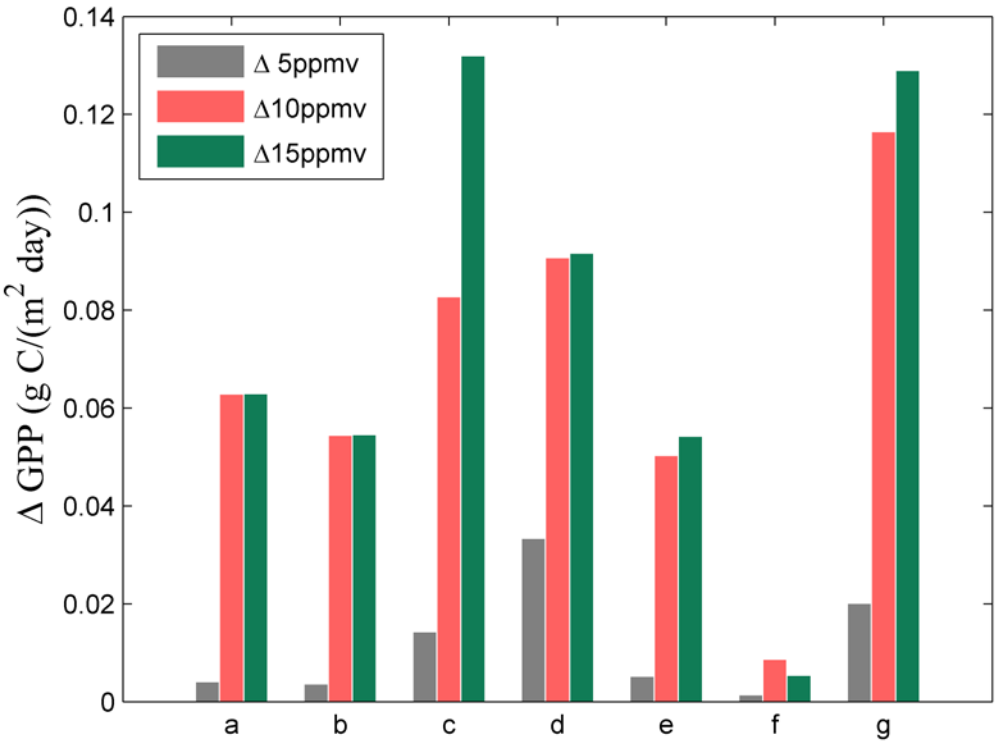

Figure 2.14 The daily GPP sensitivity to the CO_2 input changes (±5 ppmv, ±10 ppmv and ±15 ppmv) at the seven sites: (a) Blodgett Forest (evergreen forest), (b) Morgan Monroe State Forest (deciduous forest), (c) Fort Dix (mixed forest), (d) Kenndy Scrub Oak (shrubland), (e) Tonzi Ranch (savannas), (f) Kendall Grassland (grassland), and (g) Mead Irrigated (cropland). The daily GPP sensitivity in response to the CO_2 input variation is to average the GPP absolute changes (e.g. $\Delta\ GPP_{\pm 5\ ppmv} = (|\Delta\ GPP_{+5\ ppmv}| + |\Delta\ GPP_{-5\ ppmv}|)/2$).

CHAPTER 3 USING LEAF 13C DATA TO CONSTRAIN THE UNCERTAINTY OF THE CARBON DYNAMICS OF TEMPERATE FOREST ECOSYSTEMS

Abstract: Data-model fusion approach is widely used for ecosystem model parameter optimization and uncertainty quantification. The carbon isotope (13C) discrimination by terrestrial plants, involves the biophysical and biogeochemistry processes and exhibits seasonal and spatial variations, which may provide additional constraints on model parameters. In this study, we incorporated three stomatal model schemes (Ball-Berry, Leuning and Optimal) into a process-based land surface model considering the carbon isotope discrimination during photosynthesis. The key model parameters were first calibrated against observation data of gross primary productivity (GPP) and net ecosystem productivity (NEP) with and without the additional foliar 13C composition constraint, respectively. The two sets of parameters were then used for simulating the carbon dynamics of global temperate forest ecosystems. Our results indicated that, without foliar 13C composition constraints, a wide range of parameter values was found to capture in-situ GPP and NEP data with a relatively large regional carbon flux uncertainty. In contrast, using foliar 13C composition data, model parameters were constrained to a relatively narrow space and the site-level model simulations were slightly better than that without the foliar 13C constraint. The model extrapolations with three stomatal schemes all showed that the estimation uncertainties of regional carbon fluxes were reduced by about 40%. Our analysis further demonstrated that the invariant model parameters constrained by in-situ observation flux data combined with additional foliar 13C composition data at a single site were

imperfect. The vegetation and climate dependent parameters across space and time may potentially improve our future quantification of ecosystem carbon dynamics.

3.1 Introduction

Quantification of ecosystem carbon fluxes and their responses to environmental changes would improve our understanding to the carbon cycling and its feedbacks to the atmosphere. Land surface models (LSMs) incorporated with key biophysical and biochemical processes including photosynthesis, respiration, and evapotranspiration are important tools to understanding and predicting carbon exchanges between terrestrial biosphere and the atmosphere (IPCC, 2014). These process-based LSMs contain some parameters to be calibrated. The non-Bayesian calibration methods generally produce a set of optimum parameters, which may be imperfectly or poorly constrained. Tang and Zhuang (2008, 2009) showed that the Terrestrial Ecosystem Model (TEM) calibrated using eddy flux tower data was able to reproduce the observed carbon fluxes with similar accuracies, with very different sets of parameters. Therefore, a proper uncertainty analysis is desirable to provide a confidence range instead of one specific output (Beven, 2001) and it is essential to evaluate how the parameter uncertainty affects model simulations especially for complex ecological models (Keenan et al., 2011; Wang et al., 2009).

To date, the data-fusion approach encompassing model parameter optimization and uncertainty quantification using eddy flux tower-based observation (e.g., carbon and water fluxes) has been widely used for quantifying the land surface processes in response to changing climate. As an important tracer in the biogeochemical process, 13C provides novel insights on how plant physiological, soil biological, physical and chemical processes interact with and affect ecosystem processes, and therefore can be used to constrain the process-based ecosystem models. At regional and global scales, the carbon isotope ratio of atmosphere CO_2 ($13CO_2$) provides an

additional constraint on the carbon budget quantifications as the discrimination by ocean uptake is 10 times lower than that by terrestrial plant photosynthesis (Tans et al., 1993; Ciais et al., 1995). The ratio data also helps to examine the relative contribution of C3 and C4 to total primary productivity (Sage et al., 1999; Griffis et al., 2010). At the local scale, the 13C signal data have been widely used in ecological research as tracers and integrators of how organisms interact with and respond to the environment changes. For example, the variation of plant 13C tissue can improve our understanding on the response of plants to changes in precipitation, vapor pressure deficit (Farquhar and Richards, 1984; Bowling et al., 2002; Diefendorf et al., 2010) and the intrinsic water use efficiency (Saurer et al., 2004; Seibt et al., 2008). In addition, the high-frequency in-situ measurement $13CO_2$ provides a novel tool to partitioning the net ecosystem exchange (NEE) into photosynthesis and respiration (Bowling et al., 2001).

Abundant in-situ foliar 13C measurements have been published and the relationship between the foliar 13C variation and environmental conditions (Marshall et al., 2007), edaphic factors (Arens et al., 2000) and plant attributes (Kaplan et al., 2002) has been well investigated. Consequently, a theoretical equation of carbon isotope discrimination (the offset between atmospheric CO_2 isotope ratio and foliar 13C) in C3 and C4 photosynthesis (Farquhar and Richards, 1984) has been incorporated into some LSMs to calculate plant carbon discrimination (Fung et al., 1997; Suits et al., 2005; Scholze et al., 2008) at different spatial and temporal scales. As for the 13C fractionation process during photosynthesis, the following equation (3.1) is generally used to represent the 13C discrimination in C3 plants:

$$\Delta = a + (b - a) * C_i / C_a \tag{3.1}$$

where a (4.4‰) and b (28‰) are constants representing fractionation due to diffusion and carboxylation, respectively. C_a represents atmospheric CO_2 concentrations (ppmv), C_i represents

the intercellular CO_2 concentration. According to Farquhar photosynthesis formula (Farquhar et al., 1980), the carbon assimilation rate is a function of the intercellular CO_2 concentration, therefore, the in-situ observation of carbon fluxes combined with the measurements of isotopic signal of plant tissues, which integrate all the biophysical and biogeochemical processes, may have good constraints on the parameters related to biophysical and biochemical processes at the canopy scale. To date, very few studies have used the foliar 13C composition data for the LSMs calibration. For example, Aranibar et al (2006) reported the simulations of the temporal variability of canopy-scale C3 photosynthesis carbon isotope discrimination in ISOLSM model and the results showed that measured leaf 13C composition data place an additional constraint on the stomatal conductance.

In this study, we examined if the 13C discrimination during photosynthesis can constrain the key parameters related to the carbon fluxes for a process-based ecosystem model (iTEM; Chen and Zhuang, 2012; Liu et al., 2014, 2016). As the stomatal conductance dominates the exchange of carbon between biosphere and the atmosphere, we especially incorporated three stomatal models (Ball-Berry, Leuning and Optimal) into iTem. In addition, we were also interested in exploring if the invariant model parameters constrained with additional foliar 13C composition data at site level were sufficient for regional simulations.

3. 2 Method

3.2.1 Overview

We chose three stomatal model schemes (Ball-Berry (Ball et al., 1987), Leuning (Leuning 1995) and Optimal (Medlyn et al. 2011)) to be integrated into a process-based ecosystem model iTEM. The key model parameters were first calibrated using forest sites' observation data of gross primary productivity (GPP) and net ecosystem productivity (NEP) with and without the additional foliar 13C composition constraint, respectively. After parameterization, we conducted

the regional carbon estimation for temperate forest ecosystems using two sets of parameters obtained without (S0 simulation) and with additional foliar 13C composition constraint (S1 simulation).

3.2.2 Process-based ecosystem model (iTEM)

In the integrated Terrestrial ecosystem model (iTem), the canopy is modeled with a one-layer, two-big-leaf approach (Dai et al., 2004), which diagnoses energy budget, leaf temperature, evapotranspiration and photosynthesis separately for sunlit and shaded leaves. The boundary layer turbulent processes are modeled based on the Monin-Obukhov Similarity Theory. The hydrological processes include the interception, through fall of precipitation, snow accumulation, sublimation and melt, surface runoff, surface evapotranspiration, water infiltration and redistribution in soil and subsurface drainage. These algorithms allow the model to simulate the response of land surface processes to changing direct and diffuse radiation regimes, such as surface energy balance, thermal dynamics, leaf and canopy conductance, and surface evapotranspiration. In addition, the iTem kept the approach of TEM in modeling ecosystem carbon and nitrogen dynamics and their interactions (Zhuang et al., 2003). Two carbon pools and four nitrogen pools are used to represent carbon and nitrogen storages in a terrestrial ecosystem, including the Vegetation Carbon (VEGC), Soil Organic Carbon (SOC), Vegetation Labile Nitrogen (LABN), Vegetation Structural Nitrogen (STRN), Soil Organic Nitrogen (SON) and Soil Inorganic Nitrogen (AVLN). More details of the iTem are documented in Chen (2013) and Liu et al (2014).

3. 2.3 Stomatal Models

The Ball-Berry model (Ball et al., 1987) is developed based on the observation that stomatal conductance is strongly correlated with assimilation rate. Based on a series of leaf gas exchange experiments, Ball et al. (1987) developed the following empirical expression for (equation 3.2):

$$g_s = g_0 + g_1 * \frac{A * RH}{C_s} \quad (3.2)$$

where g_0 and g_1 are fitted parameters, A is net assimilation rate (μmol m^{-2} s^{-1}), RH is relative humidity at the leaf surface (dimensionless) and C_s is the atmospheric CO_2 concentration at the leaf surface (μmol mol^{-1}).

The Leuning model is an alternative model incorporating an empirical dependence on leaf-to-air vapour pressure deficit (D), a proxy for transpiration, was developed by Leuning (1995). Leuning considered two alternative forms for the dependence on D, a linear and hyperbolic dependence, and found that a hyperbolic dependence provided a better fit to experimental data. The resulting model has the following form (equation 3.3):

$$g_s = g_0 + g_1 * \frac{A}{(C_s - \Gamma)(1 + D / D_0)} \quad (3.3)$$

where Γ is the CO_2 compensation point of assimilation in the presence of dark respiration. This model has three empirically fitted parameters, g_0, g_1 and Γ.

The optimal model is based on the idea that stomata should act to maximize carbon gain (photosynthesis, A) while minimizing water loss (transpiration) (Cowan and Farquhar, 1977). Medlyn et al. (2011) proposed a unified stomatal optimal formulation, which has been shown to correctly capture the responses of stomatal conductance to changing atmospheric CO_2 and environmental conditions (Duursma et al., 2013; De Kauwe et al., 2013) (equation 3.4):

$$g_s = g_0 + 1.6\left(1 + \frac{g_1}{\sqrt{D}}\right)\frac{A}{C_s} \quad (3.4)$$

3.2.4 Foliar 13C composition calculation

As for the 13C discrimination process, we used the following equations to represent the 13C fractionation during photosynthesis:

$$\Delta = a\frac{C_a - C_s}{C_a} + b\frac{C_s - C_i}{C_a} + c\frac{C_i - C_c}{C_a} + d\frac{C_c}{C_a} \quad (3.5)$$

$$C_s = C_a - \frac{A}{g_b};\ C_i = C_s - \frac{A}{g_s};\ C_c = C_i - \frac{A}{g_m} \quad (3.6)$$

$$\delta^{13}C_{leaf} = \delta^{13}C_{atm} - \Delta \quad (3.7)$$

where a (2.9‰), b (4.4‰), c (1.8‰) and d (28.2‰) were constants representing fractionation due to diffusion at the boundary layer, stomotal cavity, CO_2 entering solution and Rubisco CO_2 fixation, respectively. And C_a, C_s, C_i and C_c represented the CO_2 concentration or partial pressure in the air, at the boundary layer, stomata and chloroplasts, respectively. We followed Evans and von Caemmerer (1996), assuming mesophyll conductance (gm) is proportional (4800) to the Rubisco content (Vm). The foliar 13C composition was calculated as the difference between the atmospheric CO_2 ($\delta^{13}C_{atm}$) and discrimination (Δ) during plant photosynthesis. $\delta^{13}C_{atm}$ was assumed as constant (−7.8‰).

To get the annual averaged $\delta^{13}C_{leaf,ann}$, we calculated a seasonal weighted average based on net daily A for the minimum growing period which was taken as the period June–August (Aranibar et al., 2006):

$$\delta^{13}C_{leaf,ann} = \frac{\sum_{d=1}^{n}(\delta^{13}C_{leaf} * A_{net} * d)}{\sum_{d=1}^{n} A_{net} * d} \quad (3.8)$$

where d was the number of days since the start of the growing period and n was the number of days in the growing period.

3.2.5 Data

Model calibrations were conducted at two European flux sites and one Ameriflux site: DETha (Grunwald and Bernhofer, 2007, Conifer forest), ITCol (Valentini et al. 1996, Deciduous forest) and Harvard forest (Goulden et al., 1996, Deciduous forest) (Table.3-1). The site level forcing data including the radiation (direct, diffuse), the initial conditions, soil properties, the plant distribution and vegetation-specific parameters as well as the half-hourly meteorological data were used for model parameterization (http://www.europe-fluxdata.eu/home). The foliar 13C compositions at the two European sites were obtained from the Work Package 5 (WP5, entitled "Isotopic Studies") of CARBOEUROFLUX project (http://www.weizmann.ac.il/EPS/wp5/results.html). We assumed that foliar 13C compositions of leaves collected at the two sites reflected the annual mean photosynthetic discrimination occurring in leaves, under a wide range of environmental conditions (i.e. during and outside of the growing season). Therefore, the model parameters selected should capture foliar 13C measurements. We also used the results derived from a recent improved isotopic flux partitioning method at Harvard forest site (Wehr and Saleska., 2015). The theory of isotopic flux partitioning was extended to include photorespiration, foliar daytime dark respiration and other refinements to obtain the continuous isotopic signatures of net photosynthesis assimilations. Here we assumed that the estimated isotopic composition from Wehr and Saleska (2015) estimation reflected the “true” isotopic fractionation during photosynthesis, and its uncertainty will be discussed later. For following regional simulations, model runs were carried out at a 3-hourly time step for the period 2003-2010, and at a spatial resolution of 1°×1° for the temperate forest region at Northern

Hemisphere. The meteorological data of air temperature, wind speed, radiation, CO_2, precipitation, water vapor concentration and surface air pressure, the initial conditions, soil properties, and the vegetation distribution were from Chen and Zhuang (2014).

3.2.6 Parameterization

The foliar 13C composition collected at two European forest sites were organized into annual mean value, which was different from the foliar 13C composition obtained from Harvard forest site (daily continuous), therefore, two distinct methods were explored for parameterization. For the two European flux sites, we parameterized the iTem with a Bayesian inference method (Tang and Zhuang, 2009). The parameterization method followed the procedures described in Tang and Zhuang (2009). Firstly, 5 key parameters related with the GPP/NEP calculation (Table.3-2) were selected to conduct the parameterization according to our previous sensitivity study (Chen, 2013) and parameterization experiences. To derive the prior parameter sets of iTEM, we first assumed that they followed the uniform distributions within previous specified reasonable ranges either based on literature review or our experience (Chen, 2013). We explored the Monte Carlo simulations by sampling 150,000 sets of parameters using the Latin Hypercube Sampling technique (Iman and Helton, 1988). We then used the sampling importance resampling (SIR) technique to collect 15,000 posterior sets of parameters, which had lower estimation errors compared with observations (Tang and Zhuang, 2009). The 15,000 sets of parameters were divided into 50 levels which were sorted from the highest error level to the lowest. We randomly sampled 50 sets of parameters from each level and used the 50 sets of parameters for site validation and ensemble regional simulations of iTEM to account for the uncertainties of parameterization. As for calibration with foliar 13C composition constraint, we used the measured foliar 13C composition data (Table.3-1) to exclude parts of the 15,000 posterior

parameters, re-dividing the rest of parameters into 50 levels, and then following the steps above. Therefore, after the calibration, we had totally two sets of parameters: one with the GPP and NEP constrained, the other with both GPP and NEP and foliar 13C composition constraint. To test the performance, we ran iTEM with the two sets of parameters for the temperate forests in the Northern Hemisphere.

For Harvard forest site, since the foliar 13C composition derived from Wehr and Saleska (2015) was daily and continuous, we explored the Ensemble Kalman Filter (EnKF), which was an advanced algorithm based on Kalman filter, to optimize iTem model parameters and states variables (e.g., soil organic carbon, vegetation carbon).This method has advantage in considering the uncertainties/errors of observation during the data assimilation process. Here we briefly summarized the EnKF algorithm as follows:

1. Initialization of the model: the state variables (carbon pools and nitrogen pools) were obtained from the flux site, and parameters of iTem were set as the uniform distributions within previous specified reasonable ranges either based on literature review or our experience.

$$Y_{i,k} = \begin{pmatrix} P_{i,k} \\ S_{i,k} \\ Z_{i,k} \end{pmatrix} \tag{3.9}$$

Where $P_{i,k}$ was composed of 5 key parameters in iTem, $S_{i,k}$ representing the model states (carbon and nitrogen pools), $Z_{i,k}$ was composed of the GPP, NEP and foliar 13C composition observations. k was the time step during the assimilation process and i was the ith ensemble member. Here the ensemble size was set as 100.

2. Obtain model forecast: the forecast step of the EnKF propagated the state vector (Y) forward, using parameter values $P_{i,k-1}$ from the previous step and computed $S_{i,k}$ using iTem.

3. Update the model state variable: The vector $Y_{i,k+1}$ was updated with changes in both parameters and $P_{i,k}$ and state variables $S_{i,k}$ by a Kalman gain, which was calculated by minimizing the squared residuals between observations and model forecasts.

Since EnKF had to forecast the model output for *i*times at each time step, we explored the OPENMPI tool to write the above EnKF algorithm as parallel mode to reduce the computation cost.

We assigned the set of parameters derived from Bayesian inference method based on the two European flux sites as P1, and the set of parameters obtained from EnKF and Harvard forest site as P2. P1 was used for extrapolation to whole temperate forest grid cells and P2 was focused on the temperate deciduous forest grid cells only. Therefore, we totally had four simulations: S0-P1, S1-P1 based on Bayesian Inference method and S0-P2, S1-P2 based on EnKF.

3.3 Results

3.3.1 Parameter constrained by foliar 13C composition

For the two European flux sites' calibration using Bayesian Inference method, before using additional foliar 13C composition constraints, although the model evaluation statistics showed that all three models can reproduce the site-level derived daily GPP and NEP reasonably well (Figure 3.1, we did not show the comparison by Lenuning and Optimal models here, as they were similar with Figure 3.1), with the R^2 ranging from 0.36 to 0.69 for all three stomatal models (Table.3-3), the posterior parameters, V_{max25} and the slope of stomatal models (g1) had a relatively wide range space. For example, when iTem was incorporated with Ball-Berry model, V_{max25} and g1 ranged from 120-140 umol CO_2 m^{-2} s^{-1} and 8-11 at conifer forest site (DETha),

respectively. This was similar at the deciduous forest site (ITCol). After further constrained by the measurement of foliar 13C composition at the two sites, it was found that the posterior parameters, V_{max25} and g1, could be narrowed to a relatively small space. Therefore the uncertainties of simulated daily GPP and NEP were significantly reduced (Figure 3.1). At DETha site, without considering the foliar 13C composition constraint, the daily simulated averaged GPP and NEP were 7.32±0.9 g C day^{-1} and 3.32±0.6 g C day^{-1}, respectively, However, if the calibration was further constrained by foliar 13C composition, the uncertainty of daily simulated averaged GPP and NEP were reduced to 0.5 g C day^{-1} and 0.4 g C day^{-1}, respectively. In addition, with the foliar 13C composition additional constraint, the statistical results indicated slightly better daily GPP and NEP comparison with in-situ observations (Table.3-3). It was noted that the ranges of other three parameters, N_{fall}, N_{max} and N_{up}, did not change significantly (Figure 3.2), this may be because: 1) the three parameters were relatively well constrained or 2) the annual flux-weighted average of simulated foliar 13C composition was not sensitive to the three parameters.

For Harvard forest site's parameterization using EnKF, Figure 3.3 showed the time evolution of the 5 key parameters for the growing season. It was found that V_{cmax25} and g1 parameters converged smoothly and uncertainty bounds eventually stabilized, while for other three parameters related with nitrogen processes, the uncertainties range were much larger. It was also found (Figure 3.3) that the 5 posterior parameters were constrained to a narrower space when the continuous daily foliar 13C discrimination data were assimilated into iTem, which was similar with the case using the Bayesian Inference method at the two European forest sites. The final constrained mean value of V_{cmax25} and g1 at Harvard forest site was slightly different from the ITCol site: by using Ball-Berry model scheme, V_{camx25} and g1 had the value about 85 umol CO_2 m^{-2} s^{-1} and 8, while for Harvard site, V_{cmax25} was 5% lower than that in ITCol, while g1 was 5% higher.

3.3.2 Comparison of regional simulation before and after using daily 13C discrimination data

By using Bayesian Inference method, both simulations (S0-P1 and S1-P1) can well capture the spatial GPP and NEP distribution across the temperate forest region in the North Hemisphere (Figure 3.4). Generally, S0 was slightly higher than S1, with the GPP difference ranging from 50-150 g C m^{-2} $year^{-1}$ and NEP difference from 50-100 g C m^{-2} $year^{-1}$, respectively. Lager differences were observed in regions which were characterized of high productivity, such as the Southeast US and East China. Without the foliar 13C composition constraint, the estimated GPP and NEP exhibited a larger uncertainty when compared with the estimation using additional foliar 13C composition constraint, and the spatial difference was obvious in high productivity areas. For example, compared with the standard deviation value around 180 g C m^{-2} $year^{-1}$ in Southeast US in S0, the GPP uncertainty in S1 was reduced to around 130 g C m^{-2} $year^{-1}$. This was similar with the simulations using EnKF at the temperate deciduous forest (S0-P2 and S1-P2) as shown in Figure 3.5.

The uncertainty induced by the wide parameters space also exhibited a strong seasonal variation (Figure 3.6, 3.7; the seasonal variations by S0-P2 and S1-P2 were not shown here, as they were similar with Figure 3.6 and 3.7). For both S0 and S1, the GPP and NEP uncertainty was larger in summer season (from June to Aug), but small in winter (from November to January). This was consistent with the site-level calibration and validation (Figure. 3.2), which showed a relatively larger fluctuation in growing season (Non-growing season was not shown here). It was also noted that the GPP and NEP uncertainties have the most reduction in summer season when iTem uses additional foliar 13C composition constraint. For example, the summer GPP uncertainty in Southeast US was reduced by 30%, from 40 g C m^{-2} $month^{-1}$ to 30 g C m^{-2} $month^{-1}$ and this was similar for NEP (Figure 3.7).

3.4 Discussion

3. 4.1 Parameterization Equifinality

The poorly constrained parameters without the calibration of foliar 13C composition raise the issue of parameters equifinality (Tang and Zhuang, 2008). Earth system models usually consist of multiple computational modules integrating biological, hydrological, and physical processes and also artificially groups of parameters associated with their processes and controls. In our study, most of the parameters in all three stomatal models were poorly constrained (Figure 3.2) when calibrated using the site-level carbon flux. This wide space parameter values introduced large uncertainties to regional carbon dynamics (Figure 3.4, 3.6 and 3.7). But if the calibration was conducted using additional foliar 13C composition constraints, the parameters (V_{max25} and g1) were better constrained with small deviations. Here, we used the coupled stomatal-photosynthesis model scheme (equation 3.10 to 3.12) to address how the foliar 13C composition can have further constraints on relative parameters:

$$g_s = g1\frac{A \times RH}{C_s} + b \tag{3.10}$$

$$A = (C_s - C_i) \times g_s = (C_i - C_c) \times g_m \tag{3.11}$$

$$GPP \sim f(V_{c\,\max}, C_c, ...) \tag{3.12}$$

After the foliar 13C composition constraint, the mean value of Vmax25 increased and g1 decreased at the DETha site (Figure 3.2). Therefore, in equation (3.12) the chloroplasts CO_2 pressure (C_c) should decrease to maintain GPP constant. Also according to equation (3.10), if we assume the boundary layer CO_2 pressure (C_s) is constant, the leaf stomatal conductance g_s decreases (because g1 decreases). The decreasing inter-cellular CO_2 pressure (C_i) and

chloroplasts CO_2 pressure (C_c) combined with the decreasing leaf stomatal conductance g_s and increasing mesophyll conductance g_m can still make the photosynthesis A constant (equation (3. 11)). From the foliar 13C composition aspect, the chloroplasts CO_2 pressure (C_c) is directly related with the discrimination during photosynthesis (the fractionation due to Rubisco CO_2 fixation is much larger than other fractionation processes). Therefore, the additional constraint foliar 13C composition can help reduce model parameters space and then the consequent regional estimation's uncertainty. Aranibar et al., (2006) also showed that the slope of stomatal model can be further constrained by comparing with measured foliar 13C composition at a needleaf forest site given a wide range of parameters in the ISOLSM model.

3.4.2 The g1 parameter issue

Current earth system models generally assume the slope of stomatal function, g1, is constant across all plant function types, without considering the possible differences under different climatic conditions or between vegetation types, although Ball (Ball et al., 1987) and Lin (Lin et al., 2015) indicated a large variation between different species. Here, we used previous derived parameters (Figure 3.2) from DETha and ITCol sites to validate the other eddy flux towers (Table 3-4). Generally, the simulated foliar 13C compositions had relatively large deviations from the observation (Figure 3.8). This indicates that the single site-level derived parameters may not be suitable for other sites. We also explored the Bayesian Inference method to re-constrain the parameters at these sites (Table 3.3). Our results indicate that the slopes of stomatal function (g1) were both significantly correlated with the annual average precipitation (Figure 3.9). The climate-related model parameters (slope of stomatal function) also support that spatially and temporally g1 variations may potentially improve the model estimation. De Kauwe et al. (2015) predicted the g1 parameters depending on environmental conditions and plant traits and incorporated the

spatially explicit g1 into the CABLE LSM at the global scale. Although we constrained g1 at only two sites and treated it as constant in the regional extrapolation, insights from De Kauwe et al. (2015) may improve the spatial and temporal g1 in future studies.

3.4.3 The choice of stomatal model

Previous studies have evaluated the response of different stomatal functions to environmental conditions using 13C signals. Ballantyne et al (2011) compared the simulated isotope composition of CO_2 using the Simple integrated Biosphere2 (SiB2) with in-situ atmosphere $13CO_2$ measurement to evaluate Ball-Berry and Lenuing model schemes. Bodin et al (2013) incorporated the three stomatal models into a LSM to simulate the carbon isotope ratio of tree leaves (δ13Cleaf) and tree rings (δ13Cstem) over a period of 53 years, and comparing the results with carbon isotope ratios obtained from measured at six sites in northern Europe. Although our study here is not to evaluate the three stomatal models' performance, it is still useful to compare their responses to environmental conditions. Here, we only tested the sensitivity of stomatal conductance and internal CO_2 partial pressure to the VPD variation. The environmental conditions (e.g., ambient temperature) and the corresponding parameters were documented in Table 3-5. The g1 parameter in the Ball-Berry model was set to a common value of 9 for C3 plants according to Collatz et al. (1992), which was in accordance to other land surface models. The g1 parameters in Leuning and Optimal models were derived from the Leuning (1995) and De Kauwe et al. (2015), respectively. The VPD-sensitivity parameter D0 in the Leuning model was set to 1.5 Kpa (Leuning 1995). The minimal conductance parameter g0 was kept constant at a value of 2000 umol m^{-2} s^{-1} (Leuning 1990). Figure 3.10 showed the stomatal response functions to VPD for all models using the Table 3-5 environmental conditions and parameters. All models exhibited a decreasing stomatal conductance and internal CO_2 partial pressure as VPD increased,

but the results differed in their sensitivity to VPD. As for the stomatal conductance, the Ball-Berry and Leuning models showed a linear response to VPD, and the sensitivity was larger than the Optimal model. As for the internal CO_2 partial pressure, the Leuning and Optimal showed a linear response and low sensitivity in response to VPD compared with the Ball-Berry model. There are relatively large discrepancies of estimated stomatal conductance as well as the intercellular CO_2 concentration among the three stomatal models when there was a large VPD value (>1100 Pa). Although no significant GPP and NEP differences were found in the site-level calibration, validation and regional estimation, this simple test indicated that the three models may exhibit different physiological behaviors and carbon and water fluxes (13C fractionation) under certain climate conditions (e.g., drought).

3.4 Conclusion

This study calibrated the model using the observed carbon flux data at two forest sites with and without using additional foliar 13C composition constraints, respectively. Our results indicate that a wide range of parameter values were found to be capable to capture the observation, resulting in relatively large regional carbon flux uncertainties. However, with the additional observed foliar 13C discrimination constraint, site-level comparisons showed that the model has a better performance compared with the parameterization without foliar 13C discrimination constraints, all three stomatal models also showed that the estimation uncertainties of regional carbon fluxes were reduced by about 40%. Our results further demonstrated that the invariant model parameters constrained by observation with additional foliar 13C composition from one site may still not be applicable to other sites, the vegetation- and climate-varied parameterization is necessary to improve future model estimation.

Table 3-1 The sites used for foliar 13C constraint

Site Name	Location	Vegetation Type	period	Reference
DETha	47.38 °N, 8.37 °E	ENF	2001-2002	Grunwald and Bernhofer, (2007)
ITCol	41.84 °N, 13.58 °E	DBF	2001-2002	Valentini et al., (1996)
Harvard	42.53 °N,72.17 ° W	DBF	2010	Goulden et al., (1996)

*ENF: evergreen needleaf forest; DBF: deciduous broadleaf forest.

Table 3-2 Key iTEM Parameters related with GPP/NEP calculation

Pameter	Unit	Definition	Prior range
V_{cmax25}	umol CO_2 m^{-2} s^{-1}	maximum carboxylation rate at 25 C	[10 150]
N_{fall}	g C m^{-2} s^{-1}	litter fall rates of N	[1 100]*1e-8
N_{max}	g N m^{-2} s^{-1}	rate of N uptake	[1 100]*1e-7
N_{up}	g g^{-1}	amount of N immobilized per unit of detrital C respired	[0 0.5]
g1	/	empirical coefficient for the sensitivity of stomatal conductance to photosynthesis, CO_2 concentration and relative humidity	[1 18]

Table 3-3 Statistical results of calibration at DETha and CHLae sites using Ball-Berry stomatal model

Model	Parameterization scheme	Site				
		Flux	DETha		ITCol	
			R^2	RMSE	R^2	RMSE
Ball-Berry	Before foliar ^{13}C composition constraint	GPP	0.41	2.5	0.58	1.8
		NEP	0.38	1.3	0.48	1.0
	After foliar ^{13}C composition constraint	GPP	0.48	2.1	0.61	1.6
		NEP	0.44	1.1	0.51	0.9
Lenuning	Before foliar ^{13}C composition constraint	GPP	0.42	2.5	0.60	1.7
		NEP	0.39	1.4	0.50	0.9
	After foliar ^{13}C composition constraint	GPP	0.48	2.0	0.61	1.6
		NEP	0.43	1.2	0.51	0.9
Optimal	Before foliar ^{13}C composition constraint	GPP	0.39	2.8	0.59	1.8
		NEP	0.32	1.5	0.49	1.1
	After foliar ^{13}C composition constraint	GPP	0.43	2.3	0.60	1.7
		NEP	0.36	1.2	0.50	1.0

*The units for RMSE are g C day^{-1}

Table 3-4 Eddy covariance sites used for comparison in Figure. 3.8

Site Name	Location	Vegetation Type	period	Reference
BEBra	51.30 °N, 4.52°E	MF	2001-2002	De Pury and Ceulemans. (1997)
DEHai	51.07 °N 10.45°E	ENF	2001-2002	Knohl et al. (2003)
DETha	47.38 °N, 8.37 °E	ENF	2001-2002	Bernhofer et al.(2003)
CHLae	47.47°N 8.35°E	MF	2001-2002	Gentsch et al. (2014)
ITNon	44.69 °N 11.09°E	MF	2001-2002	Nardino et al. (2002)
CZBK1	49.50 °N, 18.53°E	ENF	2001-2002	Reichstein et al. (2005)
ITCol	41.84 °N, 13.58 °E	DBF	2001-2002	Valentini et al. (1996)

Table 3-5 Environmental conditions and parameters used in Figure. 3.10

Driving data	Ta	APAR	C_a	VPD	V_m	r_b
	25	300	380	0.5~1.3	60	20
Stomatal Model		Ball-Berry		Leuning		Optimal
Parameters	B	m	D_0	g1	g1	g0
	2000	10	1	9	3.7	2000

*Ta: ambient temperature (℃); APAR: absorbed photosynthetically radiation (W m^{-2}); Ca: ambient CO_2 concentration (ppmv); Vm: maximum carboxylation rate (umol m^{-2} s^{-1}); rb: boundary layer resistance (s/m); m: empirical coefficient for the sensitivity of stomatal conductance to photosynthesis, CO_2 concentration and relative humidity in Ball-Berry model; b: minimum stomatal conductance to water vapor at the light compensation point in Ball-Berry model (umol m^{-2} s^{-1});

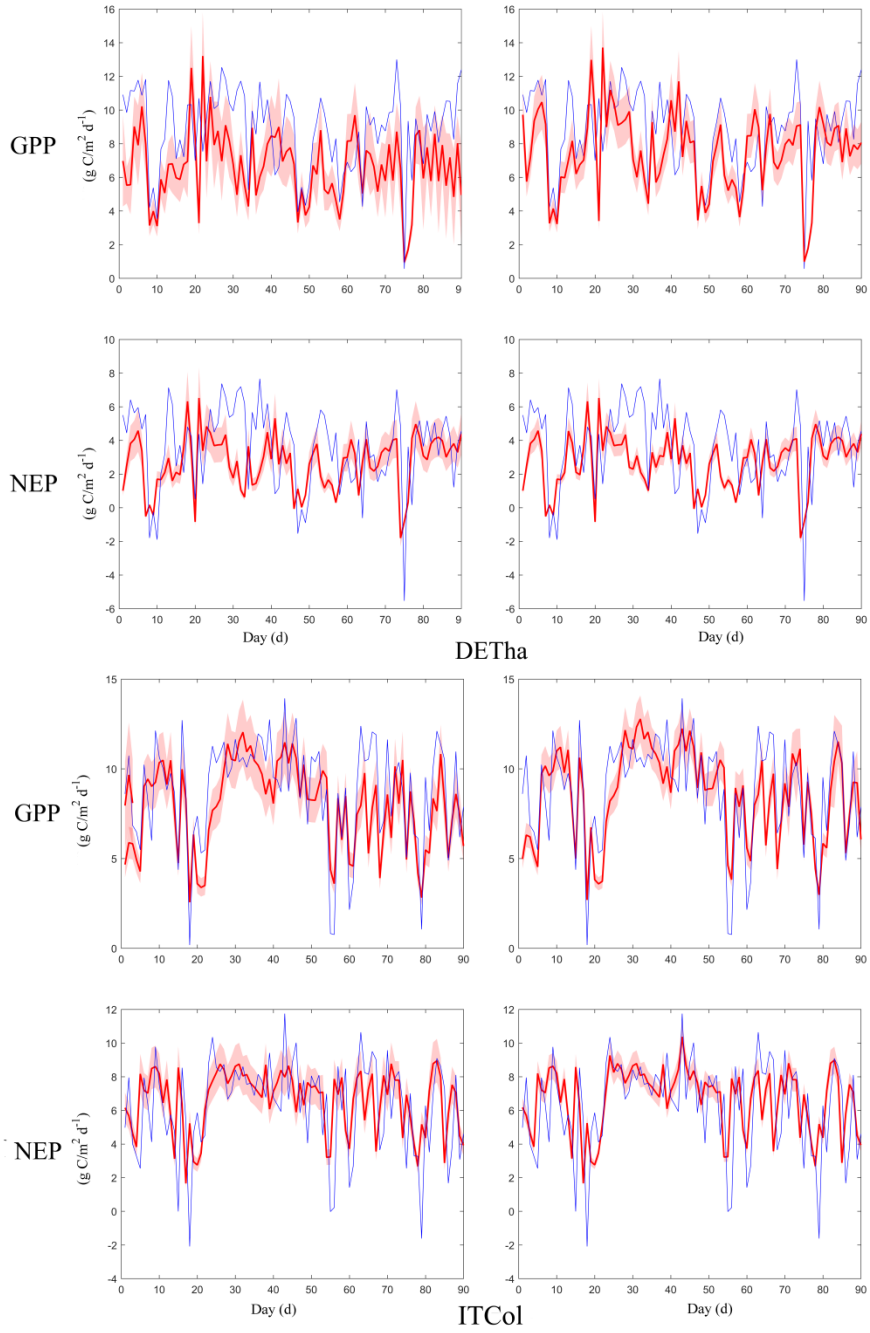

Figure 3.1 Comparison between daily GPP/NEP simulation and GPP/NEP observation (growing season, from May to August) before (leaf column) and after (right column) foliar ^{13}C composition constraint by using Ball-Berry stomatal model at DETha, ITCol site at 2002.

Before foliar ^{13}C

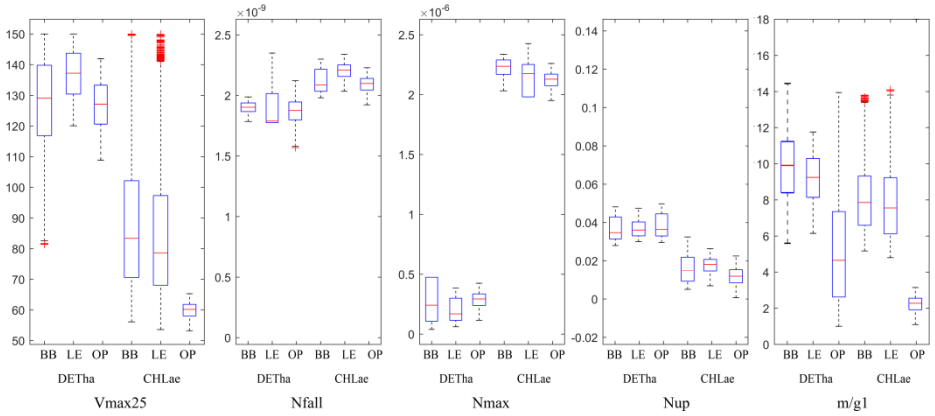

After foliar ^{13}C composition

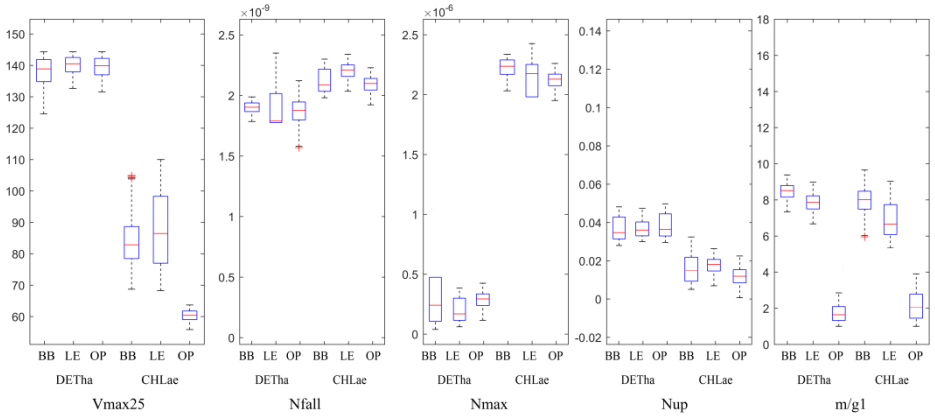

Figure 3.2 Boxplot of parameter posterior distribution that are obtained after ensemble inverse modeling for iTem at the two sites. BB, LE and OP indicate the Ball-Berry, Leuning and Optimal stomatal models, respectively. More details on the parameter description in the figure refer to Table 2.

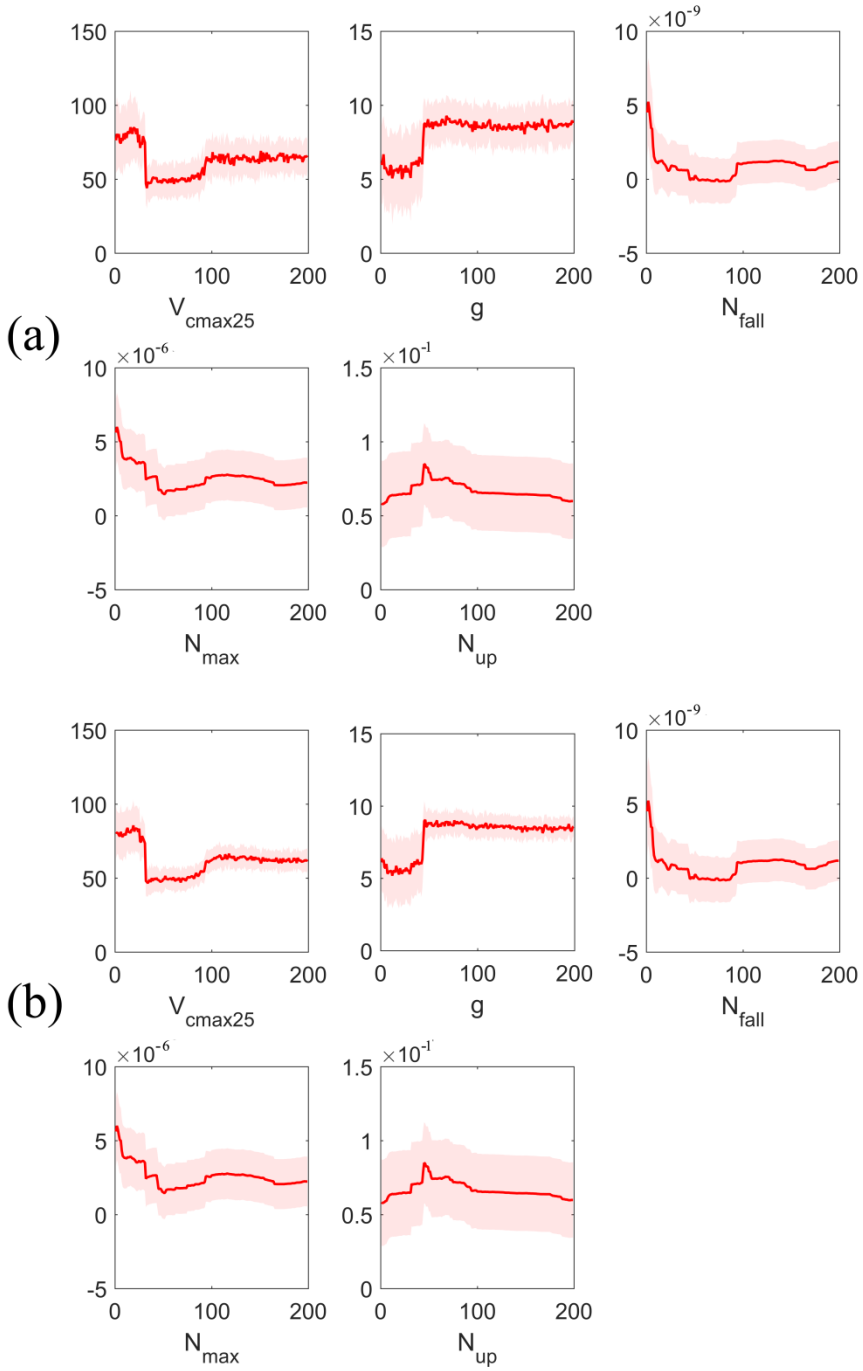

Figure 3.3 The evolution of five parameters in iTEM constrained by both GPP, NEP and isotopic signatures of net photosynthetic assimilation using Ensemble Kalman Filter (data from Wehr and Saleska 2015).

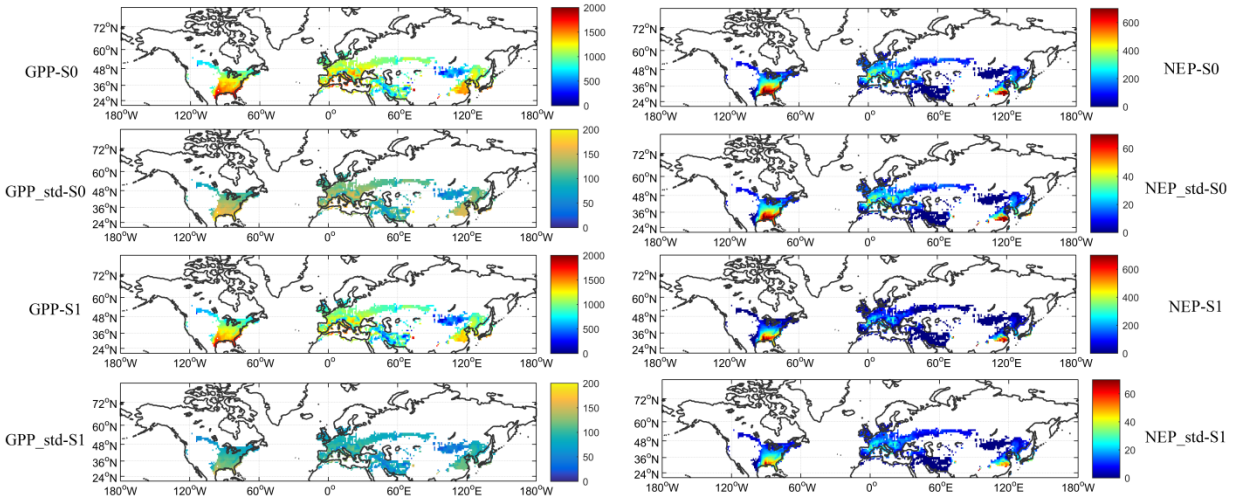

Figure 3.4 GPP/NEP estimation and its uncertainty by using Ball-Berry stomatal model in S0-P1 and S1-P1 at temperate forest region. S0, S1 stand for the estimation without and with foliar 13C discrimination constraint (Units: g C m^{-2} $year^{-1}$).

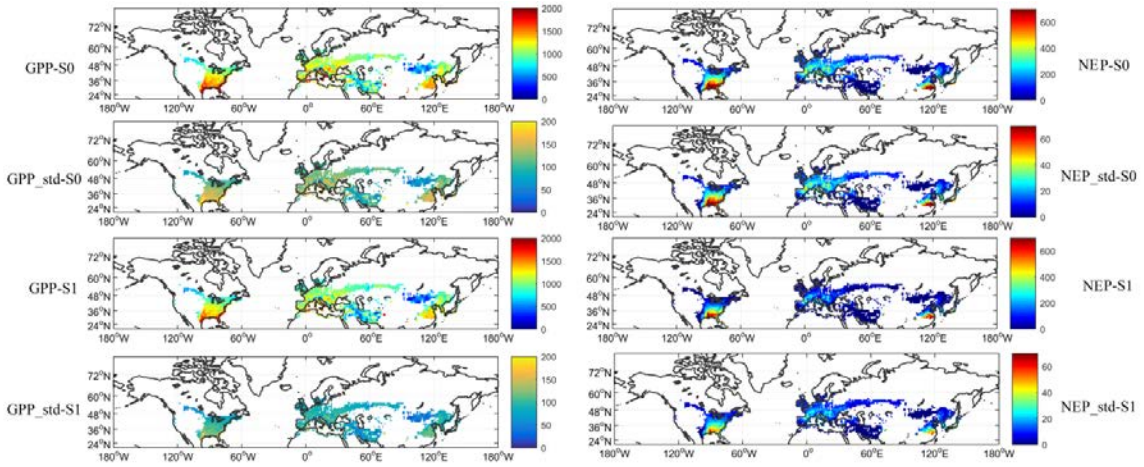

Figure 3.5 The seasonal uncertainty of GPP by using Ball-Berry stomatal model in S0-P2 and S1-P2 at temperate forest region. S0-P2, S1-P2 stand for the estimation without and with foliar 13C discrimination constraint using Ensemble Kalman Filter (Units: g C m^{-2} $month^{-1}$)

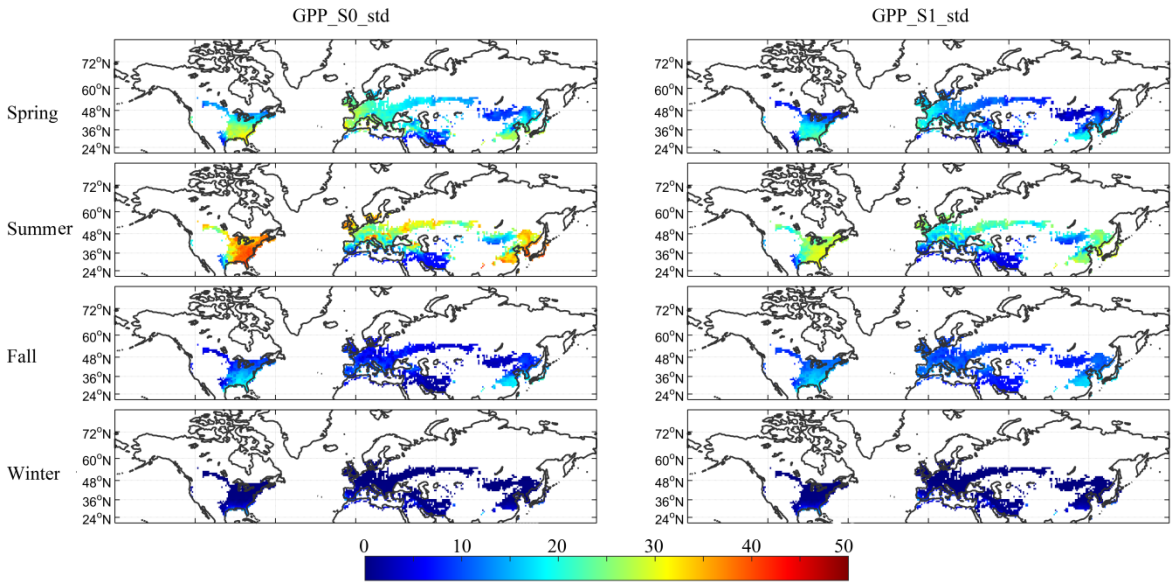

Figure 3.6 The seasonal uncertainty of GPP by using Ball-Berry stomatal model in S0-P1 and S1-P1 at temperate forest region. S0, S1 stand for the estimation without and with foliar 13C discrimination constraint (Units: g C m^{-2} $month^{-1}$).

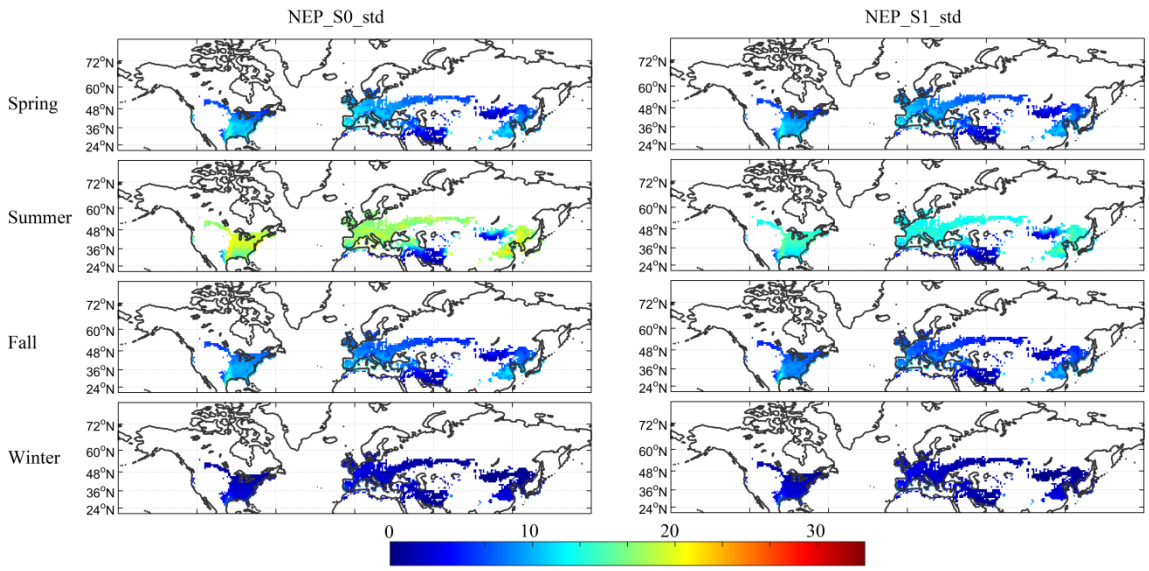

Figure 3.7 The seasonal uncertainty of NEP by using Ball-Berry stomatal model in S0-P1 and S1-P1 at temperate forest region. S0, S1 stand for the estimation without and with foliar 13C discrimination constraint (Units: g C m^{-2} $month^{-1}$).

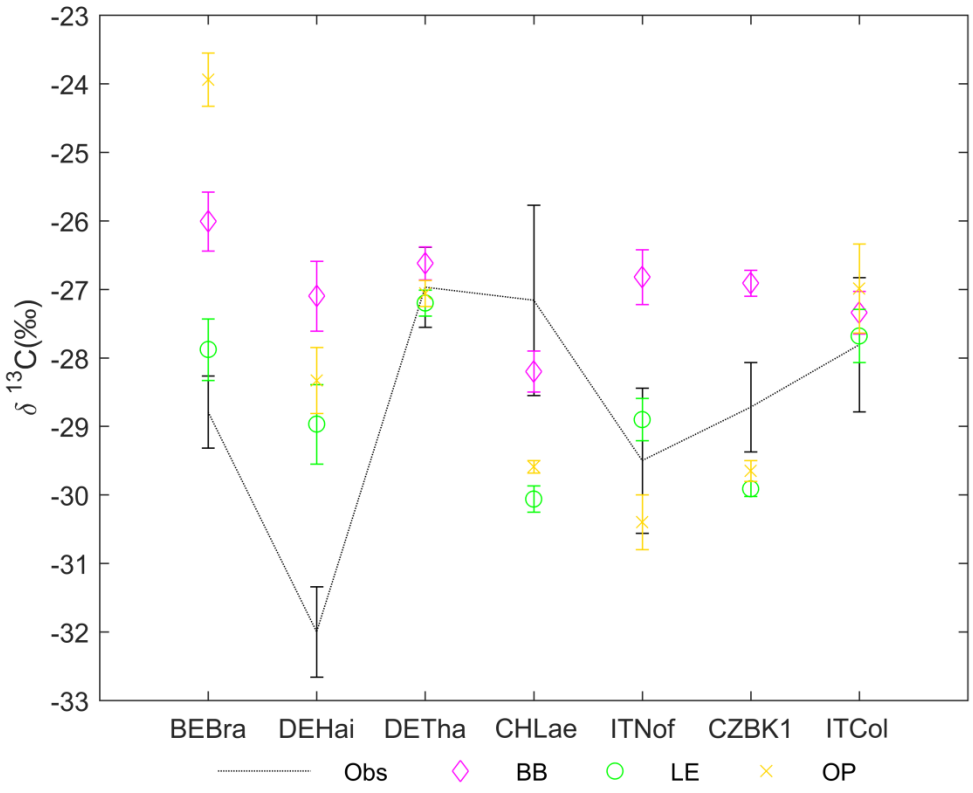

Figure 3.8 Comparison between the foliar 13C measurement and simulated 13C value by three stomatal models in eddy covariance sites in Table 3-3.

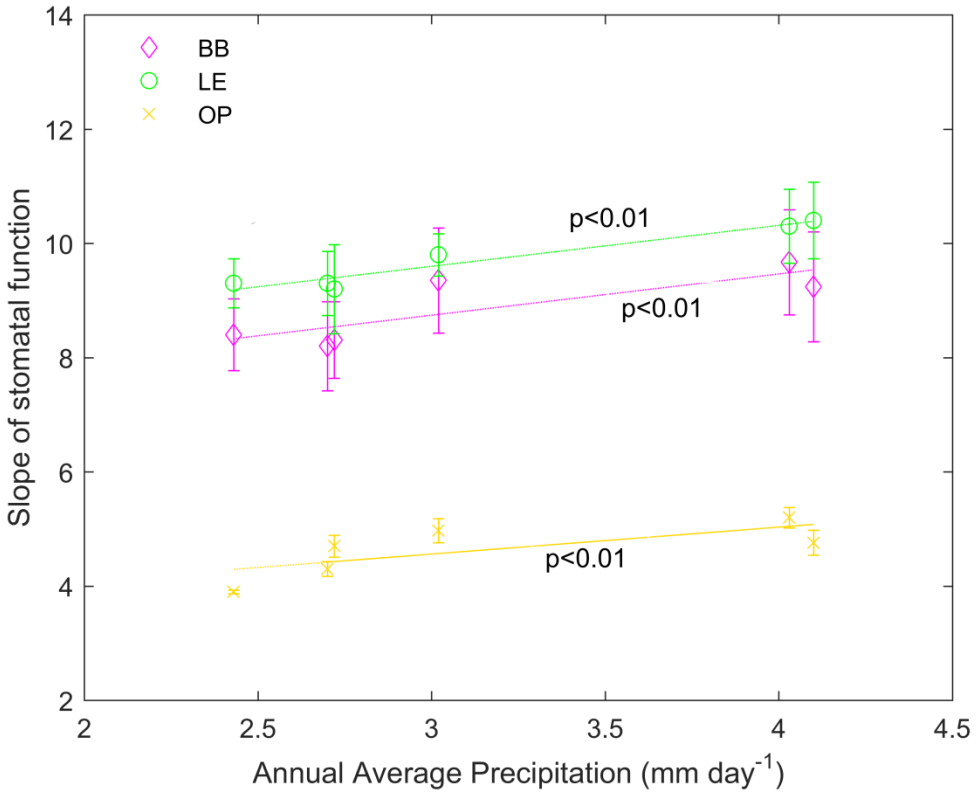

Figure 3.9 The relationship between annual precipitation and the slope of three stomatal functions among the six sites. BB, LE and OP indicate the Ball-Berry, Leuning and Optimal stomatal models, respectively.

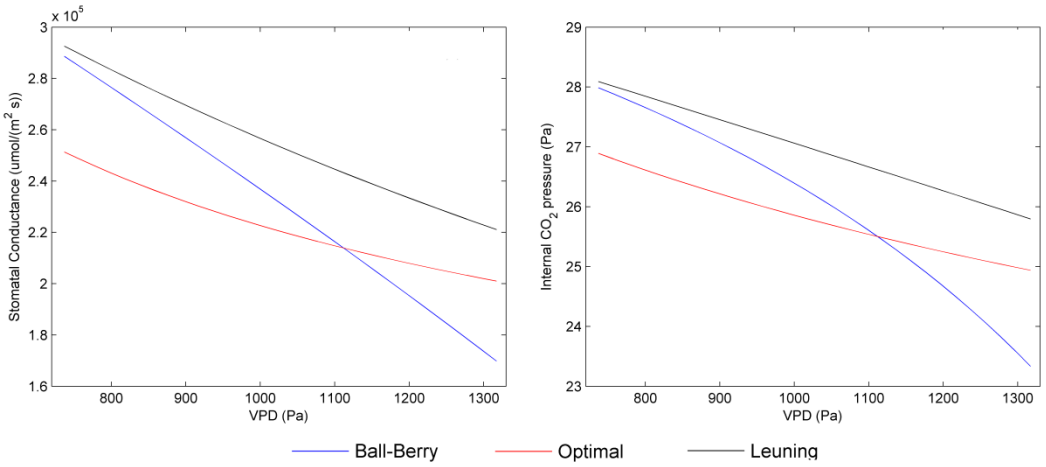

Figure 3.10 The comparison of stomatal conductance and internal CO_2 partial pressure with varying VPD using three stomatal model schemes.

CHAPTER 4 EVALUATING THE ECOSYSTEM WATER USE EFFICIENCY AND GROSS PRIMARY PRODUCTIVITY IN BOREAL FOREST BASED ON TREE RING DATA

Abstract: Climatic change affects the plant physiological and biogeochemical processes, and therefore the ecosystem water use efficiency (WUE). Therefore, a comprehensive understanding of WUE would help us understand the adaptability of ecosystems to varying climate conditions. Tree ring data have great potentials in addressing the forest response to climatic changes compared with mechanistic model simulations, eddy flux measurement and manipulative experiments. Here, we collected the tree ring isotopic carbon data at 12 boreal forest sites to develop a linear regression model, and the model was extrapolated to the whole boreal region to obtain the WUE spatial and temporal variation from 1948 to 2010. Two algorithms were also used to estimate the inter-annual gross primary productivity (GPP) based on our derived WUE. Our results demonstrated that most of boreal regions except parts of Alaska showed a significant increasing WUE trend during the study period. The spatial averaged annual mean WUE was predicted to increase by 13%, from 2.3±0.4 g C kg^{-1} H_2O at 1948 to 2.6±0.7 g C kg^{-1} H_2O at 2012, which was much higher than estimations from other land surface models. Our predicted GPP by the WUE definition algorithm was comparable with site observation, while for the revised light use efficiency algorithm, GPP estimation was higher than site observation as well as land surface model estimates. In addition, the increasing GPP trends estimated by two algorithms were similar with land surface model simulations. This is the first study to evaluate regional WUE and GPP in forest ecosystem based on tree ring data and future work should consider other variables

(including elevation and nitrogen depositions), that influence tree ring isotopic signatures and the dual-isotope approach may help improve predicting the inter-annual WUE variation.

4.1 Introduction

The carbon exchange between biosphere and the atmosphere is closely coupled with water fluxes in terrestrial ecosystems (Law et al., 2002; Niyogi et al., 2009). Water use efficiency, defined as the ratio of carbon assimilated to water transpired by plants, is an important parameter in terrestrial ecosystem models and can be used to analyze the metabolism of terrestrial ecosystems. The intrinsic water use efficiency (WUE_i) linking the gas exchange of carbon and water at the leaf level, is a good indicator of long term regulation of plant carbon uptake and water loss (Keenan et al., 2013). At the ecosystem level, the integrated WUE or ecosystem WUE, which has an additional term of atmospheric vapor pressure deficit compared with WUE_i, can be used to monitor the adaptability of an ecosystem to variable climate conditions. Therefore, a comprehensive understanding of WUE would facilitate the ecosystem management in future climatic change.

Climatic changes can affect the plant physiological and biogeochemical processes as well as the functional traits, and therefore the WUE. For example, increasing CO_2 has been demonstrated as a positive effect on the WUE_i (Keenan et al., 2013), by improving plant carbon assimilation (e.g. Li et al., 2014) and reducing stomatal conductance (Medlyn et al., 2001; Ainsworth and Rogers, 2007). Meanwhile, the increased leaf area index induced by CO_2 fertilization effect (Piao et al., 2006; Los, 2013) and the enhanced evapotranspiration (ET) would offset the positive CO_2 effect on WUE. Predicted frequent drought events (Dai, 2013) can also modify the WUE through alter the plant morphology, such as the increased carbon allocation to roots (Chapin et al., 2011). In addition, the increasing nitrogen deposition, which originates from combustion of fossil fuels and

farmland fertilization, was observed to enhance the WUE through stimulating plant photosynthetic rates (Mitchell et al., 2003; Jennings, 2013).

At present, a number of eddy flux tower sites (FLUXNET http://daac.ornl.gov/FLUXNET/fluxnet.shtml) and manipulative experiments have been operated to measure the exchanges of carbon and water fluxes continuously over a broad range of climate and biome types. Recent advance in eddy flux towers measurement have provided us insights into water and carbon cycle in various ecosystems. However, very few flux sites and experiments (e.g. free air CO_2 enrichment experiment) have long enough observations (20 years) to address the long term response of ecosystem to climate change, especially the CO_2 fertilization effect on WUE (Ainsworth and Rogers, 2007; Gagen et al., 2011). The data-fusion approach incorporated into land surface models gives us the opportunity to evaluate the WUE change across large scale for a long time period. However, these land surface models constrained with eddy flux observation are often criticized by high model complexity (Chen et al., 2011), unrealistic parameter generalization across the plant function type (Reich et al., 2007; Alton, 2011), which would induce large uncertainties.

Tree ring have great potentials to address the forest response to climatic changes compared with mechanistic model simulations, eddy flux measurement and manipulative experiments. The physiological information stored in tree ring reflects the long term information of past climate and therefore help us reconstruct the climate in the past. The isotopic records in tree rings are also sensitive to environmental change due to the stomatal regulation and photosynthetic activity. From the stable carbon isotope (13C) perspective, the fractionation occurring in the plant biogeochemical processes yield relatively lower value of 13C ratio in leaves and woods and the variation is closely related with environmental conditions. The isotopic signals in tree tissues are expressed as:

$$\delta^{13}C = \delta^{13}C_a - \Delta = \delta^{13}C_a - (a + (b-a) * {C_i}/{C_a}) \quad (4.1)$$

Where $\delta^{13}C_a$ is the atmospheric $^{13}CO_2$ ratio, a (-4.4‰) and b (-27.2‰) are the fractionation occurring during diffusion and carboxylation processes. Therefore, the ecosystem WUE value can be derived from the tree ring record, as

$$WUE = {C_a(1-(\delta^{13}C_a - \delta^{13}C - a))}/{((b-a)*1.6*VPD)} \quad (4.2)$$

Many studies have used tree ring signatures to investigate plant response to increasing CO_2 levels and changing environment across a broad climate and biomes. For example, Saurer et al (2004) investigated the response of 126 trees (Larix, Pinus and Picea) in northern Eurasia to climatic change and increasing CO_2 over the last century by using tree ring data, and their findings suggested an 19.2% increase in WUE_i in these species. Peñuelas et al (2011) conducted a meta-analysis on carbon isotopic composition of tree rings over four decades in multiple biomes, and they indicated a 20.5% increase in mature trees without significant differences among these biomes.

Right now, although most previous related work focused on site-level, few have conducted the regional WUE estimation based on the tree ring carbon data. Here we focused on the boreal forest as it is vulnerable to global warming (Parry et al., 2007) and has the greatest biogeophysical vegetation feedback to the atmosphere (Snyder et al., 2004). Twelve boreal forest sites' tree ring isotopic data and meteorological variation were collected to develop a linear regression model, and the model was extrapolated to the whole boreal region to obtain the WUE spatial and temporal variation from 1948 to 2010. We were also interested in the regional gross primary productivity (GPP) and two methods were explored to estimate the inter-annual GPP based on our derived WUE.

4.2. Method

4.2.1 Overview

Twelve boreal tree rings sites were selected to construct our predictive models (Table.4-1). We first extracted the "true" C_i/C_a from isotopic carbon data in tree ring by removing the influence of fossil fuel combustion. The linear model was used to develop the relationship between C_i/C_a variation and environmental changes and then extrapolated to the boreal region to obtain WUE from 1948 to 2012. Finally, we explored two methods to estimate the boreal GPP from 1982 to 2006 and model simulations were compared with eddy flux tower sites and land surface models (TRENDY).

4.2.2 Explanatory variables of C_i/C_a and linear regression models

The key step to derive WUE was to obtain the C_i/C_a response to environmental change. The regulation of C_i/C_a was controlled by both stomatal conductance and plant photosynthesis, as suggested by the Ficker's Law. As for the stomatal conductance, leaf gas exchange experiment and empirical statistical models (e.g. Leuning et al., 1995) suggested that the stomatal openings were negatively correlated with vapor pressure deficit (VPD) (or positively related with relative humidity). Here, we chose the air temperature as alternative explanatory variable, as temperature was highly correlated with VPD. In addition, Prentice et al (2014) derived a new C_i/C_a equation based on the optimal stomatal theory and array of leaf carbon isotope composition data, indicating the air temperature can influence the viscosity of water transporting from root to leaf and consequently the transpiration. The widely used Ball-Berry (Ball et al., 1987) and Leuning (Leuning, 1995) stomatal model had an additional environmental variable, the atmospheric CO_2 concentration. Therefore, we chose it as our second explanatory variable and expected the

negative relationship between CO_2 and C_i/C_a. We also added the moisture index (MI), which was defined as the ratio of precipitation to incoming shortwave radiation, into our predictive model. The incident radiation can significantly affect plant photosynthesis and annual mean precipitation was a good indicator of climate (dry or wet). The high moisture index indicated the plant favorable environment and we expected it had positive relationship with C_i/C_a variation. Finally, we added the C_i/C_a at previous time year as our last explanatory variable. A previous tree ring study suggested there was a significant correlation between plant growth at prior year and that at current time step (Loader and Switsur, 1996). In sum, we had four explanatory variables to predict the C_i/C_a variation in response to environmental change including: air temperature, moisture index, atmospheric CO_2 concentration and C_i/C_a at previous time year. Therefore, we had the following linear models to derive C_i/C_a:

$$\Delta C_i / C_a(t) = a * \Delta T + b * \Delta MI + c * C_a + d * C_i / C_a(t-1) + e \quad (4.3)$$

Where $\Delta C_i / C_a(t)$, ΔT , ΔMI and C_a were the difference of C_i/C_a, air temperature, moisture index, atmospheric CO_2 concentration between current and previous year, respectively. $C_i / C_a(t-1)$ was the C_i/C_a at previous year. a, b, c, d and e were the coefficients in the linear equation. The equation was first used to derive the coefficients for each tree ring site, and the 12 sets of coefficient values were averaged to conduct the extrapolation across the boreal region and the Monte Carlo method was used to get the WUE uncertainty. To be more specific, assume X1, X2 …X12 were the derived coefficient from 12 boreal tree ring sites, the mean value (X) were used to conduct the extrapolation and the 25%, 75% value would be the lower and upper bound of X, where the Monte Carlo method sampled 100 times by assuming a uniform distribution. The initial C_i/C_a at 1948 for each grid in boreal forests was obtained from “Trends in net land carbon exchange over the period 1980-2010” (TRENDY) project. TRENDY was the intercomparision project of a consortium of dynamic global vegetation models, including CLMC, CLMCN, LPJ,

LPJ-GUESS, ORCHIDEE, OCN and VEGAS (Sitch et al., 2008). The project aimed at investigating further spatial trends in Net Biome Production (NBP) and performing a factorial set of Dynamic Global Vegetation Model (DGVM) simulations over the historical period from 1901to 2010. The model simulations had three protocols: S1 (constant climate and land use data but with varying CO_2); S2 (constant land use but with varying climate and CO_2) and S3 (all of them were changing). We extracted the annual GPP and evapotranspiration (ET) from eight DGVMs S2 simulations protocols and obtained the initial C_i/C_a by using the following equation (4.4):

$$C_i/C_a = (1 - GPP / ET * 1.6 * VPD / C_a) \quad (4.4)$$

4.2.3 GPP Estimation: WUE definition and light use efficiency algorithm

One of the methods to estimate GPP was based on the ecosystem WUE definition. We explored the satellite estimation of ET, which required less data input and had simple algorithms. During the past decade, a large number of techniques have been proposed to estimate ET from satellite observations. Right now, some empirical or semi-empirical models explored meteorological variables and satellite data to derive ET. Here, we used the Landflux (http://landflux.org/Data.php) data products (Fisher et al., 2008), which explored the Priestley-Taylor method to estimate the global scale of water and energy flux between terrestrial ecosystem and the atmosphere using remote sensing observation and meteorological measurements. This product performed well in the site-level test and validation against eddy covariance measurement for all 16 flux sites.

Another method was the light use efficiency (LUE) algorithm. The LUE concept has been used in diagnostic primary production models, including the Carnegie–Ames–Stanford Approach model (Field et al., 1995), Boreal Ecosystem Productivity Simulator (Chen et al., 2003), and the

widely used MODIS GPP and NPP data products (Running et al., 2004). Wang and Prentice (2014) further developed the LUE model which considered the effect of photorespiration and substrate limitation at subsaturating CO_2 by assuming fPAR was independent of CO_2. The new algorithm used the electron-transport limitation to yield an estimate of LUE. In equation (4.5), φ_0 was the intrinsic quantum efficiency of photosynthesis, $\tilde{\alpha}$, PAR_0, $fAPAR$, and Γ^* was the leaf absorbance, accumulated PAR for the period with daily temperature above 0 °C, fractional absorbed PAR, leaf internal CO_2 concentration and photorespiratory compensation point, respectively.

$$GPP = \varphi_0 \times \tilde{\alpha} \times PAR_0 \times fAPAR \times \frac{C_i - \Gamma^*}{C_i + 2 \times \Gamma^*} \tag{4.5}$$

4.2.4 Data

4.2.4.1 Tree ring data

The selected tree ring sites spread across the boreal region, from Alaska to East Siberia (Figure 4.1 and Table. 4-1). The selected samples included the Pinus, Picea, Larix and Quercus, which represented the typical boreal species. We chose the tree ring isotope data from 1948 to 2000. In addition, due to the Sue effect caused by intensive fossil fuel combustion, we used following equation (Franks et al, 2013) to calculate the atmospheric carbon isotopic signal and obtain the "true" carbon isotope discrimination. The derived C_i/C_a in each year represented the tree response to environmental condition during growing season.

$$\delta^{13}C_a = -6.4 - (0.004 * \exp(0.0197 * (year - 1695.06))) \tag{4.6}$$

$$\Delta = (\delta^{13}C_a - \delta^{13}C_p) / (1 + \delta^{13}C_p) \tag{4.7}$$

$$\delta^{13}C = \delta^{13}C_a - \Delta = \delta^{13}C_a - (a + (b-a) * {C_i}/{C_a}) \quad (4.8)$$

4.2.4.2 Climate/remote sensing data and TRENDY products

The air temperature, precipitation, radiation during growing season (from June to August) was extracted from the CRU-NCEP climate data (Sheffield et al., 2006) for regional extrapolation. The site-level meteorological variables at 12 boreal tree ring sites were also extracted from CRU-NCEP using the nearest neighbor method. The fPAR was obtained from the Global Inventory Modeling and Mapping Studies (GIMMS) products (Tucker et al., 2004).

We also compared our predicted WUE and GPP with TRENDY project. As we mentioned above, the TRENDY project simulations had three protocols: S1 (constant climate and land use data but with varying CO_2); S2 (constant land use but with varying climate and CO_2) and S3 (all of them were changing). Here, we only extracted the TRENDY output from S2 simulations protocols for the comparison and all results were resampled to 1 degree spatial resolution to match our simulations.

4.3. Results and discussion

4.3.1 Linear regression coefficients based on tree ring data

Using the linear model, our predicted mean C_i/C_a were comparable with the observed C_i/C_a, and the R^2 ranged from 0.4 to 0.8 (Figure 4.2). Generally, the tree ring sites locating in Northern Europe had better prediction performance (e.g. B01 and B02) than other sites, such as the Alaska and East Siberia (e.g. B05 and B11). The averaged coefficients based on the 12 boreal tree ring sites were shown in Figure 4.3. The air temperature variation and C_i/C_a(t-1) exhibited negative values, indicating the opposite relationship with C_i/C_a; while for moisture index, it showed the

positive relationship with C_i/C_a variation, which was in accordance with our previous hypothesis. Although the CO_2 concentration coefficient had a relatively large range (from -0.15 to 0.09), the mean value was negative and this was consistent with the Farquhar's optimal theory (Lloyd and Farquhar, 1994) and Medlyn's developed equation (Medlyn et al., 2011). Overall, our multiple linear model exhibited a good comparison with the observation from tree ring sites, and the derived coefficients were reasonable, which could be used for following regional extrapolations.

4.3.2 Predicted WUE and GPP using linear regression models

The model simulated annual mean WUE ranging from 0.8~3.5 g C kg^{-1} H_2O (Figure 4.4). Large WUE values (>2.5 g C kg^{-1} H_2O) were generally observed at high latitudes (> 60 °N: Alaska, Norway, parts of Canada and East Serbia). Most of boreal forest region showed a significant increasing WUE trend over the period except parts of Alaska (Figure 4.5). East Europe, parts of Serbia and North America exhibited the largest increasing trend (Figure 4.5) (~0.05 g C kg^{-1} H_2O yr^{-1}). Overall, the spatial averaged annual mean WUE was predicted to increase by 13%, from 2.3±0.4 g C kg^{-1} H_2O at 1948 to 2.6±0.7 g C kg^{-1} H_2O at 2012 (Figure 4.6).

Two algorithms simulated annual mean GPP varying from 250~800 g C yr^{-1} during 1980 to 2006 (Figure 4.7). The estimated GPP for the two methods showed relatively large differences across the boreal region. For example, the LUE developed by Wang et al (2014) had higher (100~200 g C yr^{-1}) GPP estimation than that by the method of WUE definition in vast of Europe and Siberia, while in most of North America (e.g. Alaska), it generally exhibited lower (-200~-100 g C yr^{-1}) GPP values. Both algorithms showed the significant increasing trends of GPP in vast boreal region except Alaska, which was similar with the WUE temporal patterns (Figure was not shown here, as it was similar with Figure 4.5). However, the increasing trends estimated by WUE definition were around 30% larger than that by Wang's method. Correspondingly the

temporal trends of spatial averaged GPP by WUE definition was 4.2 umol C m^{-2} s^{-1} yr^{-1} during the period, which was 28% larger than that by Wang's algorithm.

4.3.3 WUE, GPP comparison with sites observation and ESMs

Previous studies by Bru¨mmer et al (2012), Buchmann and Schulze (1999) reported that the WUE of Pinus species in Canada and United Kingdom were from 0.52 to 3.71 g C kg^{-1} H_2O yr^{-1}. A recent study by Tang et al (2014) showed that the mean WUE was around 3.8 g C kg^{-1} H_2O yr^{-1} at 60 °N, and the value decreased to 1.2 g C kg^{-1} H_2O yr^{-1} at 68 °N based on eddy flux sites' observation. All the reported results above were similar with our predicted WUE based on tree ring isotopic data. From the temporal trends' perspective, few studies have reported the WUE changes in boreal forest based on observation instead of the intrinsic WUE. For example, Saurer et al (2004) investigated the response of 126 trees (Larix, Pinus and Picea) in northern Eurasia to climatic change and increasing CO_2 over the last century by using tree ring data, and their findings suggested an 19.2% increase in the intrinsic WUE in these species. The selected eddy flux sites (Table 4-2) were compared with predicted GPP using the two algorithms. Generally, GPP estimations by WUE definition were better (R^2 = 0.64 and RMSE = 102 g C m^{-2} yr^{-1}) than that by LUE algorithm developed by Wang (Figure.4.8) (R^2 = 0.46 and RMSE = 169 g C m^{-2} yr^{-1}). Both algorithms showed higher GPP estimation when the site GPP observation was low (< 500 g C m^{-2} yr^{-1}), but LUE algorithm showed much more deviation compared with WUE definition.

Our predicted WUE value was similar with most of TRENDY models during 1948-2012 (Figure 4.9), such as the CLMC, CLMCN, TRFFID, but it was higher than that in OCN and ORCHIDEE, and smaller than that in VEGAS. All models (except VEGAS) exhibited significant increasing trends, ranging from 1e-6 g C kg^{-1} H_2O yr^{-1} to 1.2e-5 g C kg^{-1} H_2O yr^{-1}. However, the increasing trend predicted by tree ring was much higher than all TRENDY models except

ORCHIDEE. For example, our predicted increasing trend was around as 9 times larger than in LPJ and 40% higher than that in TRFFID. Although tree ring based WUE was similar with most of TRENDY models, the two algorithms estimated GPP were around 15%~24% higher than that in TRENDY models. The inter-annual variability of GPP by WUE definition was comparable with TRFFID, but for the LUE algorithm developed by Wang et al (2014), the variability was generally smoother compared with other algorithms/models. Five of seven TRENDY models showed significant increasing GPP trends during the period as well as the two algorithms based GPP in this study. In addition, our predicted GPP increasing trends were also comparable with TRENDY models except the CLMC and CLMCN, ranging from 3 umol C m^{-2} s^{-1} yr^{-1} to 7 umol C m^{-2} s^{-1} yr^{-1}.

4.4 Conclusion

Twelve boreal forest sites' tree ring isotopic data were used to develop a linear regression model, and the model was extrapolated to the whole boreal region to obtain the WUE spatial and temporal variation from 1948 to 2010. Two algorithms were also explored to estimate the inter-annual gross primary productivity (GPP) based on our derived WUE. The results demonstrated that most of boreal regions showed significant increasing WUE trend during the period except parts of Alaska. The predicted spatial averaged annual mean WUE was predicted to increase by 13%, from 2.3±0.4 g C kg^{-1} H_2O at 1948 to 2.6±0.7 g C kg^{-1} H_2O at 2012, which was much higher than other land surface models. Our predicted GPP by the WUE definition algorithm was comparable with site observation, while for the light use efficiency algorithm, GPP estimation was higher than site observation as well as than land surface models. In addition, the increasing GPP trend by two algorithms was similar with land surface model simulations.

Table 4-1 Information of tree ring sites in Figure 4-1

ID	Species	Latitude	Longitude	Period	Reference
B01	Pinus sylvestris L	68.8 °N	15.4 °E	1948-2001	Young et al., (2010)
B02	Pinus sylvestris L	68.3 °N	19.7 °E	1948-2008	Loader et al., (2013)
B03	Picea abies	47.1 °N	15.4 °E	1948-1995	Anderson et al., (1998)
B04	Larix gmelinii Rupr	70.6 °N	103.4 °E	1948-2006	Sidorova et al., (2010)
B05	Larix cajanderi Mayr	70.0 °N	148.0 °E	1948-2000	Sidorova et al., (2008)
B06	Quercus robur	55.3 °N	3.4 °W	1948-2002	Loader et al., (2008)
B07	Larix cajanderi Mayr	63.0 °N	139.0 °E	1948-1999	Kirdyanov et al., (2008)
B08	Picea mariana	64.8 °N	148.0 °W	1948-1996	Beck et al., (2011)
B09	Pinus sylvestris L	68.9 °N	28.3 °E	1948-2001	Hilasvuori et al., (2009)
B10	Pinus sylvestris L	68.0 °N	27.0 °E	1948-2001	Gagen et al., (2007)
B11	Picea mariana	48.6 °N	70.4 °W	1948-1990	Simard et al., (2008)
B12	Pinus banksiana	53.9 °N	105.1 °W	1962-1993	Brooks et al., (1998)

Table 4-2 Eddy covariance sites used for GPP comparison in Figure 4.7

Site Name	Latitude	Longitude	Period	Reference
FIHYY	61.84 °N	24.29 °E	1996-2010	Suni et al., (2003)
FISOD	67.36 °N	26.63 °E	2000-2008	Thum et al., (2007)
SEFLa	64.11 °N	19.45 °E	1996-2002	Valentini et al., (2000)
SENor	60.08 °N	17.47 °E	1996-2007	Lagergren et al., (2008)
SESk1	60.13 °N	17.91 °E	2005-2008	Gioli et al., (2004)
QC	49.69 °N	74.34 °W	2003-2010	
SK	53.98 °N	105.11 °E	1996-2010	
MB	55.88 °N	98.48 °W	2007-2008	

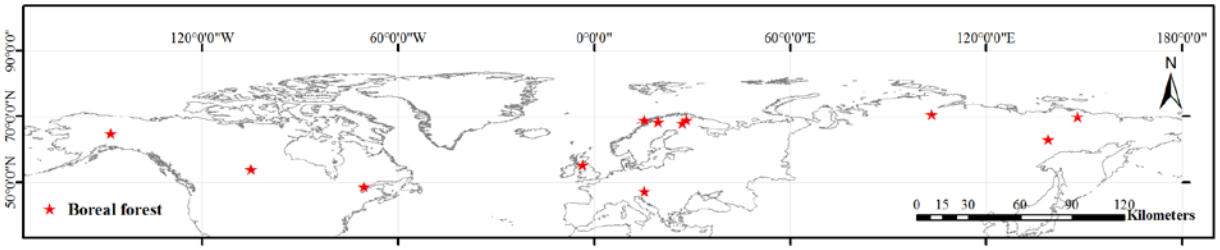

Figure 4.1 Tree ring sites of boreal forest used in this study (More information can be found in Table 4-1)

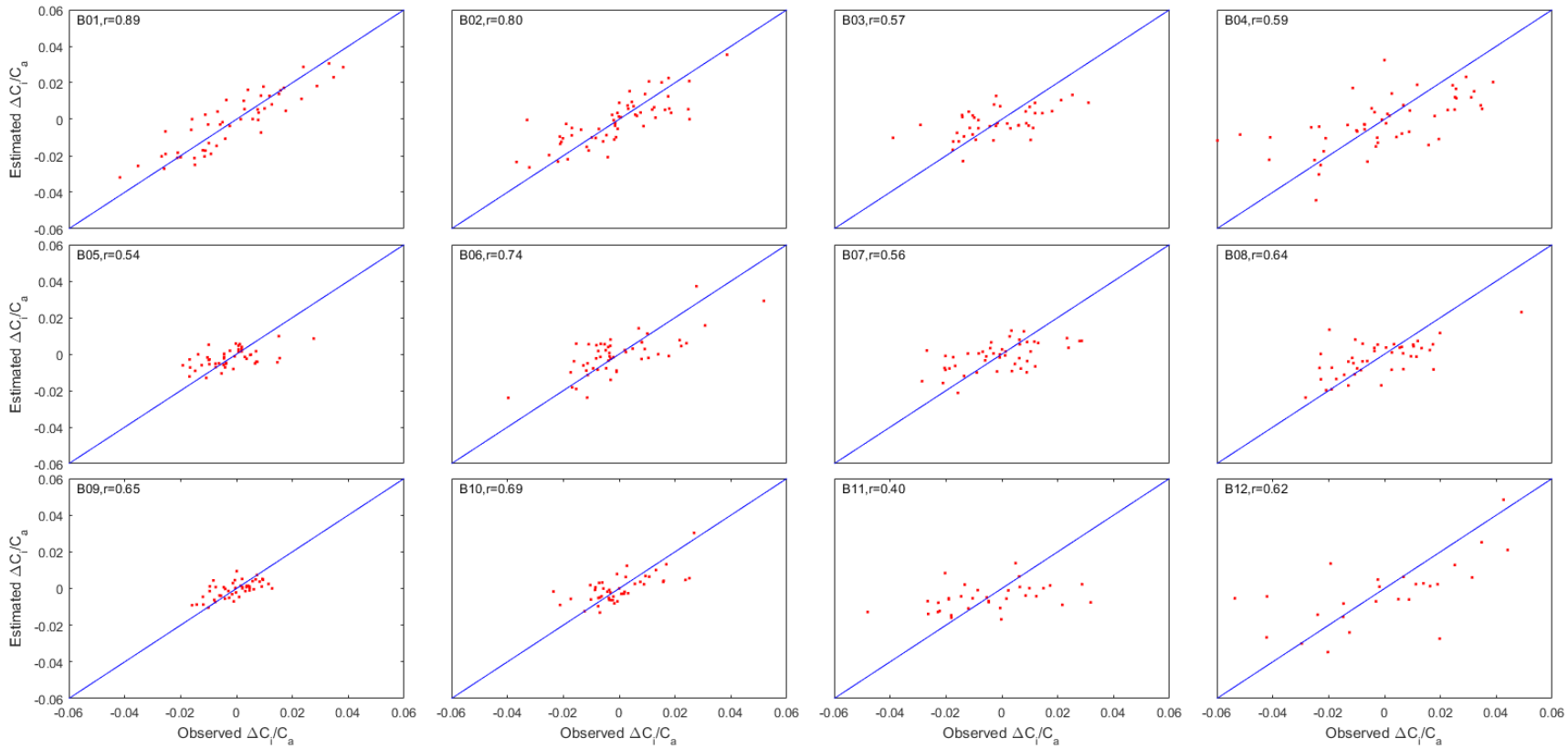

Figure 4.2 The comparison between estimated $\Delta C_i/C_a$ with derived $\Delta C_i/C_a$ from tree ring data at 12 tree ring sites. (The prediction used the multiple linear regression model as: $\Delta C_i/C_{a(t)} = a^* \Delta Temp + b^* \Delta MI + c^* \Delta Ca + d^* C_i/C_{a(t-1)} + e$; Temp: air temperature, MI: moisture index, Ca: atompsheric CO_2

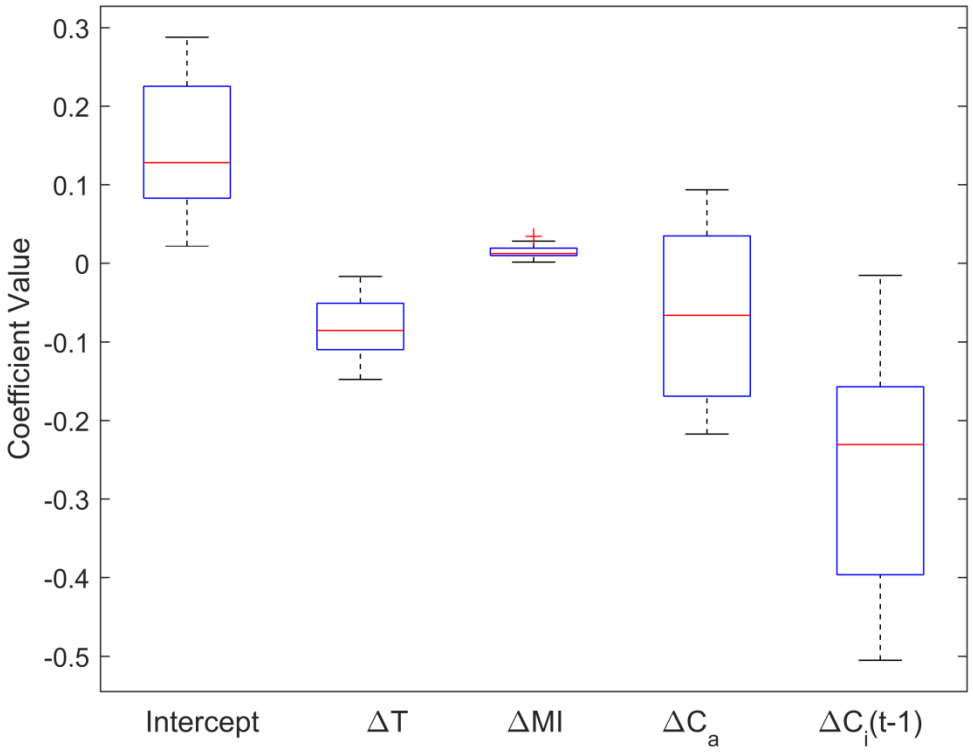

Figure 4.3 Boxplot of the five coefficients in the linear regression models (The prediction used the multiple linear regression model as: $\Delta C_i/C_{a(t)} = a^* \Delta Temp + b^* \Delta MI + c^* \Delta Ca + d^* C_i/C_{a(t-1)} + e$; Temp: air temperature, MI: moisture index, Ca: atmospheric CO_2)

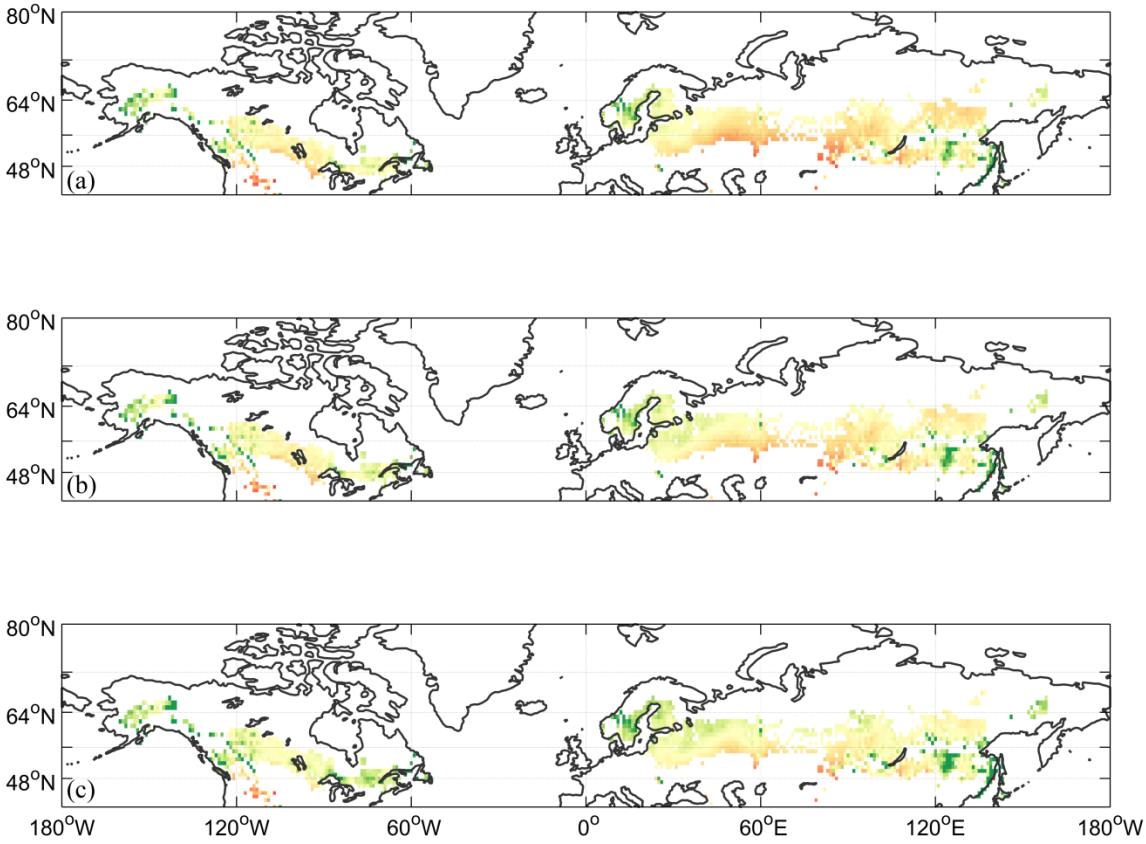

Figure 4.4 Predicted mean WUE in boreal forest in different decades ((a), (b), (c) stand for 1980~1990, 1991~2000 and 2001~2010, respectively)

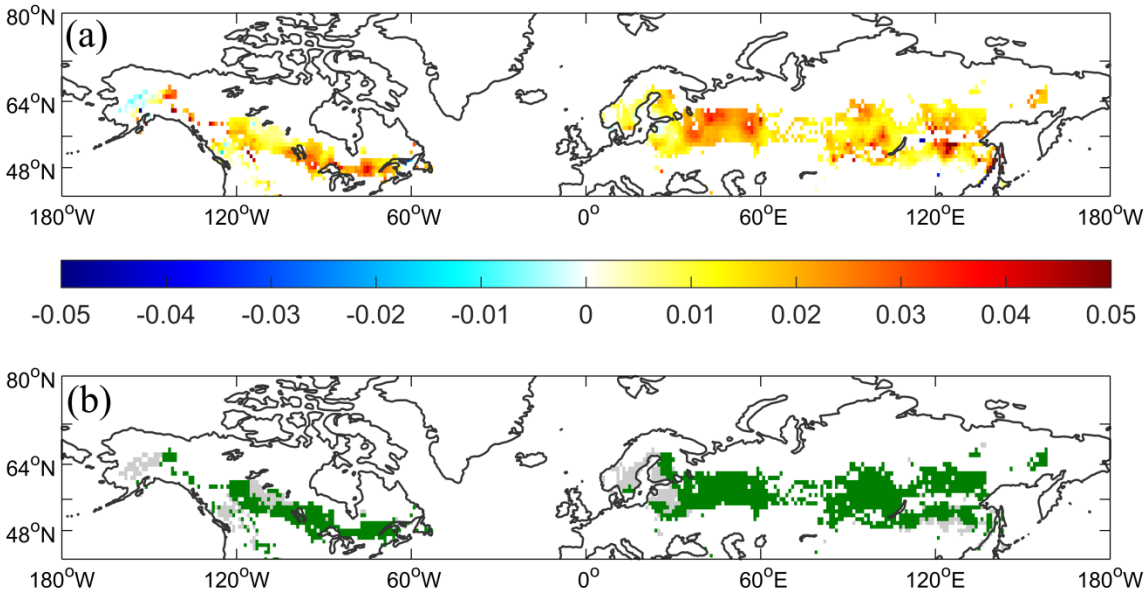

Figure 4.5 Predicted spatial WUE trends in boreal forest during the study period (a) and the trends significance (b). Green color indicates there is significant WUE changing trends ($P<0.01$), while grey one means no significance.

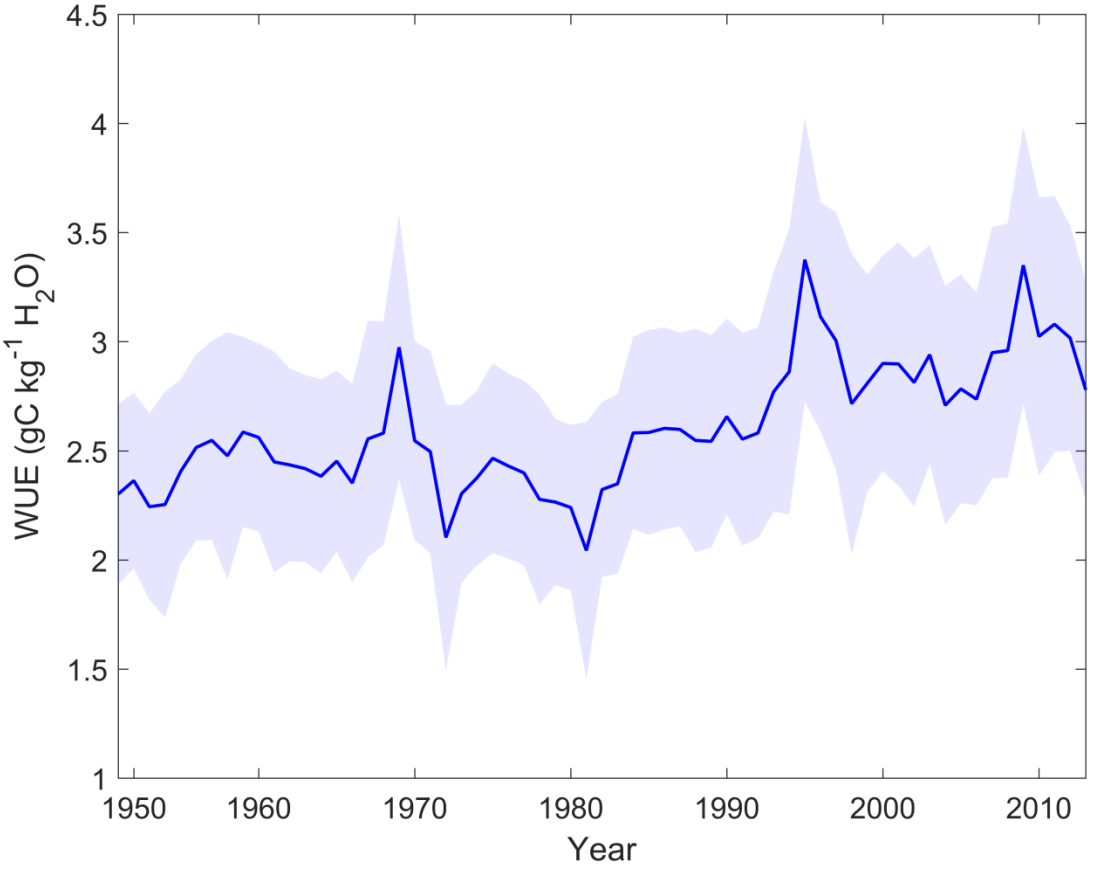

Figure 4.6 Predicted WUE in boreal forests using the linear regression model (The prediction used the multiple linear regression model as: $\Delta C_i/C_{a(t)} = a^* \Delta Temp + b^* \Delta MI + c^* \Delta Ca + d^* C_i/C_{a(t-1)} + e$; Temp: air temperature, MI: moisture index, Ca: atompsheric CO_2). Shade area stands for the estimation uncertainty induced by the regression coefficient.

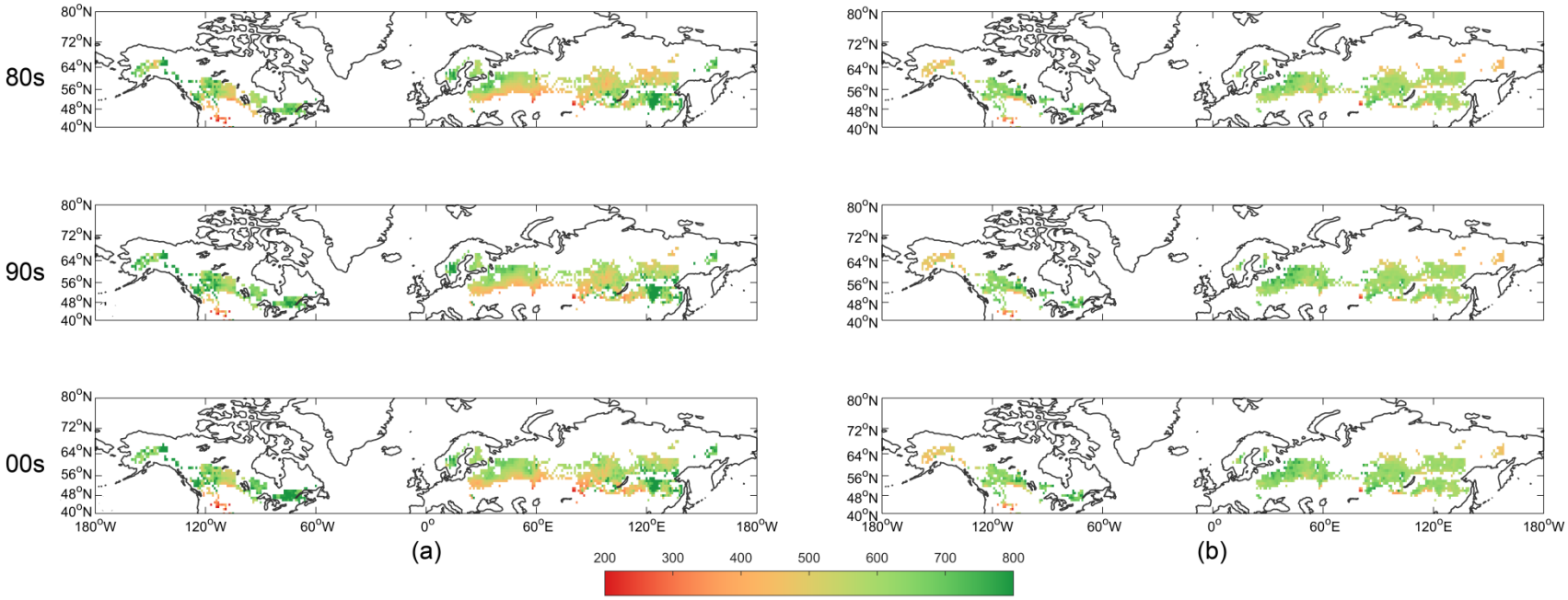

Figure 4.7 Predicted mean GPP in boreal forests using two algorithms in three decades (1980~1989, 1990~1999 and 2000~2006). a and b stand for the algorithm by WUE definition and revised LUE equation developed by Wang et al (2015).

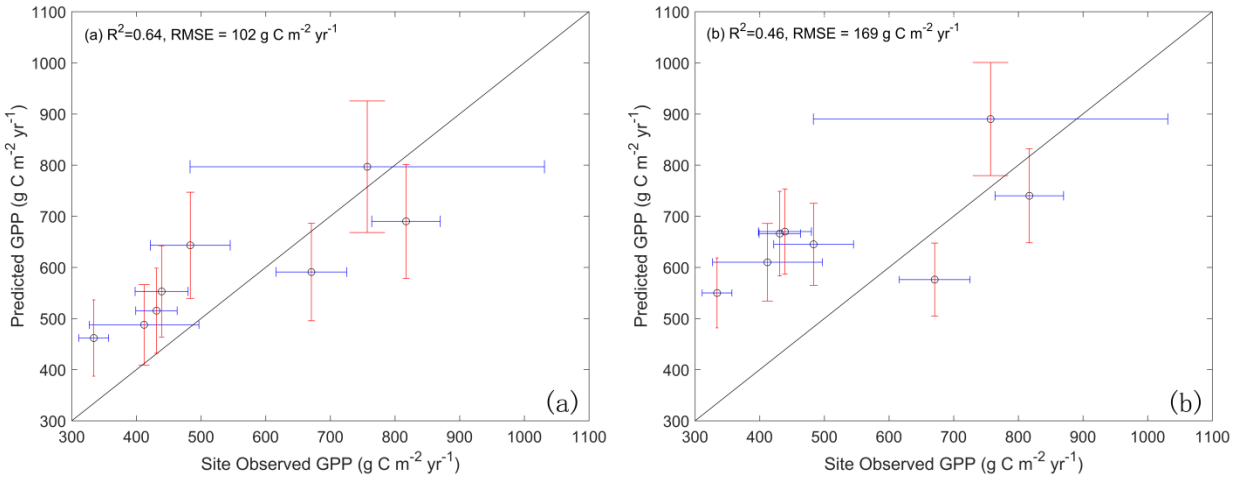

Figure 4.8 Comparison between site-observed GPP (Table 4-2) with estimated GPP by WUE definition (a) and LUE algorithm (b).

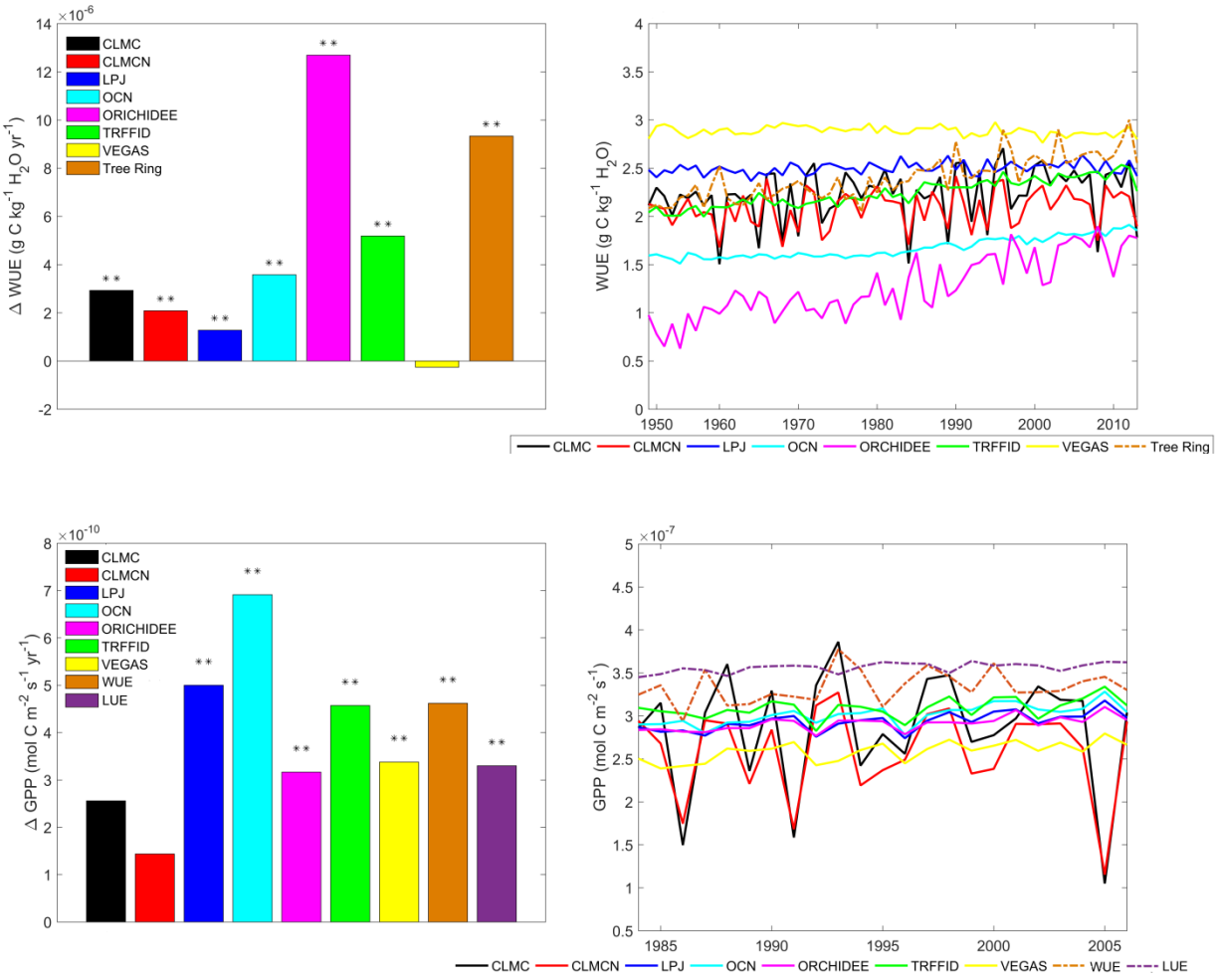

Figure 4.9 WUE and GPP trends in seven global land surface models and our study (left column) in boreal forest from 1948 to 2010 (double asterisk indicates significant increasing trend, $p<0.01$) and the spatial average WUE and GPP of 7 global land surface models and our study (right column) in boreal forest from 1948 to 2010.

CHAPTER 5 SUMMARY AND FUTURE WORK

This dissertation evaluates the regional carbon dynamics by using upscaling approach, mechanistically-based biogeochemistry models and in situ and remotely sensed data. As for the upscaling method using Fluxnet data, I focus on how and to what extent that atmospheric CO_2 effect on the carbon dynamic prediction. For mechanistically-based biogeochemistry model, I constrain the regional carbon dynamic using leaf 13C measurement. In addition, by merely using tree ring isotopic record, I also derive the inter-annual WUE and GPP variation in boreal forest.

However, the model-based studies have some drawbacks. Specific limitations and future work are listed below:

(1) In the upscaling study, first, the selected AmeriFlux sites can contribute a large uncertainty to our model development, because ANN training and validating are highly associated with the eddy flux data. The representativeness of the AmeriFlux data is crucial to scaling up site-level measurement to large regions. In our study, the criterion to select sites is based on the available CO_2 measurement from 2000 to 2006. The representativeness of the flux sites is crucial to scaling up site-level measurement and to understand the carbon dynamics across large spatial scales and quantify uncertainty. Although the global sites well represent variations in climate and ecological regions (Reichstein et al., 2014), whether the major ecoregions from North America are well represented by the AmeriFlux network has not been examined (Hargrove et al., 2003). Using a cluster analysis with 25 climatic and physiological forcing variables based on 59 AmeriFlux sites,

Hargrove et al. (2003) showed that the vast interior of the US was well-represented by the AmeriFlux network, but the Pacific Northwest, Southern, and Southwestern were under represented. In addition, the uncertain eddy flux data—due to system errors, random errors, site selection criteria (Loescher et al., 2006), and the gap-filling method (Moffat et al., 2007; Desai et al., 2008)—may affect the GPP and NEE uncertainty in the model parameterization and simulation. Second, our approach has not considered other controlling factors on the carbon fluxes. The vegetation distribution was constant without any shifts or disturbances during the study period, which might have biased estimation. Lacking the effects of land-cover changes, natural disturbances (e.g., fire, hurricane, insect infestation), economic influences (e.g., harvest) and demographic factors (Lambin et al., 2003) would also introduce uncertainties to our quantifications. Especially in the US, about half of the forest area is disturbed each decade, including the timber harvesting and grazing (Birdsey and Lewis, 2003). The forest age reflects the past disturbance history. Use of the North American forest stand age database (Pan et al., 2011) derived from forest inventory, historical fire data, and remote sensing imagery could help reduce our quantification uncertainty (Deng et al., 2013; Xiao et al., 2014). For cropland, without considering the effects of crop rotation (such as from corn to soybeans) may also introduce uncertainty. Since C4 photosynthetic capacity is different from C3 plant, explicit C3 versus C4 plant distribution data shall also help reduce the uncertainty of carbon qualification. In addition, the MODIS ecosystem distribution is not consistent with flux tower footprints (Xiao et al., 2008) and can be significantly different from the towers' vegetation type. Recent studies by Melton and Arora (2013) showed that the plant function type variability within the one-grid scale is important in simulating ecosystem responses to changing climate and atmospheric CO_2 concentration.

Third, using only seven plant functional types (PFTs) derived from the MODIS land use product may also introduce uncertainties to the carbon flux quantification. In the simulations, we assumed that, at each PFT level, the response of carbon fluxes to environmental condition changes is same.

The usefulness and accuracy of such assumption has been questioned by field ecologists and there is a significant overlap between PFTs (Reich et al., 2007). The PFT-level parameterization could be biased because it may not properly represent the functional and structural characteristics of the species within a region. The parameter values obtained at the PFT level led to diverse significant carbon dynamic quantifications (Alton, 2011; He et al., 2013). Additionally, Reichstein et al. (2014) showed that the functional biogeographical variations of ecosystem properties were only partially explained by climate and PFTs. The large variability of biogeochemical processes within each PFT (Kattge et al. 2011) depended even more on plant traits, such as allocation and stabilization of carbon in the soil. Future studies should explicitly include the site-level information and trait database to test the relation between ecosystem functions and organismic traits to accurately quantify carbon fluxes.

(2) In the second study, first, the simplification of mesophyll conduction representation may be biased. Previous leaf gas-exchange experiments suggest that the mesophyll conductance is finite and it can vary with the leaf development (Warren 2008), nutrient availability (Warren 2004), radiation (Niinemets et al., 2006; Grassi & Magnani, 2005) and leaf temperature (Bernacchi et al., 2002), thus affecting the estimation of CO_2 assimilation rate. Keenan et al (2010) indicated that the effect of mesophyll conductance was important on the leaf and ecosystem scale during the drought season. Suits et al. (2005) explored the mesophyll conductance as a function of Rubisco content, radiation, NDVI and soil water stress factor. In our study, we followed the Evans and von Caemmerer (1996), assuming that the mesophyll conductance is proportional to the Rubisco content. Recently, Sun et al (2014) suggested that assuming zero mesophyll conductance in the Community Land Model 4.5, would highly overestimate the global primary productivity. However, we have to admit that the understanding on the response of mesophyll conductance to environmental conditions is still limited (Bodin et al., 2013).

Second, we did not consider the soil water stress in the stomatal model schemes. Generally, the soil water stress and vapor pressure deficit can occur simultaneously. Substantial studies suggested that there are negative effects of soil water stress on both plant photosynthesis and stomatal conductance. However, most of the current earth surface models do not include the soil water stress factor into the stomatal models, which may impact the predictability of plant responses under drought conditions. The review by Damour et al (2010) listed a few empirical or mechanistic stomatal models considering the soil water stress, and the mechanistic or physiological knowledge is often difficult to be modeled when compared with the empirical models based on the experiment data and limited their wide use in ESMs. In addition, the modification of plant morphology was observed under water stress condition, for example, the increase root to shoot ratio. These adaptive strategies could in turn attenuate the negative effects on stomatal conductance, and should be included into models. However, whether stomatal (water stress directly influences the stomatal closure) or non-stomatal (water stress influences the photosynthetic capacity or mesophyll conductance) limitation dominates the carbon flux is still debated. As for the stomatal limitation under drought conditions, Kauwe et al (2015) explored an empirical soil water stress factor into the Leuning and Optimal model to address the stomatal conductance sensitivity to soil water limitation. While for the non stomatal limitation, Egea et al (2011) and Keenan et al (2010) both suggested that there is a critical role of non stomatal limitation in photosynthesis during drought periods.

(3) In the third study, first, the elevation's influence on tree ring isotope signals was ignored as we had no information about some tree ring sites used for developing the linear model. Previous experiment studies showed that elevation exhibited negative effect on the foliar C_i/C_a value (Kohn, 2011) due to the lower O_2 and CO_2 partial pressure as suggested by Körner et al (1991). Other studies (Hultine and Marshall, 2000) implicated that plant employed different strategies to adopt the changing environment gradient, such as decreasing stomtal density, increasing leaf

nitrogen and leaf thickness., etc. All these suggested mechanism may indirectly affect the stomatal conductance or photosynthetic capacity, therefore on the foliar/tree ring isotopic signals. Wang et al (2015) derived the empirical relationship between C_i/C_a and climate, elevation using optimal stomatal theory (Prentice et al., 2014) based on large amounts of foliar 13C composition data. Another problem was the challenge to remove the tree age influence on tree ring isotopic signals. McCarroll and Pawellek (2001) used individual trees as samples to demonstrate the age-related trend in tree ring isotopic value. The plant tissue formed during the first years of tree life was generally depleted in 13C compared with the tissue formed later. Schleser and Jayasekera (1985) suggested the age effect was caused by re-assimilation of the respired air, which may already depleted in 13C by young trees. McDowell et al (2002) suggested the variation of tree dydraulic conductivity due to tree height may explain the age effect. The decreasing hydraulic conductivity can negatively affect leaf water potential, stomatal conductance and consequently leaf carbon fractionation. Finally, increasing nitrogen deposition may also significantly impact the tree ring carbon isotopic spatial and temporal variability. The increasing atmospheric nitrogen deposition, which originated from combustion of fossil fuels and fertilization, can both affect the plant (e.g. Horswill et al., 2008) and microbial communities (Chung et al., 2007). Thus, the interactive effect of CO_2 elevation and nitrogen deposition can greatly influence the plant physiology and carbon cycling (e.g. Ollinger et al., 2002). Tree-ring studies were particularly helpful to understand tree responses to their environment in the long term. The isotopic information stored in tree ring, in spite of the complex biogeochemical processes driving the value, allowed us to evaluate the influence of environmental condition on carbon dynamics. The derived C_i/C_a in tree ring was both controlled by stomatal conductance and photosynthetic capacity. However, the 13C composition alone cannot explain whether the C_i/C_a was more affected by stomatal conductance or plant photosynthetic activity. Generally, the δ18O in plant tissue is more closely related with stomatal conductance than photosynthetic activity, which

makes it possible for us to evaluate the contribution of photosynthetic capacity and stomatal conductance to C_i/C_a. Therefore, the dual-isotope approach on tree rings may have great potential to analyze drivers of both 13C and 18O and to develop conceptual modeling framework (e.g. Scheidegger et al., 2000).

REFERENCES

REFERENCES

Ainsworth, E.A., Long, S.P., 2005. What have we learned from 15 years of free-air CO_2 enrichment (FACE)? A meta-analytic review of the responses of photosynthesis, canopy properties and plant production to rising CO_2. New Phytol. 165, 351 – 372.

Ainsworth, E.A., Rogers, A., 2007. The response of photosynthesis and stomatal conductance to rising CO_2: mechanisms and environmental interactions. Plant. Cell Environ. 30, 258–270.

Alton, P.B., 2011. How useful are plant functional types in global simulations of the carbon, water, and energy cycles? J. Geophys. Res. 116, G01030. doi:10.1029/2010JG001430

Anderson, L.O., Malhi, Y., Aragão, L.E.O.C., Ladle, R., Arai, E., Barbier, N., Phillips, O., 2010. Remote sensing detection of droughts in Amazonian forest canopies. New Phytol. 187, 733–750.

Anderson, W.T., Bernasconi, S.M., McKenzie, J.A., Sauer, M., 1998. Oxygen and carbon isotopic record of climatic variability in tree ring cellulose (Picea abies): An example from central Switzerland (1913-1995). J. Geophys. Res. 103, 31625–31636.

Andreu-Hayles, L., Planells, O., Gutirrez, E., Muntan, E., Helle, G., Anchukaitis, K.J., Schleser, G.H., 2011. Long tree-ring chronologies reveal 20th century increases in water-use efficiency but no enhancement of tree growth at five Iberian pine forests. Glob. Chang. Biol. 17, 2095–2112. doi:10.1111/j.1365-2486.2010.02373.x

Andrews, A.E., Kofler, J.D., Trudeau, M.E., Williams, J.C., Neff, D.H., Masarie, K.A., Chao, D.Y., Kitzis, D.R., Novelli, P.C., Zhao, C.L., Dlugokencky, E.J., Lang, P.M., Crotwell, M.J., Fischer, M.L., Parker, M.J., Lee, J.T., Baumann, D.D., Desai, A.R., Stanier, C.O., De Wekker, S.F.J., Wolfe, D.E., Munger, J.W., Tans, P.P., 2014. CO_2, CO, and CH_4 measurements from tall towers in the NOAA Earth System Research Laboratory's Global Greenhouse Gas Reference Network: instrumentation, uncertainty analysis, and recommendations for future high-accuracy greenhouse gas monitoring efforts. Atmos. Meas. Tech. 7, 647–687. doi:10.5194/amt-7-647-2014

ARANIBAR, J.N., BERRY, J.A., RILEY, W.J., PATAKI, D.E., LAW, B.E., EHLERINGER, J.R., 2006. Combining meteorology, eddy fluxes, isotope measurements, and modeling to understand environmental controls of carbon isotope discrimination at the canopy scale. Glob. Chang. Biol. 12, 710–730. doi:10.1111/j.1365-2486.2006.01121.x

Arens, N.C., Jahren, A.H., Amundson, R., 2000. Can C3 plants faithfully record the carbon isotopic composition of atmospheric carbon dioxide? Paleobiology 26, 137–164.

Arneth, a, Lloyd, J., Santruckova, H., Bird, M., Grigoryev, S., Kalaschnikov, Y.N., Gleixner, G., Schulze, E.D., 2002. Response of central Siberian Scots Pine to soil water deficit and long term trends in atmospheric CO_2 concentration. Global Biogeochem. Cycles 16, 1.

Aubinet, M., Grelle, A., Ibrom, A., Rannik, Ü., Moncrieff, J., Foken, T., Kowalski, A.S., Martin, P.H., Berbigier, P., Bernhofer, C., 1999. Estimates of the annual net carbon and water exchange of forests: the EUROFLUX methodology. Adv. Ecol. Res. 30, 113–175.

Babst, F., Alexander, M.R., Szejner, P., Bouriaud, O., Klesse, S., Roden, J., Ciais, P., Poulter, B., Frank, D., Moore, D.J.P., Trouet, V., 2014. A tree-ring perspective on the terrestrial carbon cycle. Oecologia 176, 307–322. doi:10.1007/s00442-014-3031-6

BALDOCCHI, D., 1997. Measuring and modelling carbon dioxide and water vapour exchange over a temperate broad-leaved forest during the 1995 summer drought. Plant, Cell Environ. 20, 1108–1122. doi:10.1046/j.1365-3040.1997.d01-147.x

Baldocchi, D., 2008. TURNER REVIEW No. 15.'Breathing'of the terrestrial biosphere: lessons learned from a global network of carbon dioxide flux measurement systems. Aust. J. Bot. 56, 1–26.

Baldocchi, D.D., Hincks, B.B., Meyers, T.P., 1988. Measuring biosphere-atmosphere exchanges of biologically related gases with micrometeorological methods. Ecology 1331–1340.

Baldocchi, D., Falge, E., Gu, L., Olson, R., Hollinger, D., Running, S., Anthoni, P., Bernhofer, C., Davis, K., Evans, R., 2001. FLUXNET: A new tool to study the temporal and spatial variability of ecosystem-scale carbon dioxide, water vapor, and energy flux densities. Bull. Am. Meteorol. Soc. 82, 2415–2434.

Ball, J.T., Woodrow, I.E., Berry, J.A., 1987. A Model Predicting Stomatal Conductance and its Contribution to the Control of Photosynthesis under Different Environmental Conditions BT - Progress in Photosynthesis Research: Volume 4 Proceedings of the VIIth International Congress on Photosynthesis Pr, in: Biggins, J. (Ed.), . Springer Netherlands, Dordrecht, pp. 221–224. doi:10.1007/978-94-017-0519-6_48

Ballantyne, A.P., Miller, J.B., Baker, I.T., Tans, P.P., White, J.W.C., 2011. Novel applications of carbon isotopes in atmospheric CO_2: what can atmospheric measurements teach us about processes in the biosphere? Biogeosciences 8, 3093–3106. doi:10.5194/bg-8-3093-2011

Barnard, D.M., Bauerle, W.L., 2013. The implications of minimum stomatal conductance on modeling water flux in forest canopies. J. Geophys. Res. Biogeosciences 118, 1322–1333. doi:10.1002/jgrg.20112

Battipaglia, G., Saurer, M., Cherubini, P., Calfapietra, C., McCarthy, H.R., Norby, R.J., Francesca Cotrufo, M., 2013. Elevated CO_2 increases tree-level intrinsic water use efficiency: insights from carbon and oxygen isotope analyses in tree rings across three forest FACE sites. New Phytol. 197, 544–54. doi:10.1111/nph.12044

Beck, P.S.A., Juday, G.P., Alix, C., Barber, V.A., Winslow, S.E., Sousa, E.E., Heiser, P., Herriges, J.D., Goetz, S.J., 2011. Changes in forest productivity across Alaska consistent with biome shift. Ecol. Lett. 14, 373–9. doi:10.1111/j.1461-0248.2011.01598.x

Beer, C., Reichstein, M., Tomelleri, E., Ciais, P., Jung, M., Carvalhais, N., Rödenbeck, C., Arain, M.A., Baldocchi, D., Bonan, G.B., 2010. Terrestrial gross carbon dioxide uptake: global distribution and covariation with climate. Science (80). 329, 834 – 838.

Bell, J.E., Weng, E., Luo, Y., 2010. Ecohydrological responses to multifactor global change in a tallgrass prairie: A modeling analysis. J. Geophys. Res. Biogeosciences 115. doi:10.1029/2009JG001120

Bernacchi, C.J., Portis, A.R., Nakano, H., von Caemmerer, S., Long, S.P., 2002. Temperature Response of Mesophyll Conductance. Implications for the Determination of Rubisco Enzyme Kinetics and for Limitations to Photosynthesis in Vivo. Plant Physiol. 130 , 1992–1998. doi:10.1104/pp.008250

Bernhofer, C., Aubinet, M., Clement, R., Grelle, A., Grünwald, T., Ibrom, A., Jarvis, P., Rebmann, C., Schulze, E.-D., Tenhunen, J.D., 2003. Spruce Forests (Norway and Sitka Spruce, Including Douglas Fir): Carbon and Water Fluxes and Balances, Ecological and Ecophysiological Determinants BT- Fluxes of Carbon, Water and Energy of European Forests, in: Valentini, R. (Ed.), . Springer Berlin Heidelberg, Berlin, Heidelberg, pp. 99–123. doi:10.1007/978-3-662-05171-9_6

Bert, D., Leavitt, S.W., Dupouey, J.-L., 1997. Variations of Wood Δ13 C and Water-Use Efficiency of Abies Alba During the Last Century. Ecology 78, 1588–1596. doi:10.1890/0012-9658(1997)078[1588:VOWCAW]2.0.CO2

Beven, K., Freer, J., 2001. Equifinality, data assimilation, and uncertainty estimation in mechanistic modelling of complex environmental systems using the GLUE methodology. J. Hydrol. 249, 11–29. doi:http://dx.doi.org/10.1016/S0022-1694(01)00421-8

Billings, S.A., Boone, A.S., Stephen, F.M., 2016. Tree-ring δ13C and δ18O, leaf δ13C and wood and leaf N status demonstrate tree growth strategies and predict susceptibility to disturbance. Tree Physiol. 36, 576–588. doi:10.1093/treephys/tpw010

Billings, S.A., Boone, A.S., Stephen, F.M., 2016. Tree-ring δ13C and δ18O, leaf δ13C and wood and leaf N status demonstrate tree growth strategies and predict susceptibility to disturbance. Tree Physiol. doi:10.1093/treephys/tpw010

Birdsey, R.A., Lewis, G.M., 2003. Current and historical trends in use, management, and disturbance of US forestlands. CRC Press, Baton Rouge, FL.

Blyth, E., Clark, D.B., Ellis, R., Huntingford, C., Los, S., Pryor, M., Best, M., Sitch, S., 2011. A comprehensive set of benchmark tests for a land surface model of simultaneous fluxes of water and carbon at both the global and seasonal scale. Geosci. Model Dev. 4, 255–269. doi:10.5194/gmd-4-255-2011

Bodin, P.E., Gagen, M., McCarroll, D., Loader, N.J., Jalkanen, R., Robertson, I., R Switsur, V., Waterhouse, J.S., Woodley, E.J., Young, G.H.F., Alton, P.B., 2013. Comparing the performance of different stomatal conductance models using modelled and measured plant carbon isotope ratios (δ13C): implications for assessing physiological forcing. Glob. Chang. Biol. 19, 1709–1719. doi:10.1111/gcb.12192

Bonan, G.B., 2008. Forests and climate change: forcings, feedbacks, and the climate benefits of forests. Science (80-.). 320, 1444–1449.

Bowling, D.R., Tans, P.P., Monson, R.K., 2001. Partitioning net ecosystem carbon exchange with isotopic fluxes of CO_2. Glob. Chang. Biol. 7, 127–145. doi:10.1046/j.1365-2486.2001.00400.x

Bowling, D.R., McDowell, N.G., Bond, B.J., Law, B.E., Ehleringer, J.R., n.d. 13C content of ecosystem respiration is linked to precipitation and vapor pressure deficit. Oecologia 131, 113–124. doi:10.1007/s00442-001-0851-y

Bracho, R., Starr, G., Gholz, H.L., Martin, T.A., Cropper, W.P., Loescher, H.W., 2012. Controls on carbon dynamics by ecosystem structure and climate for southeastern US slash pine plantations. Ecol. Monogr. 82, 101–128.

Brooks, J.R., Flanagan, L.B., Ehleringer, J.R., 1998. Responses of boreal conifers to climate fluctuations: indications from tree-ring widths and carbon isotope analyses. Can. J. For. Res. 28, 524–533.

Buchmann, N., Schulze, E.-D., 1999. Net CO_2 and H2O fluxes of terrestrial ecosystems. Global Biogeochem. Cycles 13, 751–760. doi:10.1029/1999GB900016

Bunce, J.A., 2004. Carbon dioxide effects on stomatal responses to the environment and water use by crops under field conditions. Oecologia 140, 1–10.

Canadell, J.G., Le Quéré, C., Raupach, M.R., Field, C.B., Buitenhuis, E.T., Ciais, P., Conway, T.J., Gillett, N.P., Houghton, R.A., Marland, G., 2007. Contributions to accelerating atmospheric CO_2 growth from economic activity, carbon intensity, and efficiency of natural sinks. Proc. Natl. Acad. Sci. 104, 18866–18870.

Chapin III, F.S., Matson, P.A., Vitousek, P., 2011. Principles of terrestrial ecosystem ecology. Springer Science & Business Media.

Chen, M., Zhuang, Q., Cook, D.R., Coulter, R., Pekour, M., Scott, R.L., Munger, J.W., Bible, K., 2011. Quantification of terrestrial ecosystem carbon dynamics in the conterminous United States combining a process-based biogeochemical model and MODIS and AmeriFlux data. Biogeosciences Discuss. 8, 2721.

Chung, H., Zak, D.R., Reich, P.B., Ellsworth, D.S., 2007. Plant species richness, elevated CO_2, and atmospheric nitrogen deposition alter soil microbial community composition and function. Glob. Chang. Biol. 13, 980–989.

Ciais, P., Tans, P.P., White, J.W.C., Trolier, M., Francey, R.J., Berry, J.A., Randall, D.R., Sellers, P.J., Collatz, J.G., Schimel, D.S., 1995. Partitioning of ocean and land uptake of CO_2 as inferred by δ13C measurements from the NOAA Climate Monitoring and Diagnostics Laboratory Global Air Sampling Network. J. Geophys. Res. 100, 5051. doi:10.1029/94JD02847

Collatz, G.J., Ribas-Carbo, M., Berry, J.A., 1992. Coupled Photosynthesis-Stomatal Conductance Model for Leaves of C4 Plants. Funct. Plant Biol. 19, 519–538.

Conley, M.M., Kimball, B.A., Brooks, T.J., Pinter, P.J., Hunsaker, D.J., Wall, G.W., Adam, N.R., LaMorte, R.L., Matthias, A.D., Thompson, T.L., 2001. CO_2 enrichment increases water‐use efficiency in sorghum. New Phytol. 151, 407–412.

Cowan, I.R., Farquhar, G.D., 1977. Stomatal functioning in relation to leaf metabolism and environment, in: Jennings, D.H. (Ed.), Integration of Activity in the Higher Plants. Cambridge University Press, Cambridge, UK, pp. 471–505.

Curtis, P.S., Wang, X., 1998. A meta-analysis of elevated CO_2 effects on woody plant mass, form, and physiology. Oecologia 113, 299–313.

Dai, A., 2013. Increasing drought under global warming in observations and models. Nat. Clim. Chang. 3, 52–58.

Dai, Y., Dickinson, R.E., Wang, Y.-P., 2004. A two-big-leaf model for canopy temperature, photosynthesis, and stomatal conductance. J. Clim. 17, 2281–2299.

DAMOUR, G., SIMONNEAU, T., COCHARD, H., URBAN, L., 2010. An overview of models of stomatal conductance at the leaf level. Plant. Cell Environ. 33, 1419–1438. doi:10.1111/j.1365-3040.2010.02181.x

Davis, K.J., Bakwin, P.S., Yi, C., Berger, B.W., Zhao, C., Teclaw, R.M., Isebrands, J.G., 2003. The annual cycles of CO_2 and H2O exchange over a northern mixed forest as observed from a very tall tower. Glob. Chang. Biol. 9, 1278–1293. doi:10.1046/j.1365-2486.2003.00672.x

De Kauwe, M.G., Kala, J., Lin, Y.-S., Pitman, A.J., Medlyn, B.E., Duursma, R.A., Abramowitz, G., Wang, Y.-P., Miralles, D.G., 2015. A test of an optimal stomatal conductance scheme within the CABLE land surface model. Geosci. Model Dev. 8, 431–452. doi:10.5194/gmd-8-431-2015

De Kauwe, M.G., Medlyn, B.E., Zaehle, S., Walker, A.P., Dietze, M.C., Hickler, T., Jain, A.K., Luo, Y., Parton, W.J., Prentice, I.C., Smith, B., Thornton, P.E., Wang, S., Wang, Y.-P., Wårlind, D., Weng, E., Crous, K.Y., Ellsworth, D.S., Hanson, P.J., Seok Kim, H.-, Warren, J.M., Oren, R., Norby, R.J., 2013. Forest water use and water use efficiency at elevated CO_2: a model-data intercomparison at two contrasting temperate forest FACE sites. Glob. Chang. Biol. 19, 1759–1779. doi:10.1111/gcb.12164

de Pury, D.G.G., Ceulemans, R., 1997. Scaling-Up Carbon Fluxes from Leaves to Stands in a Patchy Coniferous / Deciduous Forest BT - Impacts of Global Change on Tree Physiology and Forest Ecosystems: Proceedings of the International Conference on Impacts of Global Change on Tree Physiology and Forest Ecosystems, held 26–29 November 1996, Wageningen, The Netherlands, in: Mohren, G.M.J., Kramer, K., Sabaté, S. (Eds.), . Springer Netherlands, Dordrecht, pp. 263–272. doi:10.1007/978-94-015-8949-9_34

Dekker, S.C., Groenendijk, M., Booth, B.B.B., Huntingford, C., Cox, P.M., 2016. Spatial and temporal variations in plant water-use efficiency inferred from tree-ring, eddy covariance and atmospheric observations. Earth Syst. Dyn. 7, 525–533. doi:10.5194/esd-7-525-2016

Deng, F., Chen, J.M., Pan, Y., Peters, W., Birdsey, R., McCullough, K., Xiao, J., 2013. The use of forest stand age information in an atmospheric CO_2 inversion applied to North America. Biogeosciences 10, 5335–5348. doi:10.5194/bg-10-5335-2013

Deng, Q., Zhou, G., Liu, J., Liu, S., Duan, H., Zhang, D., 2010. Responses of soil respiration to elevated carbon dioxide and nitrogen addition in young subtropical forest ecosystems in China. Biogeosciences 7, 315–328.

Deng, X., Joly, R.J., Hahn, D.T., 1990. The influence of plant water deficit on photosynthesis and translocation of 14C‐labeled assimilates in cacao seedlings. Physiol. Plant. 78, 623‐627.

Denning, A.S., Fung, I.Y., Randall, D., 1995. Latitudinal gradient of atmospheric CO_2 due to seasonal exchange with land biota. Nature 376, 240–243.

Dermody, O., Weltzin, J.F., Engel, E.C., Allen, P., Norby, R.J., 2007. How do elevated CO_2, warming, and reduced precipitation interact to affect soil moisture and LAI in an old field ecosystem? Plant Soil 301, 255–266.

Desai, A.R., Richardson, A.D., Moffat, A.M., Kattge, J., Hollinger, D.Y., Barr, A., Falge, E., Noormets, A., Papale, D., Reichstein, M., 2008. Cross-site evaluation of eddy covariance GPP and RE decomposition techniques. Agric. For. Meteorol. 148, 821–838.

Diefendorf, A.F., Mueller, K.E., Wing, S.L., Koch, P.L., Freeman, K.H., 2010. Global patterns in leaf 13C discrimination and implications for studies of past and future climate. Proc. Natl. Acad. Sci. 107, 5738–5743.

Dijkstra, F.A., Blumenthal, D., Morgan, J.A., Pendall, E., Carrillo, Y., Follett, R.F., 2010. Contrasting effects of elevated CO_2 and warming on nitrogen cycling in a semiarid grassland. New Phytol. 187, 426–437.

Drake, B.G., Gonzàlez-Meler, M.A., Long, S.P., 1997. More efficient plants: a consequence of rising atmospheric CO_2? Annu. Rev. Plant Biol. 48, 609–639.

Dupouey, J.-L., Leavitt, S., Choisnel, E., Jourdain, S., 1993. Modelling carbon isotope fractionation in tree rings based on effective evapotranspiration and soil water status. Plant, Cell {&} Environ. 16, 939–947. doi:10.1111/j.1365-3040.1993.tb00517.x

Duquesnay, a, Breda, N., Stievenard, M., Dupouey, J.L., 1998. Changes of tree-ring delta C-13 and water-use efficiency of beech (Fagus sylvatica L.) in north-eastern France during the past century. Plant Cell Environ. 21, 565–572. doi:10.1046/j.1365-3040.1998.00304.x

Duursma, R.A., Payton, P., Bange, M.P., Broughton, K.J., Smith, R.A., Medlyn, B.E., Tissue, D.T., 2013. Near-optimal response of instantaneous transpiration efficiency to vapour pressure deficit, temperature and CO_2 in cotton (Gossypium hirsutum L.). Agric. For. Meteorol. 168, 168–176. doi:http://dx.doi.org/10.1016/j.agrformet.2012.09.005

Eby, M., Zickfeld, K., Montenegro, A., Archer, D., Meissner, K.J., Weaver, A.J., 2009. Lifetime of anthropogenic climate change: millennial time scales of potential CO_2 and surface temperature perturbations. J. Clim. 22, 2501–2511.

Egea, G., Verhoef, A., Vidale, P.L., 2011. Towards an improved and more flexible representation of water stress in coupled photosynthesis–stomatal conductance models. Agric. For. Meteorol. 151, 1370–1384. doi:http://dx.doi.org/10.1016/j.agrformet.2011.05.019

Emmett, B.A., Beier, C., Estiarte, M., Tietema, A., Kristensen, H.L., Williams, D., Penuelas, J., Schmidt, I., Sowerby, A., 2004. The response of soil processes to climate change: results from manipulation studies of shrublands across an environmental gradient. Ecosystems 7, 625–637.

Eugster, W., Zeyer, K., Zeeman, M., Michna, P., Zingg, A., Buchmann, N., Emmenegger, L., 2007. Methodical study of nitrous oxide eddy covariance measurements using quantum cascade laser spectrometery over a Swiss forest. Biogeosciences 4, 927–939. doi:10.5194/bg-4-927-2007

Evans, J.R., Von Caemmerer, S., 1996. Carbon Dioxide Diffusion inside Leaves. Plant Physiol. 110, 339–346.

Farquhar, G.D., O'Leary, M.H., Berry, J.A., 1982. On the Relationship Between Carbon Isotope Discrimination and the Intercellular Carbon Dioxide Concentration in Leaves. Funct. Plant Biol. 9, 121–137.

Farquhar, G.D., Richards, R.A., 1984. Isotopic Composition of Plant Carbon Correlates With Water-Use Efficiency of Wheat Genotypes. Funct. Plant Biol. 11, 539–552.

Farquhar, G.D., von Caemmerer, S. von, Berry, J.A., 1980. A biochemical model of photosynthetic CO_2 assimilation in leaves of C3 species. Planta 149, 78–90.

Farquhar, G.D., Ehleringer, J.R., Hubick, K.T., 1989. Carbon isotope discrimination and photosynthesis. Annu. Rev. Plant Biol. 40, 503–537.

Faure, G., Mensing, T.M., 2005. Isotopes: principles and applications. John Wiley & Sons Inc.

Feng, X., n.d. Long-term ci /ca response of trees in western North America to atmospheric CO_2 concentration derived from carbon isotope chronologies. Oecologia 117, 19–25. doi:10.1007/s004420050626

Feng, X., 1999. Trends in intrinsic water-use efficiency of natural trees for the past 100-200 years: A response to atmospheric CO_2 concentration. Geochim. Cosmochim. Acta 63, 1891–1903. doi:10.1016/S0016-7037(99)00088-5

Feng, X., Epstein, S., 1995. Carbon isotopes of trees from arid environments and implications for reconstructing atmospheric CO_2 concentration. Geochim. Cosmochim. Acta 59, 2599–2608. doi:10.1016/0016-7037(95)00152-2

Fernández-de-Uña, L., McDowell, N.G., Cañellas, I., Gea-Izquierdo, G., 2016. Disentangling the effect of competition, CO_2 and climate on intrinsic water-use efficiency and tree growth. J. Ecol. n/a–n/a. doi:10.1111/1365-2745.12544

Field, C.B., Randerson, J.T., Malmström, C.M., 1995. Global net primary production: combining ecology and remote sensing. Remote Sens. Environ. 51, 74–88.

Fisher, J.B., Tu, K.P., Baldocchi, D.D., 2008. Global estimates of the land–atmosphere water flux based on monthly AVHRR and ISLSCP-II data, validated at 16 FLUXNET sites. Remote Sens. Environ. 112, 901–919. doi:http://dx.doi.org/10.1016/j.rse.2007.06.025

Flexas, J., Díaz-Espejo, A., Conesa, M.A., Coopman, R.E., Douthe, C., Gago, J., Gallé, A., Galmés, J., Medrano, H., Ribas-Carbo, M., Tomàs, M., Niinemets, U., 2015. Mesophyll conductance to CO_2 and Rubisco as targets for improving intrinsic water use efficiency in C3 plants. Plant, Cell Environ. 965–982. doi:10.1111/pce.12622

Foken, T., Wichura, B., 1996. Tools for quality assessment of surface-based flux measurements. Agric. For. Meteorol. 78, 83–105.

Franks, P.J., Adams, M.A., Amthor, J.S., Barbour, M.M., Berry, J.A., Ellsworth, D.S., Farquhar, G.D., Ghannoum, O., Lloyd, J., McDowell, N., Norby, R.J., Tissue, D.T., von Caemmerer, S., 2013. Sensitivity of plants to changing atmospheric CO_2 concentration: from the geological past to the next century. New Phytol. 197, 1077–94. doi:10.1111/nph.12104

Friedlingstein, P., Cox, P., Betts, R., Bopp, L., von Bloh, W., Brovkin, V., Cadule, P., Doney, S., Eby, M., Fung, I., Bala, G., John, J., Jones, C., Joos, F., Kato, T., Kawamiya, M., Knorr, W., Lindsay, K., Matthews, H.D., Raddatz, T., Rayner, P., Reick, C., Roeckner, E., Schnitzler, K.-G., Schnur, R., Strassmann, K., Weaver, A.J., Yoshikawa, C., Zeng, N., 2006. Climate–Carbon Cycle Feedback Analysis: Results from the C4MIP Model Intercomparison. J. Clim. 19, 3337–3353. doi:10.1175/JCLI3800.1

Fu, D., Chen, B., Zhang, H., Wang, J., Black, T.A., Amiro, B., Bohrer, G., Bolstad, P., Coulter, R., Rahman, F., 2014. Estimating landscape net ecosystem exchange at high spatial–temporal resolution based on Landsat data, an improved upscaling model framework, and eddy covariance flux measurements. Remote Sens. Environ. 141, 90–104.

Fung, I., Field, C.B., Berry, J.A., Thompson, M. V, Randerson, J.T., Malmström, C.M., Vitousek, P.M., Collatz, G.J., Sellers, P.J., Randall, D.A., Denning, A.S., Badeck, F., John, J., 1997. Carbon 13 exchanges between the atmosphere and biosphere. Global Biogeochem. Cycles 11, 507–533. doi:10.1029/97GB01751

GAGEN, M., FINSINGER, W., WAGNER-CREMER, F., MCCARROLL, D., LOADER, N.J., ROBERTSON, I., JALKANEN, R., YOUNG, G., KIRCHHEFER, A., 2011. Evidence of changing intrinsic water-use efficiency under rising atmospheric CO_2 concentrations in Boreal Fennoscandia from subfossil leaves and tree ring δ13C ratios. Glob. Chang. Biol. 17, 1064–1072. doi:10.1111/j.1365-2486.2010.02273.x

Gagen, M., McCarroll, D., Loader, N.J., Robertson, I., Jalkanen, R., Anchukaitis, K.J., 2007. Exorcising thesegment length curse': summer temperature reconstruction since AD 1640 using non-detrended stable carbon isotope ratios from pine trees in northern Finland. The Holocene 17, 435–446.

Geels, C., Gloor, M., Ciais, P., Bousquet, P., Peylin, P., Vermeulen, A.T., Dargaville, R., Aalto, T., Brandt, J., Christensen, J.H., Frohn, L.M., Haszpra, L., Karstens, U., Rödenbeck, C., Ramonet, M., Carboni, G., Santaguida, R., 2007. Comparing atmospheric transport models for future regional inversions over Europe ; Part 1: mapping the atmospheric CO_2 signals. Atmos. Chem. Phys. 7, 3461–3479. doi:10.5194/acp-7-3461-2007

Gentsch, L., Hammerle, A., Sturm, P., Ogée, J., Wingate, L., Siegwolf, R., Plüss, P., Baur, T., Buchmann, N., Knohl, A., 2014. Carbon isotope discrimination during branch photosynthesis of Fagus sylvatica: a Bayesian modelling approach. Plant. Cell Environ. 37, 1516–1535.

Gill, R.A., Polley, H.W., Johnson, H.B., Anderson, L.J., Maherali, H., Jackson, R.B., 2002. Nonlinear grassland responses to past and future atmospheric CO_2. Nature 417, 279–282.

Gioli, B., Miglietta, F., De Martino, B., Hutjes, R.W.A., Dolman, H.A.J., Lindroth, A., Schumacher, M., Sanz, M.J., Manca, G., Peressotti, A., others, 2004. Comparison between tower and aircraft-based eddy covariance fluxes in five European regions. Agric. For. Meteorol. 127, 1–16.

GOULDEN, M.L., MUNGER, J.W., FAN, S.-M., DAUBE, B.C., WOFSY, S.C., 1996. Measurements of carbon sequestration by long-term eddy covariance: methods and a critical evaluation of accuracy. Glob. Chang. Biol. 2, 169–182. doi:10.1111/j.1365-2486.1996.tb00070.x

GRASSI, G., MAGNANI, F., 2005. Stomatal, mesophyll conductance and biochemical limitations to photosynthesis as affected by drought and leaf ontogeny in ash and oak trees. Plant. Cell Environ. 28, 834–849. doi:10.1111/j.1365-3040.2005.01333.x

Griepentrog, M., Eglinton, T.I., Hagedorn, F., Schmidt, M.W.I., Wiesenberg, G.L.B., 2015. Interactive effects of elevated CO_2 and nitrogen deposition on fatty acid molecular and isotope composition of above- and belowground tree biomass and forest soil fractions. Glob. Chang. Biol. 21, 473–486. doi:10.1111/gcb.12666

Griffis, T.J., Baker, J.M., Sargent, S.D., Erickson, M., Corcoran, J., Chen, M., Billmark, K., 2010. Influence of C4 vegetation on $13CO_2$ discrimination and isoforcing in the upper Midwest, United States. Global Biogeochem. Cycles 24. doi:10.1029/2009GB003768

Groenendijk, M., 2015. Spatial and temporal variations in plant Water Use Efficiency inferred from tree-ring, eddy covariance and atmospheric observations. PhD Propos. 1, 1–25. doi:10.1017/CBO9781107415324.004

GRÜNWALD, T., BERNHOFER, C., 2007. A decade of carbon, water and energy flux measurements of an old spruce forest at the Anchor Station Tharandt. Tellus B 59, 387–396. doi:10.1111/j.1600-0889.2007.00259.x

Gu, Y., Brown, J.F., Verdin, J.P., Wardlow, B., 2007. A five-year analysis of MODIS NDVI and NDWI for grassland drought assessment over the central Great Plains of the United States. Geophys. Res. Lett. 34.

Gu, Y., Hunt, E., Wardlow, B., Basara, J.B., Brown, J.F., Verdin, J.P., 2008. Evaluation of MODIS NDVI and NDWI for vegetation drought monitoring using Oklahoma Mesonet soil moisture data. Geophys. Res. Lett. 35.

Hanan, N.P., Burba, G., Verma, S.B., Berry, J.A., Suyker, A., Walter-Shea, E.A., 2002. Inversion of net ecosystem CO_2 flux measurements for estimation of canopy PAR absorption. Glob. Chang. Biol. 8, 563–574. doi:10.1046/j.1365-2486.2002.00488.x

Hanson, P.J., Amthor, J.S., Wullschleger, S.D., Wilson, K.B., Grant, R.F., Hartley, A., Hui, D., Hunt E Raymond, J., Johnson, D.W., Kimball, J.S., 2004. Oak forest carbon and water simulations: model intercomparisons and evaluations against independent data. Ecol. Monogr. 74, 443–489.

Hargrove, W.W., Hoffman, F.M., Law, B.E., 2003. New analysis reveals representativeness of the AmeriFlux network. Eos, Trans. Am. Geophys. Union 84, 529–535.

Hartmann, J., West, A.J., Renforth, P., Köhler, P., De La Rocha, C.L., Wolf-Gladrow, D.A., Dürr, H.H., Scheffran, J., 2013. Enhanced chemical weathering as a geoengineering strategy to reduce atmospheric carbon dioxide, supply nutrients, and mitigate ocean acidification. Rev. Geophys. 51, 113–149.

Hasper, T.B., Wallin, G., Lamba, S., Hall, M., Jaramillo, F., Laudon, H., Linder, S., Medhurst, J.L., Räntfors, M., Sigurdsson, B.D., Uddling, J., 2016. Water use by Swedish boreal forests in a changing climate. Funct. Ecol. 30, 690–699. doi:10.1111/1365-2435.12546

Haszpra, L., Barcza, Z., Hidy, D., Szilágyi, I., Dlugokencky, E., Tans, P., 2008. Trends and temporal variations of major greenhouse gases at a rural site in Central Europe. Atmos. Environ. 42, 8707–8716. doi:10.1016/j.atmosenv.2008.09.012

He, Y., Zhuang, Q., David McGuire, A., Liu, Y., Chen, M., 2013. Alternative ways of using field-based estimates to calibrate ecosystem models and their implications for carbon cycle studies. J. Geophys. Res. Biogeosciences. doi:10.1002/jgrg.20080

Helama, S., Arppe, L., Uusitalo, J., Mäkelä, H.M., Oinonen, M., Mielikäinen, K., 2016. Coexisting responses in tree-ring δ13C to high-latitude climate variability under elevated CO_2: A critical examination of climatic effects and systematic discrimination rate changes. Agric. For. Meteorol. 226-227, 199–212. doi:10.1016/j.agrformet.2016.06.005

Helliker, B.R., 2004. Estimates of net CO_2 flux by application of equilibrium boundary layer concepts to CO_2 and water vapor measurements from a tall tower. J. Geophys. Res. 109, D20106. doi:10.1029/2004JD004532

Hilasvuori, E., Berninger, F., Sonninen, E., Tuomenvirta, H., Jungner, H., 2009. Stability of climate signal in carbon and oxygen isotope records and ring width from Scots pine (Pinus sylvestris L.) in Finland. J. Quat. Sci. 24, 469–480.

Hirata, R., Saigusa, N., Yamamoto, S., Ohtani, Y., Ide, R., Asanuma, J., Gamo, M., Hirano, T., Kondo, H., Kosugi, Y., 2008. Spatial distribution of carbon balance in forest ecosystems across East Asia. Agric. For. Meteorol. 148, 761–775.

Holzkämper, S., Kuhry, P., Kultti, S., Gunnarson, B., Sonninen, E., 2009. Stable Isotopes in Tree Rings as Proxies for Winter Precipitation Changes in the Russian Arctic over the Past 150 Years. Geochronometria 32, 37–46. doi:10.2478/v10003-008-0025-6

Horswill, P., O'Sullivan, O., Phoenix, G.K., Lee, J.A., Leake, J.R., 2008. Base cation depletion, eutrophication and acidification of species-rich grasslands in response to long-term simulated nitrogen deposition. Environ. Pollut. 155, 336–349.

Hovenden, M.J., Newton, P.C.D., Carran, R.A., Theobald, P., Wills, K.E., Vander Schoor, J.K., Williams, A.L., Osanai, Y., 2008. Warming prevents the elevated CO_2-induced reduction in available soil nitrogen in a temperate, perennial grassland. Glob. Chang. Biol. 14, 1018–1024.

Hsieh, P., Veeramah, K.R., Lachance, J., Tishkoff, S.A., Wall, J.D., Hammer, M.F., Gutenkunst, R.N., Biology, E., Biology, C., Francisco, S., Brook, S., 2015. 1,2* ,. doi:10.1074/jbc.M115.679969

Huang, M., Piao, S., Sun, Y., Ciais, P., Cheng, L., Mao, J., Poulter, B., Shi, X., Zeng, Z., Wang, Y., 2015. Change in terrestrial ecosystem water-use efficiency over the last three decades. Glob. Chang. Biol. 21, 2366–78. doi:10.1111/gcb.12873

Huang, M., Piao, S., Zeng, Z., Peng, S., Ciais, P., Cheng, L., Mao, J., Poulter, B., Shi, X., Yao, Y., Yang, H., Wang, Y., 2015. Seasonal responses of terrestrial ecosystem water-use efficiency to climate change. Glob. Chang. Biol. doi:10.1111/gcb.13180

Huete, A., Didan, K., Miura, T., Rodriguez, E.P., Gao, X., Ferreira, L.G., 2002. Overview of the radiometric and biophysical performance of the MODIS vegetation indices. Remote Sens. Environ. 83, 195–213.

Hultine, K.R., Marshall, J.D., 2000. Altitude trends in conifer leaf morphology and stable carbon isotope composition. Oecologia 123, 32–40.

Iman, R.L., Helton, J.C., 1988. An Investigation of Uncertainty and Sensitivity Analysis Techniques for Computer Models. Risk Anal. 8, 71–90. doi:10.1111/j.1539-6924.1988.tb01155.x

Ito, A., Inatomi, M., 2012. Water-Use Efficiency of the Terrestrial Biosphere: A Model Analysis Focusing on Interactions between the Global Carbon and Water Cycles. J. Hydrometeorol. 13, 681–694. doi:10.1175/JHM-D-10-05034.1

Janssens, I.A., Freibauer, A., Ciais, P., Smith, P., Nabuurs, G.-J., Folberth, G., Schlamadinger, B., Hutjes, R.W.A., Ceulemans, R., Schulze, E.-D., 2003. Europe's terrestrial biosphere absorbs 7 to 12% of European anthropogenic CO_2 emissions. Science (80-.). 300, 1538–1542.

Jasechko, S., Sharp, Z.D., Gibson, J.J., Birks, S.J., Yi, Y., Fawcett, P.J., 2013. Terrestrial water fluxes dominated by transpiration. Nature 496, 347–350.

Jennings, K., 2013. Response of tree growth and water use efficiency to climate and nitrogen deposition in a temperate deciduous forest in the northeastern US. UNIVERSITY OF NEW HAMPSHIRE.

Jennings, K.A., Guerrieri, R., Vadeboncoeur, M.A., Asbjornsen, H., 2016. Response of Quercus velutina growth and water use efficiency to climate variability and nitrogen fertilization in a temperate deciduous forest in the northeastern USA. Tree Physiol. . doi:10.1093/treephys/tpw003

Jung, M., Verstraete, M., Gobron, N., Reichstein, M., Papale, D., Bondeau, A., Robustelli, M., Pinty, B., 2008. Diagnostic assessment of European gross primary production. Glob. Chang. Biol. 14, 2349–2364.

Kaplan, J.O., Prentice, I.C., Buchmann, N., 2002. The stable carbon isotope composition of the terrestrial biosphere: Modeling at scales from the leaf to the globe. Global Biogeochem. Cycles 16, 8–11. doi:10.1029/2001GB001403

Kato, T., Tang, Y., 2008. Spatial variability and major controlling factors of CO_2 sink strength in Asian terrestrial ecosystems: evidence from eddy covariance data. Glob. Chang. Biol. 14, 2333–2348.

Kattge, J., Diaz, S., Lavorel, S., Prentice, I.C., Leadley, P., Bönisch, G., Garnier, E., Westoby, M., Reich, P.B., Wright, I.J., 2011. TRY–a global database of plant traits. Glob. Chang. Biol. 17, 2905–2935.

Keeling, C.D., Whorf, T.P., Wahlen, M., Plicht, J. van der, 1995. Interannual extremes in the rate of rise of atmospheric carbon dioxide since 1980. Nature 375, 666–670.

Keenan, T., Garc'\ia, R., Friend, A.D., Zaehle, S., Gracia, C., Sabate, S., 2009. Improved understanding of drought controls on seasonal variation in Mediterranean forest canopy CO_2 and water fluxes through combined in situ measurements and ecosystem modelling. Biogeosciences 6, 1423–1444. doi:10.5194/bg-6-1423-2009

Keenan, T.F., Carbone, M.S., Reichstein, M., Richardson, A.D., 2011. The model–data fusion pitfall: assuming certainty in an uncertain world. Oecologia 167, 587–597. doi:10.1007/s00442-011-2106-x

Keenan, T.F., Hollinger, D.Y., Bohrer, G., Dragoni, D., Munger, J.W., Schmid, H.P., Richardson, A.D., 2013. Increase in forest water-use efficiency as atmospheric carbon dioxide concentrations rise. Nature 499, 324–327.

KEENAN, T., SABATE, S., GRACIA, C., 2010. The importance of mesophyll conductance in regulating forest ecosystem productivity during drought periods. Glob. Chang. Biol. 16, 1019–1034. doi:10.1111/j.1365-2486.2009.02017.x

Keppel‐Aleks, G., Wolf, A.S., Mu, M., Doney, S.C., Morton, D.C., Kasibhatla, P.S., Miller, J.B., Dlugokencky, E.J., Randerson, J.T., 2014. Separating the influence of temperature, drought, and fire on interannual variability in atmospheric CO_2. Global Biogeochem. Cycles.

Kirdyanov, A. V, Treydte, K.S., Nikolaev, A., Helle, G., Schleser, G.H., 2008. Climate signals in tree-ring width, density and δ13 C from larches in Eastern Siberia (Russia). Chem. Geol. 252, 31–41.

Kirschbaum, M.U.F., King, D.A., Comins, H.N., McMurtrie, R.E., Medlyn, B.E., Pongracic, S., Murty, D., Keith, H., Raison, R.J., Khanna, P.K., 1994. Modelling forest response to increasing CO_2 concentration under nutrient‐limited conditions. Plant. Cell Environ. 17, 1081–1099.

Knohl, A., Schulze, E.-D., Kolle, O., Buchmann, N., 2003. Large carbon uptake by an unmanaged 250-year-old deciduous forest in Central Germany. Agric. For. Meteorol. 118, 151–167.

Knorr, W., Heimann, M., 1995. Impact of drought stress and other factors on seasonal land biosphere CO_2 exchange studied through an atmospheric tracer transport model. Tellus B 47, 471–489.

Knorr, W., Scholze, M., Gobron, N., Pinty, B., Kaminski, T., 2005. Global‐scale drought caused atmospheric CO_2 increase. Eos, Trans. Am. Geophys. Union 86, 178‐181.

Körner, C., Farquhar, G.D., Wong, S.C., 1991. Carbon isotope discrimination by plants follows latitudinal and altitudinal trends. Oecologia 88, 30–40. doi:10.1007/BF00328400

Lagergren, F., Lindroth, A., Dellwik, E., Ibrom, A., Lankreijer, H., Launiainen, S., Mölder, M., Kolari, P., Pilegaard, K.I.M., Vesala, T., 2008. Biophysical controls on CO_2 fluxes of three northern forests based on long-term eddy covariance data. Tellus B 60, 143–152.

Lambers, H., Chapin, F.S., Pons, T.L., 2008. Plant Water Relations BT - Plant Physiological Ecology, in: Lambers, H., Chapin, F.S., Pons, T.L. (Eds.), . Springer New York, New York, NY, pp. 163–223. doi:10.1007/978-0-387-78341-3_5

Lambin, E.F., Geist, H.J., Lepers, E., 2003. Dynamics of land-use and land-cover change in tropical regions. Annu. Rev. Environ. Resour. 28, 205–241.

Larsen, K.S., Andresen, L.C., Beier, C., Jonasson, S., Albert, K.R., Ambus, P.E.R., Arndal, M.F., Carter, M.S., Christensen, S., Holmstrup, M., 2011. Reduced N cycling in response to elevated CO_2, warming, and drought in a Danish heathland: synthesizing results of the CLIMAITE project after two years of treatments. Glob. Chang. Biol. 17, 1884–1899.

Lauvaux, T., Schuh, A.E., Bocquet, M., Wu, L., Richardson, S., Miles, N., Davis, K.J., 2012. Network design for mesoscale inversions of CO_2 sources and sinks. Tellus B; Vol 64.

Law, B.E., Anthoni, P.M., Aber, J.D., 2000. Measurements of gross and net ecosystem productivity and water vapour exchange of a Pinus ponderosa ecosystem, and an evaluation of two generalized models. Glob. Chang. Biol. 6, 155–168.

Law, B.E., Falge, E., Gu, L. V, Baldocchi, D.D., Bakwin, P., Berbigier, P., Davis, K., Dolman, A.J., Falk, M., Fuentes, J.D., 2002. Environmental controls over carbon dioxide and water vapor exchange of terrestrial vegetation. Agric. For. Meteorol. 113, 97 – 120.

Le Quere, C., Raupach, M.R., Canadell, J.G., Marland et al., G., 2009. Trends in the sources and sinks of carbon dioxide. Nat. Geosci 2, 831–836.

Leavitt, S.W., 1988. Stable Carbon Isotope Chronologies from Trees in the Southwestern United States. Global Biogeochem. Cycles 2, 189–198. doi:10.1029/GB002i003p00189

LEUNING, R., 1995. A critical appraisal of a combined stomatal-photosynthesis model for C3 plants. Plant. Cell Environ. 18, 339–355. doi:10.1111/j.1365-3040.1995.tb00370.x

Leuning, R., 1990. Modelling Stomatal Behaviour and and Photosynthesis of Eucalyptus grandis. Funct. Plant Biol. 17, 159–175.

Li, C., Wang, K., 2003. Differences in drought responses of three contrasting Eucalyptus microtheca F. Muell. populations. For. Ecol. Manage. 179, 377–385.

Lin, Y.-S., Medlyn, B.E., Duursma, R.A., Prentice, I.C., Wang, H., Baig, S., Eamus, D., de Dios, V.R., Mitchell, P., Ellsworth, D.S., de Beeck, M.O., Wallin, G., Uddling, J., Tarvainen, L., Linderson, M.-L., Cernusak, L.A., Nippert, J.B., Ocheltree, T.W., Tissue, D.T., Martin-StPaul, N.K., Rogers, A., Warren, J.M., De Angelis, P., Hikosaka, K., Han, Q., Onoda, Y., Gimeno, T.E., Barton, C.V.M., Bennie, J., Bonal, D., Bosc, A., Low, M., Macinins-Ng, C., Rey, A., Rowland, L., Setterfield, S.A., Tausz-Posch, S., Zaragoza-Castells, J., Broadmeadow, M.S.J., Drake, J.E., Freeman, M., Ghannoum, O., Hutley, L.B., Kelly, J.W., Kikuzawa, K., Kolari, P., Koyama, K., Limousin, J.-M., Meir, P., Lola da Costa, A.C., Mikkelsen, T.N., Salinas, N., Sun, W., Wingate, L., 2015. Optimal stomatal behaviour around the world. Nat. Clim. Chang. 5, 459–464.

Linares, J.C., Delgado-Huertas, A., Camarero, J.J., Merino, J., Carreira, J.A., 2009. Competition and drought limit the response of water-use efficiency to rising atmospheric carbon dioxide in the Mediterranean fir Abies pinsapo. Oecologia 161, 611–624. doi:10.1007/s00442-009-1409-7

Liu, S., Chen, M., Zhuang, Q., 2014. Aerosol effects on global land surface energy fluxes during 2003–2010. Geophys. Res. Lett. 41, 7875–7881.

Liu, S., Zhuang, Q., Chen, M., Gu, L., 2016. Quantifying spatially and temporally explicit CO_2 fertilization effects on global terrestrial ecosystem carbon dynamics. Ecosphere 7. doi:10.1002/ecs2.1391

Lloyd, J., Taylor, J.A., 1994. On the Temperature Dependence of Soil Respiration. Funct. Ecol. 8, 315–323. doi:10.2307/2389824

Loader, N.J., Santillo, P.M., Woodman-Ralph, J.P., Rolfe, J.E., Hall, M.A., Gagen, M., Robertson, I., Wilson, R., Froyd, C.A., McCarroll, D., 2008. Multiple stable isotopes from oak trees in southwestern Scotland and the potential for stable isotope dendroclimatology in maritime climatic regions. Chem. Geol. 252, 62–71.

Loader, N.J., Switsur, V.R., 1996. Reconstructing Past Environmental Change Using Stable Isotopes in Tree-rings. Bot. J. Scotl. 48, 65–78. doi:10.1080/03746609609480374

Loader, N.J., Young, G.H., McCarroll, D., Wilson, R.J., 2013. Quantifying uncertainty in isotope dendroclimatology. The Holocene 23, 1221–1226. doi:10.1177/0959683613486945

Loescher, H.W., Law, B.E., Mahrt, L., Hollinger, D.Y., Campbell, J., Wofsy, S.C., 2006. Uncertainties in, and interpretation of, carbon flux estimates using the eddy covariance technique. J. Geophys. Res. Atmos. 111.

Los, S.O., 2013. Analysis of trends in fused AVHRR and MODIS NDVI data for 1982–2006: Indication for a CO_2 fertilization effect in global vegetation. Global Biogeochem. Cycles 27, 318–330.

Lund, M., Lafleur, P.M., Roulet, N.T., Lindroth, A., Christensen, T.R., Aurela, M., Chojnicki, B.H., Flanagan, L.B., Humphreys, E.R., Laurila, T., 2010. Variability in exchange of CO_2 across 12 northern peatland and tundra sites. Glob. Chang. Biol. 16, 2436–2448.

Luo, Y., Jackson, R.B., Field, C.B., Mooney, H.A., 1996. Elevated CO_2 increases belowground respiration in California grasslands. Oecologia 108, 130–137.

Luo, Y., Keenan, T.F., Smith, M., 2015. Predictability of the terrestrial carbon cycle. Glob. Chang. Biol. 21, 1737–1751. doi:10.1111/gcb.12766

Luo, Y., Su, B.O., Currie, W.S., Dukes, J.S., Finzi, A., Hartwig, U., Hungate, B., McMurtrie, R.E., Oren, R.A.M., Parton, W.J., 2004. Progressive nitrogen limitation of ecosystem responses to rising atmospheric carbon dioxide. Bioscience 54, 731–739.

Madani, N., Kimball, J.S., Affleck, D.L.R., Kattge, J., Graham, J., Bodegom, P.M., Reich, P.B., Running, S.W., 2014. Improving ecosystem productivity modeling through spatially explicit estimation of optimal light use efficiency. J. Geophys. Res. Biogeosciences 119, 1755–1769.

Marshall, J.D., Brooks, J.R., Lajtha, K., 2007. Sources of Variation in the Stable Isotopic Composition of Plants, in: Stable Isotopes in Ecology and Environmental Science. Blackwell Publishing Ltd, pp. 22–60. doi:10.1002/9780470691854.ch2

Masarie, K.A., Petron, G., Andrews, A., Bruhwiler, L., Conway, T.J., Jacobson, A.R., Miller, J.B., Tans, P.P., Worthy, D.E., Peters, W., 2011. Impact of CO_2 measurement bias on CarbonTracker surface flux estimates. J. Geophys. Res. Atmos. 116.

McCarroll, D., Loader, N.J., 2004. Stable isotopes in tree rings. Quat. Sci. Rev. 23, 771–801. doi:10.1016/j.quascirev.2003.06.017

McCarroll, D., Pawellek, F., 2001. Stable carbon isotope ratios of Pinus sylvestris from northern Finland and the potential for extracting a climate signal from long Fennoscandian chronologies. The Holocene 11, 517–526.

McDowell, G.R., Harireche, O., 2002. Discrete element modelling of yielding and normal compression of sand. GEOTECHNIQUE-LONDON- 52, 299–304.

McDowell, N.G., Bond, B.J., Dickman, L.T., Ryan, M.G., Whitehead, D., 2011. Relationships Between Tree Height and Carbon Isotope Discrimination BT - Size- and Age-Related Changes in Tree Structure and Function, in: Meinzer, C.F., Lachenbruch, B., Dawson, E.T. (Eds.), . Springer Netherlands, Dordrecht, pp. 255–286. doi:10.1007/978-94-007-1242-3_10

Medlyn, B.E., Barton, C.V.M., Broadmeadow, M.S.J., Ceulemans, R., De Angelis, P., Forstreuter, M., Freeman, M., Jackson, S.B., Kellomäki, S., Laitat, E., 2001. Stomatal conductance of forest species after long‐term exposure to elevated CO_2 concentration: A synthesis. New Phytol. 149, 247–264.

MEDLYN, B.E., DUURSMA, R.A., EAMUS, D., ELLSWORTH, D.S., PRENTICE, I.C., BARTON, C.V.M., CROUS, K.Y., DE ANGELIS, P., FREEMAN, M., WINGATE, L., 2011. Reconciling the optimal and empirical approaches to modelling stomatal conductance. Glob. Chang. Biol. 17, 2134–2144. doi:10.1111/j.1365-2486.2010.02375.x

Melton, J.R., Arora, V.K., 2013. Sub-grid scale representation of vegetation in global land surface schemes: implications for estimation of the terrestrial carbon sink. Biogeosciences Discuss. 10, 16003–16041.

Mesinger, F., DiMego, G., Kalnay, E., Mitchell, K., Shafran, P.C., Ebisuzaki, W., Jovic, D., Woollen, J., Rogers, E., Berbery, E.H., 2006. North American regional reanalysis. Bull. Am. Meteorol. Soc. 87, 343–360.

Migliavacca, M., Reichstein, M., Richardson, A.D., Mahecha, M.D., Cremonese, E., Delpierre, N., Galvagno, M., Law, B.E., Wohlfahrt, G., Black, T.A., Carvalhais, N., Ceccherini, G., Chen, J., Gobron, N., Koffi, E., Munger, J.W., Perez-Priego, O., Robustelli, M., Tomelleri, E., Cescatti, A., 2015. Influence of physiological phenology on the seasonal pattern of ecosystem respiration in deciduous forests. Glob. Chang. Biol. 21, 363–76. doi:10.1111/gcb.12671

Miles, N.L., Richardson, S.J., Davis, K.J., Lauvaux, T., Andrews, A.E., West, T.O., Bandaru, V., Crosson, E.R., 2012. Large amplitude spatial and temporal gradients in atmospheric boundary layer CO 2 mole fractions detected with a tower-based network in the U.S. upper Midwest. J. Geophys. Res. Biogeosciences 117. doi:10.1029/2011JG001781

Miralles, D.G., Holmes, T.R.H., De Jeu, R.A.M., Gash, J.H., Meesters, A.G.C.A., Dolman, A.J., 2011. Global land-surface evaporation estimated from satellite-based observations. Hydrol. Earth Syst. Sci. 15, 453–469. doi:10.5194/hess-15-453-2011

MITCHELL, C.E., REICH, P.B., TILMAN, D., GROTH, J. V, 2003. Effects of elevated CO_2, nitrogen deposition, and decreased species diversity on foliar fungal plant disease. Glob. Chang. Biol. 9, 438–451. doi:10.1046/j.1365-2486.2003.00602.x

Moffat, A.M., Papale, D., Reichstein, M., Hollinger, D.Y., Richardson, A.D., Barr, A.G., Beckstein, C., Braswell, B.H., Churkina, G., Desai, A.R., 2007. Comprehensive comparison of gap-filling techniques for eddy covariance net carbon fluxes. Agric. For. Meteorol. 147, 209–232.

Mohren, G.M.J., Kramer, K., Sabaté, S., 2013. Impacts of Global Change on Tree Physiology and Forest Ecosystems: Proceedings of the International Conference on Impacts of Global Change on Tree Physiology and Forest Ecosystems, held 26--29 November 1996, Wageningen, The Netherlands. Springer Science & Business Media.

Morecroft, M.D., Stokes, V.J., Morison, J.I.L., 2003. Seasonal changes in the photosynthetic capacity of canopy oak (Quercus robur) leaves: the impact of slow development on annual carbon uptake. Int. J. Biometeorol. 47, 221–226.

Morgan, J.A., Pataki, D.E., Körner, C., Clark, H., Del Grosso, S.J., Grünzweig, J.M., Knapp, A.K., Mosier, A.R., Newton, P.C.D., Niklaus, P.A., 2004. Water relations in grassland and desert ecosystems exposed to elevated atmospheric CO_2. Oecologia 140, 11–25.

Mortazavi, B., Chanton, J.P., Prater, J.L., Oishi, A.C., Oren, R., Katul, G., 2005. Temporal variability in 13C of respired CO_2 in a pine and a hardwood forest subject to similar climatic conditions. Oecologia 142, 57–69. doi:10.1007/s00442-004-1692-2

Myneni, R.B., Hoffman, S., Knyazikhin, Y., Privette, J.L., Glassy, J., Tian, Y., Wang, Y., Song, X., Zhang, Y., Smith, G.R., 2002. Global products of vegetation leaf area and fraction absorbed PAR from year one of MODIS data. Remote Sens. Environ. 83, 214–231.

Nardino, M., Georgiadis, T., Rossi, F., Ponti, F., Miglietta, F., Magliulo, V., 2002. Primary productivity and evapotranspiration of a mixed forest, in: Congress CNR-ISA Fo., Istituto per I Sistemi Agricoli E Forestali Del Mediterraneo, Portici. pp. 24–25.

NIINEMETS, Ü.L.O., CESCATTI, A., RODEGHIERO, M., TOSENS, T., 2006. Complex adjustments of photosynthetic potentials and internal diffusion conductance to current and previous light availabilities and leaf age in Mediterranean evergreen species Quercus ilex. Plant. Cell Environ. 29, 1159–1178. doi:10.1111/j.1365-3040.2006.01499.x

Niyogi, D., Alapaty, K., Raman, S., Chen, F., 2009. Development and Evaluation of a Coupled Photosynthesis-Based Gas Exchange Evapotranspiration Model (GEM) for Mesoscale Weather Forecasting Applications. J. Appl. Meteorol. Climatol. 48, 349–368. doi:10.1175/2008JAMC1662.1

Nock, C.A., Baker, P.J., Wanek, W., Leis, A., Grabner, M., Bunyavejchewin, S., Hietz, P., 2011. Long-term increases in intrinsic water-use efficiency do not lead to increased stem growth in a tropical monsoon forest in western Thailand. Glob. Chang. Biol. 17, 1049–1063. doi:10.1111/j.1365-2486.2010.02222.x

Norby, R.J., Warren, J.M., Iversen, C.M., Medlyn, B.E., McMurtrie, R.E., 2010. CO_2 enhancement of forest productivity constrained by limited nitrogen availability. Proc. Natl. Acad. Sci. 107, 19368–19373.

Nowak, R.S., Ellsworth, D.S., Smith, S.D., 2004. Functional responses of plants to elevated atmospheric CO_2–do photosynthetic and productivity data from FACE experiments support early predictions? New Phytol. 162, 253–280.

Ollinger, S. V, Aber, J.D., Reich, P.B., Freuder, R.J., 2002. Interactive effects of nitrogen deposition, tropospheric ozone, elevated CO_2 and land use history on the carbon dynamics of northern hardwood forests. Glob. Chang. Biol. 8, 545–562.

O'Reilly Sternberg, L. da S.L., 2009. Oxygen stable isotope ratios of tree-ring cellulose: the next phase of understanding. New Phytol. 181, 553–62. doi:10.1111/j.1469-8137.2008.02661.x

Oren, R., Ellsworth, D.S., Johnsen, K.H., Phillips, N., Ewers, B.E., Maier, C., Schäfer, K.V.R., McCarthy, H., Hendrey, G., McNulty, S.G., 2001. Soil fertility limits carbon sequestration by forest ecosystems in a CO_2-enriched atmosphere. Nature 411, 469–472.

Pan, Y., Chen, J.M., Birdsey, R., McCullough, K., He, L., Deng, F., 2011. Age structure and disturbance legacy of North American forests. Biogeosciences 8, 715–732. doi:10.5194/bg-8-715-2011

Park, S., Feddema, J.J., Egbert, S.L., 2004. Impacts of hydrologic soil properties on drought detection with MODIS thermal data. Remote Sens. Environ. 89, 53–62.

Parry, M.L., Canziani, O.F., Palutikof, J.P., der Linden, P.J., Hanson, C.E., 2007. Contribution of working group II to the fourth assessment report of the intergovernmental panel on climate change, 2007. Clim. Chang. 2007 Work. Gr. II Impacts, Adapt. Vulnerability.

Peltola, H., Kilpeläinen, A., Kellomäki, S., 2002. Diameter growth of Scots pine (Pinus sylvestris) trees grown at elevated temperature and carbon dioxide concentration under boreal conditions. Tree Physiol. 22, 963–972.

Peñuelas, J., Canadell, J.G., Ogaya, R., 2011. Increased water-use efficiency during the 20th century did not translate into enhanced tree growth. Glob. Ecol. Biogeogr. 20, 597–608. doi:10.1111/j.1466-8238.2010.00608.x

Peñuelas, J., Hunt, J.M., Ogaya, R., Jump, A.S., 2008. Twentieth century changes of tree-ring $δ$13C at the southern range-edge of Fagus sylvatica: Increasing water-use efficiency does not avoid the growth decline induced by warming at low altitudes. Glob. Chang. Biol. 14, 1076–1088. doi:10.1111/j.1365-2486.2008.01563.x

Peters, W., Jacobson, A.R., Sweeney, C., Andrews, A.E., Conway, T.J., Masarie, K., Miller, J.B., Bruhwiler, L.M.P., Petron, G., Hirsch, A.I., 2007. An atmospheric perspective on North American carbon dioxide exchange: CarbonTracker. Proc. Natl. Acad. Sci. 104, 18925–18930.

Phoenix, G.K., Emmett, B.A., Britton, A.J., Caporn, S.J.M., Dise, N.B., Helliwell, R., Jones, L., Leake, J.R., Leith, I.D., Sheppard, L.J., Sowerby, A., Pilkington, M.G., Rowe, E.C., Ashmore, M.R., Power, S.A., 2012. Impacts of atmospheric nitrogen deposition: Responses of multiple plant and soil parameters across contrasting ecosystems in long-term field experiments. Glob. Chang. Biol. 18, 1197–1215. doi:10.1111/j.1365-2486.2011.02590.x

Piao, S., Friedlingstein, P., Ciais, P., Zhou, L., Chen, A., 2006. Effect of climate and CO_2 changes on the greening of the Northern Hemisphere over the past two decades. Geophys. Res. Lett. 33, L23402. doi:10.1029/2006GL028205

Prentice, I.C., Dong, N., Gleason, S.M., Maire, V., Wright, I.J., 2014. Balancing the costs of carbon gain and water transport: Testing a new theoretical framework for plant functional ecology. Ecol. Lett. 17, 82–91. doi:10.1111/ele.12211

Prentice, I.C., Liang, X., Medlyn, B.E., Wang, Y.P., 2015. Reliable, robust and realistic: The three R's of next-generation land-surface modelling. Atmos. Chem. Phys. 15, 5987–6005. doi:10.5194/acp-15-5987-2015

Prince, S.D., Goward, S.N., 1995. Global primary production: a remote sensing approach. J. Biogeogr. 815–835.

Raczka, B., Duarte, H.F., Koven, C.D., Ricciuto, D., Thornton, P.E., Lin, J.C., Bowling, D.R., 2016. An observational constraint on stomatal function in forests: evaluating coupled carbon and water vapor exchange with carbon isotopes in the Community Land Model (CLM 4.5). Biogeosciences Discuss. 2016, 1–46. doi:10.5194/bg-2016-73

Rahman, A.F., 2005. Potential of MODIS EVI and surface temperature for directly estimating per-pixel ecosystem C fluxes. Geophys. Res. Lett. 32, L19404. doi:10.1029/2005GL024127

Raich, J.W., Rastetter, E.B., Melillo, J.M., Kicklighter, D.W., Steudler, P.A., Peterson, B.J., Grace, A.L., Moore Iii, B., Vörösmarty, C.J., 1991. Potential net primary productivity in South America: application of a global model. Ecol. Appl. 399–429.

RAICH, J.W., SCHLESINGER, W.H., 1992. The global carbon dioxide flux in soil respiration and its relationship to vegetation and climate. Tellus B 44, 81–99. doi:10.1034/j.1600-0889.1992.t01-1-00001.x

Reich, P.B., Hobbie, S.E., Lee, T.D., 2014. Plant growth enhancement by elevated CO_2 eliminated by joint water and nitrogen limitation. Nat. Geosci.

Reich, P.B., Wright, I.J., Lusk, C.H., 2007. PREDICTING LEAF PHYSIOLOGY FROM SIMPLE PLANT AND CLIMATE ATTRIBUTES: A GLOBAL GLOPNET ANALYSIS. Ecol. Appl. 17, 1982–1988. doi:10.1890/06-1803.1

Reichstein, M., Bahn, M., Mahecha, M.D., Kattge, J., Baldocchi, D.D., 2014. Linking plant and ecosystem functional biogeography. Proc. Natl. Acad. Sci. 111, 13697–13702. doi:10.1073/pnas.1216065111

Reichstein, M., Falge, E., Baldocchi, D., Papale, D., Aubinet, M., Berbigier, P., Bernhofer, C., Buchmann, N., Gilmanov, T., Granier, A., Grünwald, T., Havránková, K., Ilvesniemi, H., Janous, D., Knohl, A., Laurila, T., Lohila, A., Loustau, D., Matteucci, G., Meyers, T., Miglietta, F., Ourcival, J.-M., Pumpanen, J., Rambal, S., Rotenberg, E., Sanz, M., Tenhunen, J., Seufert, G., Vaccari, F., Vesala, T., Yakir, D., Valentini, R., 2005. On the separation of net ecosystem exchange into assimilation and ecosystem respiration: review and improved algorithm. Glob. Chang. Biol. 11, 1424–1439. doi:10.1111/j.1365-2486.2005.001002.x

Reichstein, M., Tenhunen, J.D., Roupsard, O., Ourcival, J., Rambal, S., Miglietta, F., Peressotti, A., Pecchiari, M., Tirone, G., Valentini, R., 2002. Severe drought effects on ecosystem CO_2 and H2O fluxes at three Mediterranean evergreen sites: revision of current hypotheses? Glob. Chang. Biol. 8, 999–1017.

Robertson, I., Switsur, V.R., Carter, a H.C., Barker, a C., Waterhouse, J.S., Briffa, K.R., Jones, P.D., 1997. Signal strength and climate relationships in 13C/12C ratios of tree ring cellulose from oak in east England. J. Geophys. Res. 102, 19507–19519. doi:10.1029/97JD01226

Ruehr, N.K., Offermann, C.A., Gessler, A., Winkler, J.B., Ferrio, J.P., Buchmann, N., Barnard, R.L., 2009. Drought effects on allocation of recent carbon: from beech leaves to soil CO_2 efflux. New Phytol. 184, 950–961.

Running, S.W., Nemani, R.R., Heinsch, F.A., Zhao, M., Reeves, M., Hashimoto, H., 2004. A continuous satellite-derived measure of global terrestrial primary production. Bioscience 54, 547–560.

Running, S.W., Thornton, P.E., Nemani, R., Glassy, J.M., 2000. Global terrestrial gross and net primary productivity from the earth observing system. Methods Ecosyst. Sci. 44–57.

Sage, R.F., 1999. 1 - Why C4 Photosynthesis? BT - C4 Plant Biology, in: Physiological Ecology. Academic Press, San Diego, pp. 3–16. doi:http://dx.doi.org/10.1016/B978-012614440-6/50002-1

Saurer, M., Siegenthaler, U., Schweingruber, F., 1995. The climate-carbon isotope relationship in tree rings and the significance of site conditions. Tellus B. doi:10.1034/j.1600-0889.47.issue3.4.x

Saurer, M., Siegwolf, R.T.W., Schweingruber, F.H., 2004. Carbon isotope discrimination indicates improving water-use efficiency of trees in northern Eurasia over the last 100 years. Glob. Chang. Biol. 10, 2109–2120. doi:10.1111/j.1365-2486.2004.00869.x

Scheidegger, Y., Saurer, M., Bahn, M., Siegwolf, R., 2000. Linking stable oxygen and carbon isotopes with stomatal conductance and photosynthetic capacity: a conceptual model. Oecologia 125, 350–357. doi:10.1007/s004420000466

Schleser, G.H., Jayasekera, R., 1985. δ13C-variations of leaves in forests as an indication of reassimilated CO_2 from the soil. Oecologia 65, 536–542.

Scholze, M., Ciais, P., Heimann, M., 2008. Modeling terrestrial 13C cycling: Climate, land use and fire. Global Biogeochem. Cycles 22. doi:10.1029/2006GB002899

Schwarz, P.A., Law, B.E., Williams, M., Irvine, J., Kurpius, M., Moore, D., 2004. Climatic versus biotic constraints on carbon and water fluxes in seasonally drought-affected ponderosa pine ecosystems. Global Biogeochem. Cycles 18. doi:10.1029/2004GB002234

Seibt, U., Rajabi, A., Griffiths, H., Berry, J. a., 2008. Carbon isotopes and water use efficiency: Sense and sensitivity. Oecologia 155, 441–454. doi:10.1007/s00442-007-0932-7

Sheffield, J., Goteti, G., Wood, E.F., 2006. Development of a 50-Year High-Resolution Global Dataset of Meteorological Forcings for Land Surface Modeling. J. Clim. 19, 3088–3111. doi:10.1175/JCLI3790.1

Sidorova, O. V, Siegwolf, R.T.W., Saurer, M., Naurzbaev, M.M., Shashkin, A. V, Vaganov, E.A., 2010. Spatial patterns of climatic changes in the Eurasian north reflected in Siberian larch tree-ring parameters and stable isotopes. Glob. Chang. Biol. 16, 1003 – 1018. doi:10.1111/j.1365-2486.2009.02008.x

Sidorova, O. V, Siegwolf, R.T.W., Saurer, M., Naurzbaev, M.M., Vaganov, E.A., 2008. Isotopic composition (??13C, ??18O) in wood and cellulose of Siberian larch trees for early Medieval and recent periods. J. Geophys. Res. Biogeosciences 113, 1–13. doi:10.1029/2007JG000473

Sidorova, O.V., Siegwolf, R.T.W., Saurer, M., Shashkin, A. V, Knorre, A.A., Prokushkin, A.S., Vaganov, E.A., Kirdyanov, A. V, 2009. Do centennial tree-ring and stable isotope trends of Larix gmelinii (Rupr.) Rupr. indicate increasing water shortage in the Siberian north? Oecologia 161, 825–835. doi:10.1007/s00442-009-1411-0

Silva, L.C.R., Anand, M., 2013. Probing for the influence of atmospheric CO_2 and climate change on forest ecosystems across biomes. Glob. Ecol. Biogeogr. 22, 83–92. doi:10.1111/j.1466-8238.2012.00783.x

Silva, L.C.R., Anand, M., Leithead, M.D., 2010. Recent widespread tree growth decline despite increasing atmospheric CO_2. PLoS One 5. doi:10.1371/journal.pone.0011543

Simard, S., Elhani, S., Morin, H., Krause, C., Cherubini, P., 2008. Carbon and oxygen stable isotopes from tree-rings to identify spruce budworm outbreaks in the boreal forest of Québec. Chem. Geol. 252, 80–87.

Singh, R.P., Roy, S., Kogan, F., 2003. Vegetation and temperature condition indices from NOAA AVHRR data for drought monitoring over India. Int. J. Remote Sens. 24, 4393–4402.

SITCH, S., HUNTINGFORD, C., GEDNEY, N., LEVY, P.E., LOMAS, M., PIAO, S.L., BETTS, R., CIAIS, P., COX, P., FRIEDLINGSTEIN, P., JONES, C.D., PRENTICE, I.C., WOODWARD, F.I., 2008. Evaluation of the terrestrial carbon cycle, future plant geography and climate-carbon cycle feedbacks using five Dynamic Global Vegetation Models (DGVMs). Glob. Chang. Biol. 14, 2015–2039. doi:10.1111/j.1365-2486.2008.01626.x

Snyder, P.K., Delire, C., Foley, J.A., 2004. Evaluating the influence of different vegetation biomes on the global climate. Clim. Dyn. 23, 279–302. doi:10.1007/s00382-004-0430-0

Son, N.T., Chen, C.F., Chen, C.R., Chang, L.Y., Minh, V.Q., 2012. Monitoring agricultural drought in the Lower Mekong Basin using MODIS NDVI and land surface temperature data. Int. J. Appl. Earth Obs. Geoinf. 18, 417–427.

Song, X., Saito, G., Kodama, M., Sawada, H., 2004. Early detection system of drought in East Asia using NDVI from NOAA/AVHRR data. Int. J. Remote Sens. 25, 3105–3111.

Soudant, A., Loader, N.J., Bäck, J., Levula, J., Kljun, N., 2016. Intra-annual variability of wood formation and δ13C in tree-rings at Hyytiälä, Finland. Agric. For. Meteorol. 224, 17–29. doi:10.1016/j.agrformet.2016.04.015

Sowerby, A., Emmett, B.A., Tietema, A., Beier, C., 2008. Contrasting effects of repeated summer drought on soil carbon efflux in hydric and mesic heathland soils. Glob. Chang. Biol. 14, 2388–2404.

Specht, D.F., 1991. A general regression neural network. Neural Networks, IEEE Trans. 2, 568–576.

Suits, N.S., Denning, a. S., Berry, J. a., Still, C.J., Kaduk, J., Miller, J.B., Baker, I.T., 2005. Simulation of carbon isotope discrimination of the terrestrial biosphere. Global Biogeochem. Cycles 19, 1–15. doi:10.1029/2003GB002141

Sun, Y., Gu, L., Dickinson, R.E., Norby, R.J., Pallardy, S.G., Hoffman, F.M., 2014. Impact of mesophyll diffusion on estimated global land CO_2 fertilization. Proc. Natl. Acad. Sci. 111 , 15774–15779. doi:10.1073/pnas.1418075111

Suni, T., Rinne, J., Reissell, A., Altimir, N., Keronen, P., Rannik, U., Kulmala, M., Vesala, T., 2003. Long-term measurements of surface fluxes above a Scots pine forest in Hyytiala, southern Finland, 1996-2001. Boreal Environ. Res. 8, 287–302.

Tang, J., Zhuang, Q., 2009. A global sensitivity analysis and Bayesian inference framework for improving the parameter estimation and prediction of a process-based Terrestrial Ecosystem Model. J. Geophys. Res. Atmos. 114. doi:10.1029/2009JD011724

Tang, J., Zhuang, Q., 2008. Equifinality in parameterization of process-based biogeochemistry models: A significant uncertainty source to the estimation of regional carbon dynamics. J. Geophys. Res. Biogeosciences 113. doi:10.1029/2008JG000757

Tang, X., Li, H., Desai, A.R., Nagy, Z., Luo, J., Kolb, T.E., Olioso, A., Xu, X., Yao, L., Kutsch, W., others, 2014. How is water-use efficiency of terrestrial ecosystems distributed and changing on Earth? Sci. Rep. 4, 7483.

Tans, P.P., Berry, J.A., Keeling, R.F., 1993. Oceanic 13 C/12 C observations: A new window on ocean CO 2 uptake. Global Biogeochem. Cycles 7, 353–368. doi:10.1029/93GB00053

Tans, P.P., Fung, I.Y., Takahashi, T., 1990. Observational contrains on the global atmospheric CO_2 budget. Science (80-). 247, 1431–1438.

Thum, T., Aalto, T., Laurila, T., Aurela, M., Kolari, P., Hari, P., 2007. Parametrization of two photosynthesis models at the canopy scale in a northern boreal Scots pine forest. Tellus B 59, 874–890.

Tingey, D.T., Mckane, R.B., Olszyk, D.M., Johnson, M.G., Rygiewicz, P.T., Henry Lee, E., 2003. Elevated CO_2 and temperature alter nitrogen allocation in Douglas‐fir. Glob. Chang. Biol. 9, 1038–1050.

Todd-Brown, K.E.O., Randerson, J.T., Post, W.M., Hoffman, F.M., Tarnocai, C., Schuur, E.A.G., Allison, S.D., 2013. Causes of variation in soil carbon simulations from CMIP5 Earth system models and comparison with observations. Biogeosciences 10, 1717–1736. doi:10.5194/bg-10-1717-2013

Tucker, C.J., 1979. Red and photographic infrared linear combinations for monitoring vegetation. Remote Sens. Environ. 8, 127–150.

Turner, D.P., Ritts, W.D., Cohen, W.B., Gower, S.T., Running, S.W., Zhao, M., Costa, M.H., Kirschbaum, A.A., Ham, J.M., Saleska, S.R., Ahl, D.E., 2006. Evaluation of MODIS NPP and GPP products across multiple biomes. Remote Sens. Environ. 102, 282–292. doi:10.1016/j.rse.2006.02.017

Turner, D.P., Ritts, W.D., Cohen, W.B., Gower, S.T., Zhao, M., Running, S.W., Wofsy, S.C., Urbanski, S., Dunn, A.L., Munger, J.W., 2003. Scaling gross primary production (GPP) over boreal and deciduous forest landscapes in support of MODIS GPP product validation. Remote Sens. Environ. 88, 256–270.

Vaganov, E.A., Schulze, E.-D., Skomarkova, M. V, Knohl, A., Brand, W.A., Roscher, C., 2009. Intra-annual variability of anatomical structure and δ13C values within tree rings of spruce and pine in alpine, temperate and boreal Europe. Oecologia 161, 729–745. doi:10.1007/s00442-009-1421-y

Valentini, R., Angelis, P. de, Matteucci, G., Monaco, R., Dore, S., Mucnozza, G.E.S., 1996. Seasonal net carbon dioxide exchange of a beech forest with the atmosphere. Glob. Chang. Biol. 2, 199–207.

Valentini, R., Matteucci, G., Dolman, A.J., Schulze, E.-D., Rebmann, C., Moors, E.J., Granier, A., Gross, P., Jensen, N.O., Pilegaard, K., 2000. Respiration as the main determinant of carbon balance in European forests. Nature 404, 861–865.

Verma, S.B., 1990. Micrometeorological methods for measuring surface fluxes of mass and energy. Remote Sens. Rev. 5, 99–115.

Vetter, M., Churkina, G., Jung, M., Reichstein, M., Zaehle, S., Bondeau, A., Chen, Y., Ciais, P., Feser, F., Freibauer, A., 2008. Analyzing the causes and spatial pattern of the European 2003 carbon flux anomaly using seven models. Biogeosciences 5, 561–583.

Voelker, S.L., Brooks, J.R., Meinzer, F.C., Anderson, R., Bader, M.K.-F., Battipaglia, G., Becklin, K.M., Beerling, D., Bert, D., Betancourt, J.L., Dawson, T.E., Domec, J.-C., Guyette, R.P., Körner, C., Leavitt, S.W., Linder, S., Marshall, J.D., Mildner, M., Ogée, J., Panyushkina, I., Plumpton, H.J., Pregitzer, K.S., Saurer, M., Smith, A.R., Siegwolf, R.T.W., Stambaugh, M.C., Talhelm, A.F., Tardif, J.C., Van de Water, P.K., Ward, J.K., Wingate, L., 2016. A dynamic leaf gas-exchange strategy is conserved in woody plants under changing ambient CO_2 : evidence from carbon isotope discrimination in paleo and CO_2 enrichment studies. Glob. Chang. Biol. 22, 889–902. doi:10.1111/gcb.13102

Walker, A.P., Zaehle, S., Medlyn, B.E., De Kauwe, M.G., Asao, S., Hickler, T., Parton, W., Ricciuto, D.M., Wang, Y.-P., Wårlind, D., Norby, R.J., 2015. Predicting long-term carbon sequestration in response to CO_2 enrichment: How and why do current ecosystem models differ? Global Biogeochem. Cycles 29, 476–495. doi:10.1002/2014GB004995

Wall, G.W., Brooks, T.J., Adam, N.R., Cousins, A.B., Kimball, B.A., Pinter, P.J., LaMorte, R.L., Triggs, J., Ottman, M.J., Leavitt, S.W., 2001. Elevated atmospheric CO_2 improved sorghum plant water status by ameliorating the adverse effects of drought. New Phytol. 152, 231–248.

Wan, S., Norby, R.J., Ledford, J., Weltzin, J.F., 2007. Responses of soil respiration to elevated CO_2, air warming, and changing soil water availability in a model old‐field grassland. Glob. Chang. Biol. 13, 2411‐2424.

Wan, Z., Wang, P., Li, X., 2004. Using MODIS land surface temperature and normalized difference vegetation index products for monitoring drought in the southern Great Plains, USA. Int. J. Remote Sens. 25, 61–72.

Wan, Z., Zhang, Y., Zhang, Q., Li, Z., 2002. Validation of the land-surface temperature products retrieved from Terra Moderate Resolution Imaging Spectroradiometer data. Remote Sens. Environ. 83, 163–180.

Wang, H., Prentice, I.C., Davis, T.W., 2014. Biophsyical constraints on gross primary production by the terrestrial biosphere. Biogeosciences 11, 5987–6001. doi:10.5194/bg-11-5987-2014

Wang, Y.-P., Trudinger, C.M., Enting, I.G., 2009. A review of applications of model–data fusion to studies of terrestrial carbon fluxes at different scales. Agric. For. Meteorol. 149, 1829–1842. doi:http://dx.doi.org/10.1016/j.agrformet.2009.07.009

Warren, C.R., 2004. The photosynthetic limitation posed by internal conductance to CO_2 movement is increased by nutrient supply. J. Exp. Bot. 55 , 2313–2321. doi:10.1093/jxb/erh239

Warren, C.R., 2008. Stand aside stomata, another actor deserves centre stage: the forgotten role of the internal conductance to CO_2 transfer. J. Exp. Bot. 59 , 1475–1487. doi:10.1093/jxb/erm245

Wehr, R., Saleska, S.R., 2015. An improved isotopic method for partitioning net ecosystem–atmosphere CO_2 exchange. Agric. For. Meteorol. 214–215, 515–531. doi:http://dx.doi.org/10.1016/j.agrformet.2015.09.009

White, M.A., Thornton, P.E., Running, S.W., Nemani, R.R., 2000. Parameterization and sensitivity analysis of the BIOME-BGC terrestrial ecosystem model: net primary production controls. Earth Interact. 4, 1–85.

Whitman, T., Lehmann, J., 2015. A dual-isotope approach to allow conclusive partitioning between three sources. Nat Commun 6.

Williams, M., Richardson, a. D., Reichstein, M., Stoy, P.C., Peylin, P., Verbeeck, H., Carvalhais, N., Jung, M., Hollinger, D.Y., Kattge, J., Leuning, R., Luo, Y., Tomelleri, E., Trudinger, C., Wang, Y.-P., 2009. Improving land surface models with FLUXNET data. Biogeosciences Discuss. 6, 2785–2835. doi:10.5194/bgd-6-2785-2009

Xia, J., Luo, Y., Wang, Y.-P., Hararuk, O., 2013. Traceable components of terrestrial carbon storage capacity in biogeochemical models. Glob. Chang. Biol. 19, 2104–2116. doi:10.1111/gcb.12172

Xiao, J., Chen, J., Davis, K.J., Reichstein, M., 2012. Advances in upscaling of eddy covariance measurements of carbon and water fluxes. J. Geophys. Res. Biogeosciences 117. doi:10.1029/2011JG001889

Xiao, J., Ollinger, S. V., Frolking, S., Hurtt, G.C., Hollinger, D.Y., Davis, K.J., Pan, Y., Zhang, X., Deng, F., Chen, J., Baldocchi, D.D., Law, B.E., Arain, M.A., Desai, A.R., Richardson, A.D., Sun, G., Amiro, B., Margolis, H., Gu, L., Scott, R.L., Blanken, P.D., Suyker, A.E., 2014. Data-driven diagnostics of terrestrial carbon dynamics over North America. Agric. For. Meteorol. 197, 142–157. doi:10.1016/j.agrformet.2014.06.013

Xiao, J., Zhuang, Q., Baldocchi, D.D., Law, B.E., Richardson, A.D., Chen, J., Oren, R., Starr, G., Noormets, A., Ma, S., 2008. Estimation of net ecosystem carbon exchange for the conterminous United States by combining MODIS and AmeriFlux data. Agric. For. Meteorol. 148, 1827–1847.

Xiao, J., Zhuang, Q., Law, B.E., Chen, J., Baldocchi, D.D., Cook, D.R., Oren, R., Richardson, A.D., Wharton, S., Ma, S., 2010. A continuous measure of gross primary production for the conterminous United States derived from MODIS and AmeriFlux data. Remote Sens. Environ. 114, 576–591. doi:10.1016/j.rse.2009.10.013

Xue, B.-L., Guo, Q., Otto, A., Xiao, J., Tao, S., Li, L., 2015. Global patterns, trends, and drivers of water use efficiency from 2000 to 2013. Ecosphere 6, 1–18. doi:10.1890/ES14-00416.1

Yang, F., Ichii, K., White, M.A., Hashimoto, H., Michaelis, A.R., Votava, P., Zhu, A., Huete, A., Running, S.W., Nemani, R.R., 2007. Developing a continental-scale measure of gross primary production by combining MODIS and AmeriFlux data through Support Vector Machine approach. Remote Sens. Environ. 110, 109–122.

Yang, F., Zhu, A., Ichii, K., White, M.A., Hashimoto, H., Nemani, R.R., 2008. Assessing the representativeness of the AmeriFlux network using MODIS and GOES data. J. Geophys. Res. Biogeosciences 113.

Yi, C., Davis, K.J., Berger, B.W., Bakwin, P.S., 2001. Long-Term Observations of the Dynamics of the Continental Planetary Boundary Layer. J. Atmos. Sci. 58, 1288–1299. doi:10.1175/1520-0469(2001)058

Young, G.H.F., McCarroll, D., Loader, N.J., Kirchhefer, A.J., 2010. A 500-year record of summer near-ground solar radiation from tree-ring stable carbon isotopes. The Holocene 20, 315–324. doi:10.1177/0959683609351902

Yu, G., Zhu, X., Fu, Y., He, H., Wang, Q., Wen, X., Li, X., Zhang, L., Zhang, L., Su, W., 2013. Spatial patterns and climate drivers of carbon fluxes in terrestrial ecosystems of China. Glob. Chang. Biol. 19, 798–810.

Yuan, W., Liu, S., Yu, G., Bonnefond, J.-M., Chen, J., Davis, K., Desai, A.R., Goldstein, A.H., Gianelle, D., Rossi, F., 2010. Global estimates of evapotranspiration and gross primary production based on MODIS and global meteorology data. Remote Sens. Environ. 114, 1416–1431.

Zaehle, S., Medlyn, B.E., De Kauwe, M.G., Walker, A.P., Dietze, M.C., Hickler, T., Luo, Y., Wang, Y.-P., El-Masri, B., Thornton, P., Jain, A., Wang, S., Warlind, D., Weng, E., Parton, W., Iversen, C.M., Gallet-Budynek, A., McCarthy, H., Finzi, A., Hanson, P.J., Prentice, I.C., Oren, R., Norby, R.J., 2014. Evaluation of 11 terrestrial carbon–nitrogen cycle models against observations from two temperate Free-Air CO_2 Enrichment studies. New Phytol. 202, 803–822. doi:10.1111/nph.12697

Zhang, Y., Song, C., Sun, G., Band, L.E., McNulty, S., Noormets, A., Zhang, Q., Zhang, Z., 2016. Development of a coupled carbon and water model for estimating global gross primary productivity and evapotranspiration based on eddy flux and remote sensing data. Agric. For. Meteorol. 223, 116–131. doi:10.1016/j.agrformet.2016.04.003

Zhu, X.-J., Yu, G.-R., He, H.-L., Wang, Q.-F., Chen, Z., Gao, Y.-N., Zhang, Y.-P., Zhang, J.-H., Yan, J.-H., Wang, H.-M., Zhou, G.-S., Jia, B.-R., Xiang, W.-H., Li, Y.-N., Zhao, L., Wang, Y.-F., Shi, P.-L., Chen, S.-P., Xin, X.-P., Zhao, F.-H., Wang, Y.-Y., Tong, C.-L., Fu, Y.-L., Wen, X.-F., Liu, Y.-C., Zhang, L.-M., Zhang, L., Su, W., Li, S.-G., Sun, X.-M., 2014. Geographical statistical assessments of carbon fluxes in terrestrial ecosystems of China: Results from upscaling network observations. Glob. Planet. Change 118, 52–61. doi:10.1016/j.gloplacha.2014.04.003

Zhu, X., Zhuang, Q., Qin, Z., Glagolev, M., Song, L., 2013. Estimating wetland methane emissions from the northern high latitudes from 1990 to 2009 using artificial neural networks. Global Biogeochem. Cycles 27, 592–604.

ZHUANG, Q., McGUIRE, A.D., MELILLO, J.M., CLEIN, J.S., DARGAVILLE, R.J., KICKLIGHTER, D.W., MYNENI, R.B., DONG, J., ROMANOVSKY, V.E., HARDEN, J., HOBBIE, J.E., 2003. Carbon cycling in extratropical terrestrial ecosystems of the Northern Hemisphere during the 20th century: a modeling analysis of the influences of soil thermal dynamics. Tellus B 55, 751–776. doi:10.1034/j.1600-0889.2003.00060.x

Zhuang, Q., Lu, Y., Chen, M., 2012. An inventory of global N_2O emissions from the soils of natural terrestrial ecosystems. Atmos. Environ. 47, 66–75.

VITA

VITA

SHAOQING LIU

Department of Earth, Atmospheric, and Planetary Sciences

Purdue University

550 Stadium mall Dr. West Lafayette, IN 47907

Email: liu955@purdue.edu Tel: +1 765 775 6329

Education

- 09/2012-12/2016 Ph.D., Earth, Atmospheric and Planetary Science, Purdue University
- 09/2009-07/2012 M.S., Environmental Science and Engineering, Beijing Normal University
- 09/2005-07/2009 B.S., Environmental Science, Beijing Normal University

Qualification & Skills

- Experienced in land surface biophysical-biochemical model operation, optimization and data assimilation
- Experienced in C++, C programming and OPENMPI
- Full proficiencies in Unix bash script, R, Matlab

PUBLICATIONS

Liu, S., Zhuang, Q., Chen, M., Gu, L., 2016. Quantifying spatially and temporally explicit CO_2 fertilization effects on global terrestrial ecosystem carbon dynamics. *Ecosphere* 7(7). doi:10.1002/ecs2.1391

Liu, S., Chen, M., and Zhuang, Q. (2016). Direct radiative effects of tropospheric aerosols on changes of global surface soil moisture. *Climatic Change*, 1–13. http://doi.org/10.1007/s10584-016-1611-7

Liu, S., Zhuang, Q., He, Y., Noormets, A., Chen, J., and Gu, L. (2016). Evaluating atmospheric CO_2 effects on gross primary productivity and net ecosystem exchanges of terrestrial ecosystems in the conterminous United States using the AmeriFlux data and an artificial neural network approach. *Agricultural and Forest Meteorology*, 220, 38–49.

Liu, S., Chen, M., & Zhuang, Q. (2014). Aerosol effects on global land surface energy fluxes during 2003–2010. *Geophysical Research Letters*, 41(22), 7875-7881.

Hao, G., Zhuang, Q., Pan, J., Jin, Z., Zhu, X., & **Liu, S**. (2014). Soil thermal dynamics of terrestrial ecosystems of the conterminous United States from 1948 to 2008: an analysis with a process-based soil physical model and AmeriFlux data. *Climatic Change*, 126(1-2), 135-150.